UNIVERSITY OF OSLO
Department of Informatics

Study of radiation effects in COTS semiconductors for use in high energy physics experiments

Cand. Scient Thesis

Hallvard Kvedalen

May 2002

Preface

This document is written as the main report for the Candidatus Scientiarum (Cand. Scient) degree at the University of Oslo, Norway, Department of Informatics.

The work that is described in this thesis is based on the work that I did during my one year stay at the European Organization for Nuclear Research (CERN) as a technical student (2000 - 2001). During my stay at CERN I worked in the Detector Control System group at the ATLAS detector which is under construction at CERN. The work that I did consisted of many different jobs, but the main work was focused around radiation testing of a part of the front-end electronics to be used in the control system in the ATLAS detector. The radiation test itself was not the most time consuming part of the work, but the preparation of the radiation tests and the analysis of the measured data were the main work. It should be mentioned that the preparation of the radiation tests consisted of software development and preparation of the measurement hardware used during the test.

I would like to thank my teaching supervisors Professor Steinar Stapnes at the Department of Physics, and Professor Oddvar Søråsen at the Department of Informatics at the University of Oslo. In addition I would like to thank my supervisor Dr. Helfried Burckhart at CERN, and my colleague Björn Inge Hallgren at CERN for an eventful and a great year.

It should be mentioned that the thesis is written as a complete report on the various radiation tests, and not a report on what I did related to the radiation testing. This means that not all of the described work has been done by me. This is because the radiation testing was done as teamwork. I have chosen to write the thesis in this way since this gives a more natural progress in the thesis and to give the reader a complete picture of the various radiation tests.

In addition to the work related to the radiation testing, I was also involved in other projects. I was involved in PCB design (the motherboard which will be mentioned later) and making of prototype test equipment for testing of the ATLAS DCS front-end electronics.

It should also be mentioned that I participated in several courses during my stay at CERN.

- One week course in the Supervisory Control and Data Acquisition system which is used in the ATLAS DCS system.
- 60 hours basic French course.
- One day CAN field bus course.
- One day CANopen field bus protocol course.

Contents

List of Figures

List of Tables

Introduction

This thesis is based on the work that I did during my stay at CERN. During my stay I was involved in various development work for the ATLAS detector control system, but radiation testing of electronics was the main topic, and this is also the topic of this thesis. To be more specific, I was involved in radiation testing of the front-end field bus node that is intended to be used in the ATLAS detector control system. This field bus node is based on the CAN field bus technology. The field bus node is referred to as the ELMB (Embedded Local Monitor Board). This is a general-purpose node that can be used to measure various sensor voltages via an onboard ADC and to read/write digital signals via the onboard microcontrolles.

All electronics that is to be used in the ATLAS experiment area must be tested and qualified to be radiation tolerant. The purpose of the radiation tests which is presented in this thesis was to find out if the components that are used in the ELMB design could be used in an environment with high radiation. In other words, the results presented in this thesis are used as a foundation for the selection of the components that is used in the ELMB.

The work concerning the radiation testing consisted of planning of the various tests, the preparation of the tests and the testing itself. In addition the results has been analyzed and the results has been presented in the ATLAS-DCS internal working notes [6], [7], [8] and [9]. The results has also been presented at the "7th Workshop on Electronics for LHC Experiments", Stockholm, Sweden, 10 to 14 September, 2001 [5].

The front-end electronics needed to undergo three different kinds of radiation tests, a Total Ionizing Dose (TID) test, a Non Ionizing Energy Loss test (NIEL) and a Single Event Effect (SEE) test. During my stay at CERN I was only involved in the TID and the SEE test, but the electronics has now been tested for all three types of radiation. This thesis will mostly discuss the TID and the SEE testing which I took part of.

The radiation tests has been performed at three different locations:

- The first TID test was done at the PAGURE irradiation facility. This facility is operated by CIS bio international. The facility is located at Gif-Sur-Yvette outside Paris, France.
- The two last TID tests was done at the Gamma Irradiation Facility located at CERN.
- The SEE test was performed with the cyclotron at the Louvain-la-neuve of the Université Catholique de Louvain in Belgium.

Chapter 1 gives an introduction to the new LHC accelerator and the ATLAS detector. This is a basic introduction.

Chapter 2 gives a description of the ATLAS Detector Control System. Further, the front-end

electronics that is used in some parts of the control system is described. Also a brief description of the CAN field bus and the CANopen application protocol is given.

Chapter 3 gives a theoretical base for radiation testing of electronics. The intention of the chapter is to highlight some of the most distinct effects that we can encounter during radiation testing.

Chapter 4 describes the test setup, the test locations and the test procedures that were used during the radiation tests. In addition the ATLAS rules for radiation testing of electronics are discussed.

Chapter 5 describes the results from the various radiation tests. The two types of radiation tests (TID and SEE) are presented in two sections with a summary in each section.

Chapter 6 summarizes the thesis with a conclusion and suggestions to further work.

Chapter 1

Physics experiments at CERN

This chapter describes the LHC project and it gives an overview of the ATLAS detector.

1.1 The LHC accelerator

The Large Hadron Collider (LHC) is the new and powerful accelerator under construction at CERN. The accelerator will be located in the same tunnel as the former LEP accelerator[1]. This accelerator will be the worlds largest and most powerful accelerator ever built. It will have four different detectors (ALICE, ATLAS, CMS and LHCb). They will be located at four different locations in the tunnel. Figure 1.1 shows a map of the CERN location with the LEP/LHC tunnel marked. The length of the tunnel is 27 km, and as seen, the tunnel is located at the borderline between France and Switzerland (around 100 m deep).

The "A Toroidal LHC ApparatuS" (ATLAS) detector will be located at point 1, close to the CERN main entrance, while the "Compact Muon Solenoid" (CMS) detector will be located at the opposite part of the circle, point 5. The two other detectors which will be located in the LHC accelerator is the "A Large Ion Collider Experiment" (ALICE) detector and the "Large Hadron Collider beauty experiment" (LHCb).

In the LEP experiment, electrons and positrons were accelerated in the LEP tunnel and lead into head on collisions at four places - the places were the detectors were located. The LEP experiment gave the physicists a lot of new information, but to be able penetrate even deeper into the nuclear world even higher energy levels are needed. This will be achieved with the LHC accelerator that will have two beams of protons instead of the electrons and positrons as used in the LEP. The two proton beams will be located inside two vacuum tubes, where they will be steered by a strong magnetic field. The magnetic field will steer the proton beams and overcome the centrifugal force on the proton beam. The magnetic field required to do this job is quite strong, and therefore special magnets are required. The magnets used in the LHC are so-called super-conducting magnets. This means that the magnets will be made of a super conducting material, and they will be totally immersed in liquid helium, which gives them a temperature close to absolute zero. The protons will be accelerated by an electric filed created at some locations in the accelerator. The maximum energy to the protons is 7TeV.

[1]The LEP (Large Electron-Positron Colider) experiment was an experiment where electrons and positrons were accelerated and collided in four different detectors. This experiment was operational for over ten years, but has now been stopped.

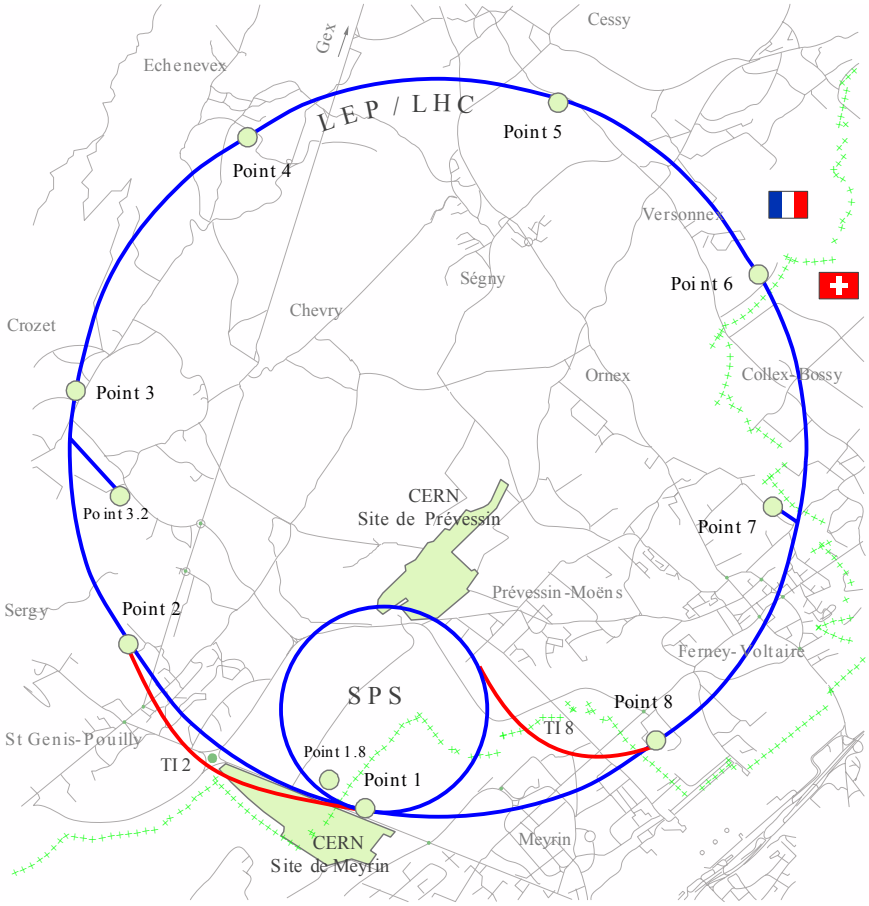

Figure 1.1: *Geographic map of the LHC accelerator location.*

To get enough data from the rare events expected in the LHC accelerator a high number of collisions are needed. To achieve a high number of collisions per second, the accelerator tubes will contain many protons. Each of the tubes will contain 2835 bunches with protons. Each proton bunch will have around 10^{11} protons. When the 2835 bunches are spread equally in the tube there will be 7.5 meters between each particle bunch. Since the protons are moving at almost the speed of light there will be a collision every 25 nS in each detector. This high collision rate will create a huge amount of physics data that must be handled and stored. The protons, which will be used in this experiment will be produced and pre-accelerated in the Super Proton Synchrotron (SPS) and the Proton Synchrotron (PS) already located at CERN. The protons will be accelerated further in the LHC accelerator by the accelerating cavities before the proton bunches can be steered towards each other to create a collision, the collision will only take place in each detector [52].

1.2 The ATLAS detector

One of the detectors in the LHC accelerator is the ATLAS detector (short for A Toroidal LHC ApparatuS). This detector is the biggest detector in the LHC accelerator. The overall size of the detector is something like 40×20 meters and it will weight around 7000 tons. An artistic drawing of the detector inside the cavern is shown in figure 1.2.

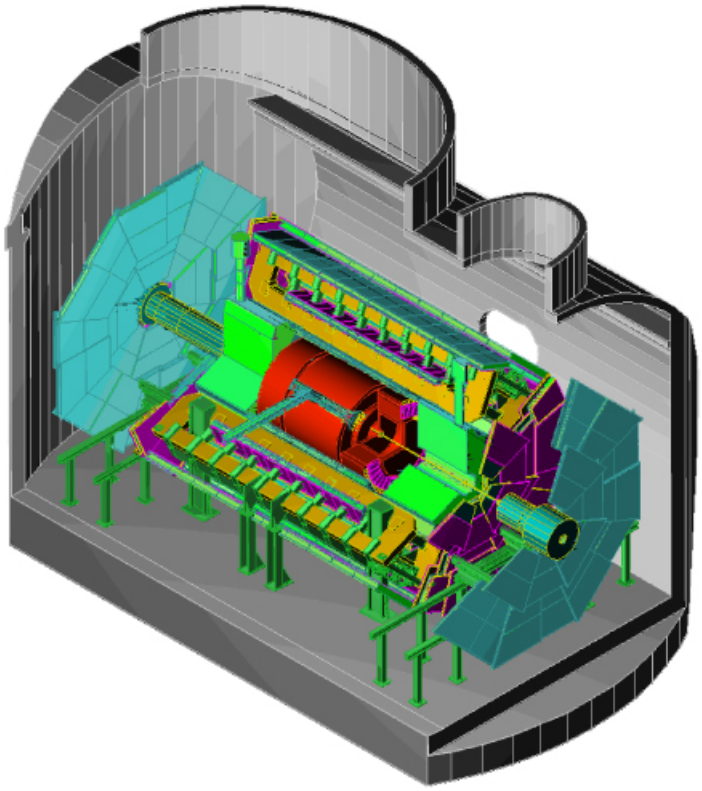

Figure 1.2: *Artistic drawing of the ATLAS detector in the cavern.*

The ATLAS detector will be a gigantic and accurate instrument for the particle physicists. There will be something like one billion collision events every second. This is a huge amount of data and the detector must be able to select interesting data events and reduce the rate down to 10 - 100 events per second, which is stored for further analysis. The detector have many purposes in experimental particle physics, but one important goal is the search for the origin of mass (the search for the Higgs particle) [11]. To achieve this, the detector must be able to measure the direction of particles, the momentum, polarity, and energy. It must also be able it identify particles and be able to identify if some of the particles was created outside the main collision pint. The ATLAS detector is divided into several layers. Each of these layers serves specific proposes, i.e. different parts of the detector is responsible for the detection of different particles.

1.2.1 ATLAS inner detector

The inner detector will measure the directions, the momenta and the charge of electrically charged particles. The inner detector is built of several layers with different sensors. The innermost part is made of so-called pixel detectors. This type of detector element consists of several silicon wafers which is 16×60mm large. Each wafer consists of 50000 pixels with a size of 50×400 microns. These pixel wafers will be mounted onto 1500 modules that will make the pixel detector. The pixel detector is 1.4m long and 0.5m in diameter and is the innermost part visible on the figure 1.3. The pixel modules are mounted both axial and radially in the detector. The modules which are mounted parallel to the beam axis will detect particles with a large angle between the particle beam axis and the particle path. To be able to detect particles with a small angle, the modules will also be placed on several discs. These discs are placed further away from the collision point.

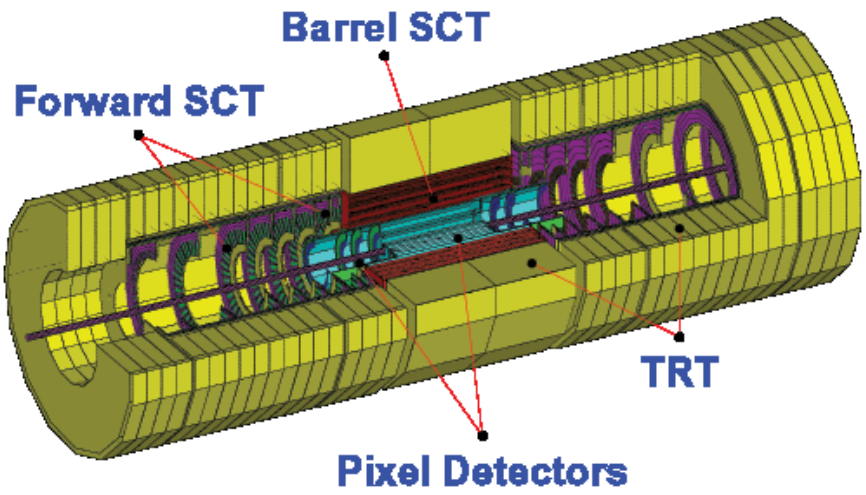

Figure 1.3: *Artistic drawing of the ATLAS inner detector.*

For even better position measurements additional layers of detectors are added. The next layer in the inner detector is the semiconductor tracker (SCT). The SCT is made of so-called silicon microstrip technology. The strips are about 80 microns wide and several centimeters long. The strip detectors are mounted the same way as the pixels. In the area closest to the collision point the stripes are mounted parallel to the beam axis. This part of the detector is referred to as the Barrel SCT. The SCT are also mounted onto disks. These disks are located further away from the collision point. This part of the detector is called the Forward SCT.

Due to the high cost of pixel detectors and strip detectors it is not possible to use this kind of detectors in the outermost part of the inner detector. In this part the Transition Radiation Tracker (TRT) detector is used. The sensor element in the TRT is a gas filled straw tube. Between the tube wall and the wire a high tension is applied. When a particle travels through the straw tube it creates a shower of electrons and positrons, which contributes to a charge change that can be measured. With accurate timing it is possible to determine how far from the wire the particle passed.

1.2.2 ATLAS calorimetry

Figure 1.4 shows a drawing of the calorimeter in the detector. The purpose of the calorimeter is to measure the energy of electrons/protons and photons, which traverses the calorimeter.

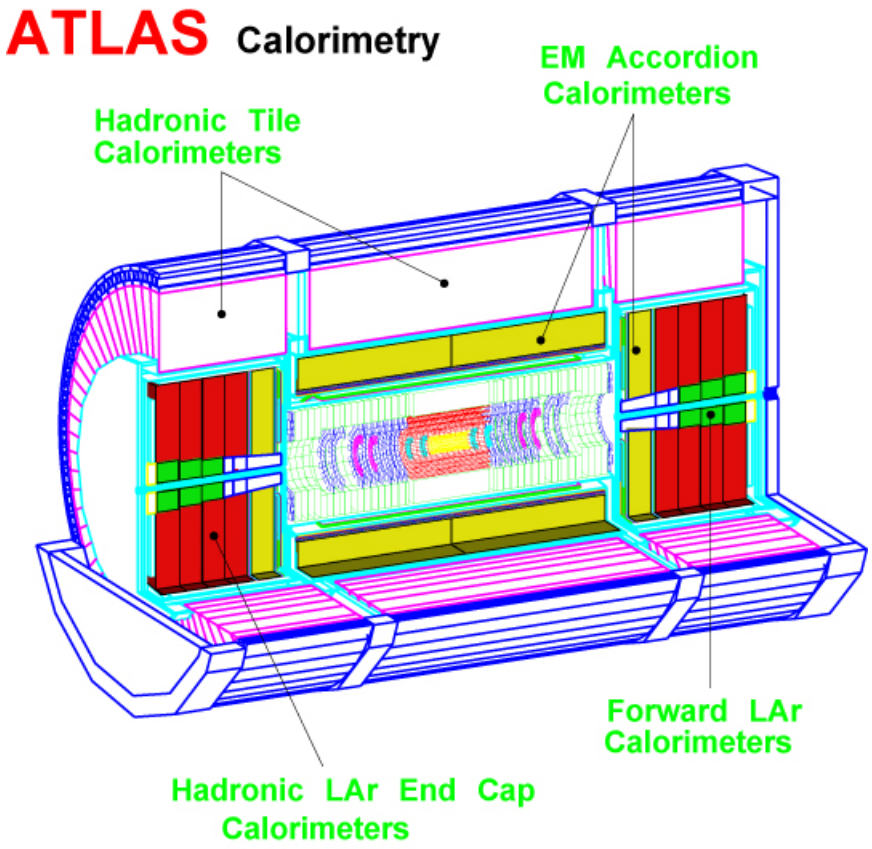

Figure 1.4: *Artistic drawing of the calorimeter part of the ATLAS detector.*

The electromagnetic calorimeter is made like a sandwich. The layers are made of thin lead plates fully immersed in liquid argon. Each of these layers is connected to some current measuring equipment. Between each lead plate there is also an electric field. When a fast moving electron/positron or a photon traverses this "sandwich" it will create a particle shower from the lead plate and into the liquid argon. When the electrons from the shower reaches the liquid argon they hit some argon atoms and crate ions and free electrons. The electrons will drift to the positive side in the electric field and a current proportional to the energy can be measured.

The hadronic calorimeter surrounds the electromagnetic calorimeter. The purpose of this calorimeter is to measure the energies of hadrons. Since jets are created from a quark or a gluon and these two particles can not be observed directly it is of great interest to measure these jets. This should also be

The hadronic calorimeter will be able to measure the energy and the direction of jets. The principle of operation of the hadronic calorimeter is a bit like the electromagnetic calorimeter. The calorimeter consists of metal layers of copper and steal. When a hadron traverse into the calorimeter it will create a hadronic shower consisting of hadrons with lower energies. The shower

of hadrons will travel through the plastic sintillator and excite the nearby atoms in the plastic. When the atoms in the sintillator falls back to the ground state they emit photons (light) which can be measured.

1.2.3 ATLAS muon detector

Figure 1.5 shows a drawing of the muon detector in the ATLAS detector. The muon detector detects high-energy muons. The detector determines the polarity and the momenta of the muons. The muon detector is made of many individual gas-filled chambers where it is possible to measure a charge change. When the muon passes this chamber is will create a shower of electron/positron pairs and ions. This will create a charge change that can be measured. The muon detector is made with several layers with these gas-filled chambers. When a muon passes several of these chambers it is possible to reconstruct the muon path. To be able to measure the momenta and the polarity it is necessary to deflect the muon and measure the radius in the particle path. The muon is deflected by a toroid magnet system. The magnet system consists of eight coils.

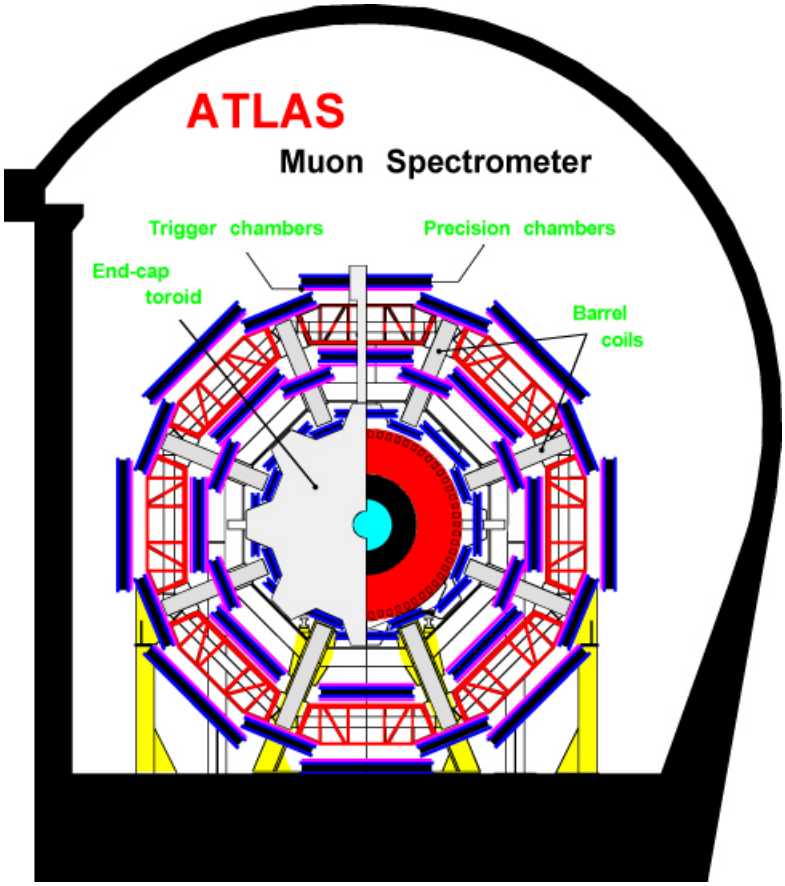

Figure 1.5: *Artistic drawing of the muon detector part of the ATLAS detector.*

1.2.4 Trigger - DAQ

The ATLAS detector consists of many different detector types with an extremely high number of output channels with physics data. Due to the high number of channels and the high collision frequency it is necessary to reduce the amount of data. The trigger/DAQ (data acquisition) system is responsible for the data fetching from the front-end electronics in the various detectors, and the selection of interesting data. Figure 1.6 shows a drawing of the trigger system.

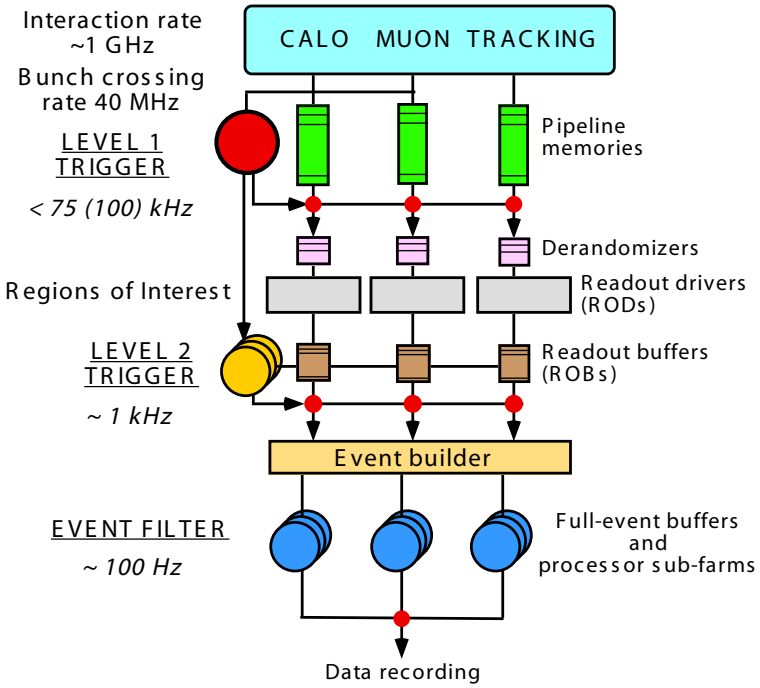

Figure 1.6: *ATLAS trigger/DAQ system, figure is taken from [13].*

The interaction rate in the ATLAS detector will be 10^9Hz. This rate must be reduced down to about 100Hz for permanent storage of the data [13]. This means that a lot of physics data must be rejected, the system must therefore be able to recognize new and interesting events, like the Higgs boson decay.

The trigger/DAQ system is made of two triggers, the level-1 trigger (LVL1) and the level-2 trigger (LVL2). The LVL1 trigger is the first trigger in the trigger/DAQ chain and can be programmed to select different kinds of events. This trigger is fed with event data from the front-end electronics from the various detectors. The data from the LVL1 trigger is placed in the Readout buffers (ROBs) in the trigger chain. The LVL2 trigger will do a second decision on the data from the detectors. This selection is based on detection of interesting event signatures. If an interesting event is found, the data will moved from the ROBs and to the event builder. The event data in the ROBs is composed of data from different parts of the detector. In order to select an interesting event, it is necessary to use the event builder. The event builder collects the data associated with the event and places this data in some memory with a label (identifier) that can be used for further selection. The event filter is used to filter out the various events which has been collected by the event builder, only the most interesting events will be selected and transferred to the storage system.

Chapter 2

ATLAS Detector Control System

This chapter describes the ATLAS detector control system and the CAN bus front-end node which will be tested in the radiation test. Also a short description of the CAN bus and the CANopen application protocol is included.

2.1 The Detector Control System

Nowadays physics experiments have become so big that it is impossible to have fully control over the experiment without the use of a specially dedicated control system. For a safe and reliable operation of the detector a Detector Control System (DCS) is required. The main task of the DCS is to have supervision of the sub-detectors inside the detector and to communicate with the outside world. In this context, the outside world means communication with the LHC accelerator, the general infrastructure of the experiment and the CERN infrastructure. Figure 2.1 show a diagram of the various connections to and from the DCS. As we can see, the DCS system is connected to smaller groups in the detector that called sub-detectors. For instance the Semiconductor Tracking Detector (SCT) or the Liquid Argon (LAr). These groups are responsible for a smaller part of the detector, but the DCS should collect information from all these sub-detectors.

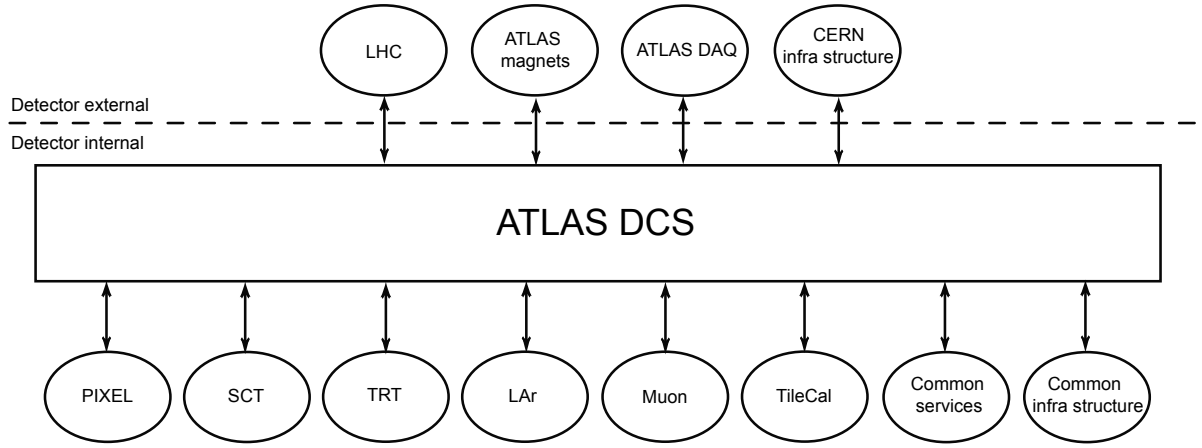

Figure 2.1: *The logical structure of DCS.*

The complement to the DCS is the Data Acquisition (DAQ) system. This system is responsible for the physics event data and is only operational when the experiment is running. On the contrary, the DCS is operational all the time and the data have a time stamp.

The ATLAS DCS is a distributed control system and it consists of two main parts. The Supervisory Control and Data Acquisition system (SCADA) and the front-end system. The SCADA system is a system that collects data, performs data processing, archiving of data in a real-time database and presentation of the data for the end user. The front-end system is described as devices and I/O points. This means everything from simple I/O nodes to larger computer systems.

The structure of the ATLAS DCS is divided into three zones. Figure 2.2 shows a layout of the three zones. The main control room is located in the SCX1 zone. This is located at the surface (ground level) in the ATLAS main building. The USA15 zone is the electronics area. This zone is underground and is always accessible for personnel. The UX15 area is the experiment cavern. This area is exposed to high radiation and magnetic fields, and is therefore not accessible during beam time.

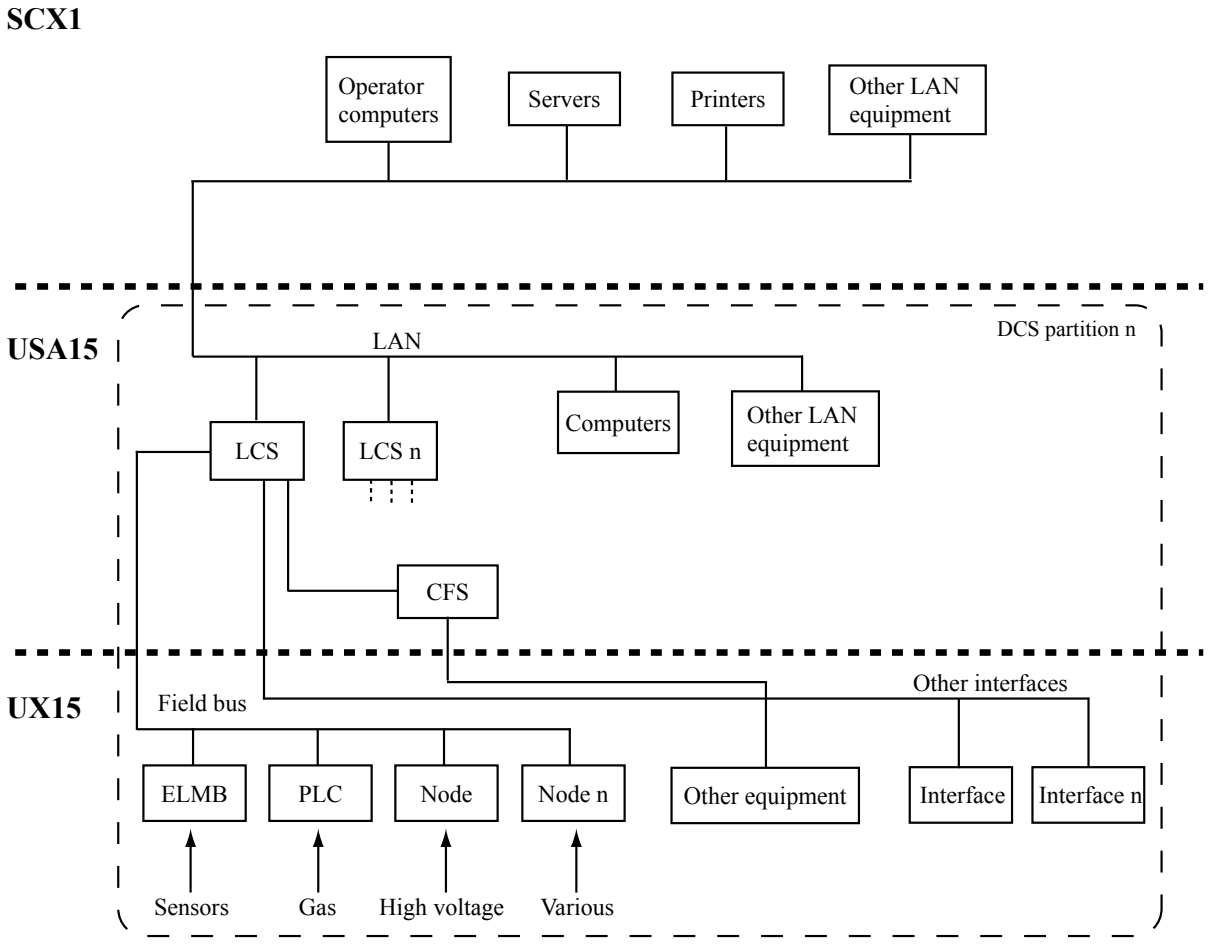

Figure 2.2: *The distribution of the DCS architecture in the ATLAS detector complex.*

The figure shows a sketch of one DCS partition, the complete system will have several such partitions. The figure also indicates what the DCS system consists of, and how the system is

connected together. As seen, the front-end I/O system is distributed in the USA15 and the UX15 areas. Since the size of the detector is quite big, and there is a demand for many I/O channels it is necessary to use intelligent I/O nodes that are connected via field buses to the SCADA system. Without the field buses it would be impossible to have all the I/O channels required in the detector. In some cases one might be using a Local Area Network (LAN) for distribution of measurement data. This is the case if you want to connect many SCADA systems together (see top of figure). The idea of the system is to distribute the field buses in the detector and connect them to a so-called Local Control Station (LCS). The LCS is running a SCADA system which is responsible for collection of data, and control of the nodes in that DCS partition. The LCS is connected to various computers where personnel can control each LCS. As seen, the LCS is connected to the control/supervision computers via a LAN connection. The CFS (Complex Front-end System) block shown in the figure is a stand-alone computer system used to perform a specific task. The top down structure on the DCS system is referred to as a vertical slice [10] [12].

2.2 The front-end IO

The front-end I/O system consists of many different I/O devices. This depends on the local system and its requirements. If you have a closed loop system and you want a fast feedback (no time for data to travel through the vertical slice into SCADA and back for a response), you might want to use a Programmable Logic Controller (PLC) for fast feedback. On the other hand, if you just need to monitor the status, or the response in your system is not critical, you can use some kind of a field bus I/O node that is controlled entirely of the SCADA system. The DCS system is quite complex, and there is a demand for many I/O channels. Due to this demand, the limited space, and the harsh environment it would be difficult to use only commercial I/O nodes. Therefore the ALTAS Detector Control System group (ATLAS-DCS) started to investigate, and design a field bus node with a high number of I/O channels. Since the environment where the nodes are supposed to operate has a strong magnetic field and a high radiation level it must be radiation and magnetic field tolerant. Another important factor for the I/O system is that it should be flexible, i.e. it should be possible to use the same node for many applications (cost effective). The field bus itself is also very important. The bus system should be reliable, a message sent, should arrive at the destination node without message corruption. At CERN a field bus survey [28] has been performed, and three field buses are recommended for use in the detectors. The buses are the CAN bus, Worldfip and the Profibus. The CAN bus has been chosen by the DCS as the standard bus for the field bus nodes.

The I/O node which was designed were called the “Local Monitor Box” (LMB). The LMB is a CAN field bus node and is intended to be a front-end data acquisition node for the slow control system. The LMB concept is shown in figure 2.3. The LMB consists of a main part and several add on modules. The main module is the control part of the LMB system. It has an interface to the CAN bus and an internal serial bus carrying data and power. Various add-on modules can be attached to this serial bus. This makes the LMB concept quite flexible since each node can be customized to each application. If your system requires some analog input channels you can just attach an ADC module. In total the control module can handle seven of these add on modules. The LMB are designed so it can be mounted onto a standard DIN rail as shown in the figure. It can be powered through the CAN bus, or locally with the auxiliary power connector.

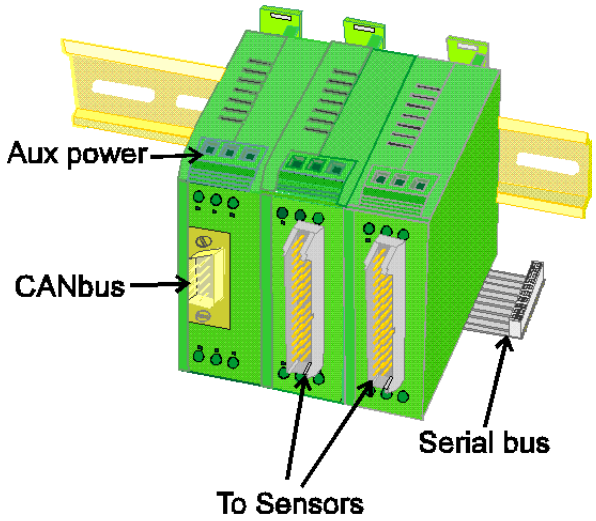

Figure 2.3: *The LMB concept. The figure shows an artistic drawing of the main module and two add on modules. The figure shows two analog input boxes with 16 channels each.*

After successful testing of the LMB, the successor of the LMB was designed. The successor to the LMB is called the Embedded Local Monitor Board (ELMB). It has been designed to give the user even more features on a smaller area. As the name says, the ELMB is an embedded solution. The ELMB is simply a small card that can be embedded into a larger electronic system where the functionality offered by the ELMB is required. The card is quite small, it is just 50×67 mm. Figure 2.4 show the front side of the card, and figure 2.5 show the back side of the card. The front side holds the digital part and the CAN part, while the backside holds the analog part.

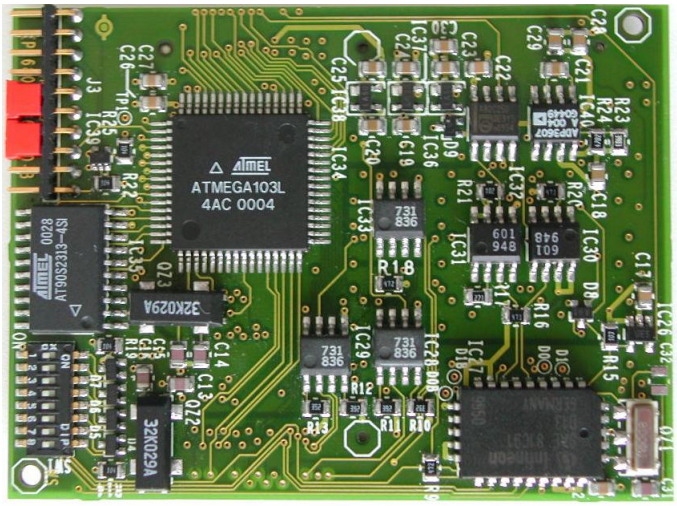

Figure 2.4: *Front side of the ELMB PCB. The digital part and the CAN part is located on this side.*

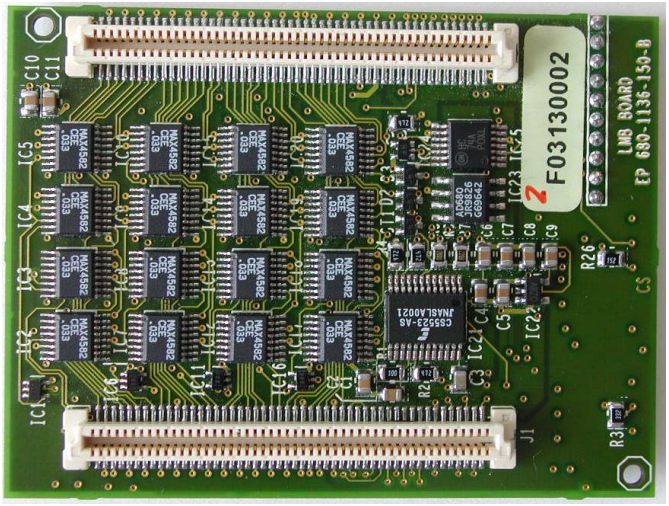

Figure 2.5: *Back side of the ELMB PCB. The analog part of the ELMB is located on this side.*

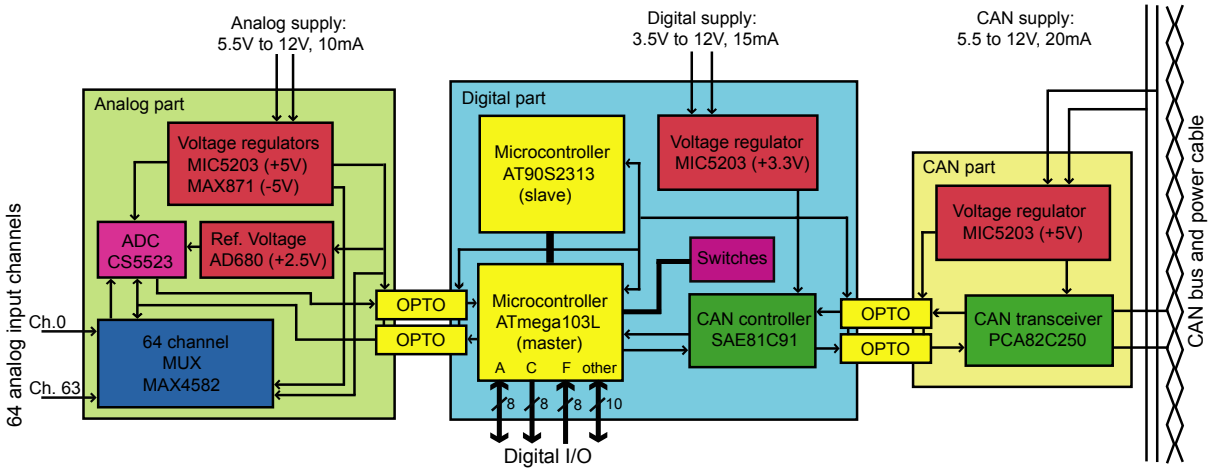

Figure 2.6: *Block diagram of the ELMB.*

As mentioned, the ELMB is separated into an analog, a digital and a CAN part. The separation of the powering is done to avoid and to reduce problems with noise and grounding loops. This is clearly shown in figure 2.6 where the three parts are depicted. Each part is galvanic separated by opto-couplers.

The digital part of the ELMB is based around two microcontrollers from the AVR microcontroller series from Atmel. The rather big ATmega103L is used as the main processor, while the smaller AT90S2313 is used as a slave processor. Both of these microcontrollers are so-called *In System Programmable* (ISP). This means that the controllers can be programmed while soldered onto the PCB. This feature is a major advantage since this makes it easy to change and upgrade the software. This is especially useful when the ELMB is mounted onto some other electronic that is hard to "get to" in the detector. The microcontrollers are also connected in a way so that they can program each other. This functionality is implemented in the current ELMB firmware. With this firmware it is possible to download new firmware via the CAN bus and to program

the controllers. The controller that does not undergo programming handles the programming.

A second reason for the two microcontrollers instead of one is the possibility to recover from problems related to radiation. The idea is that if a problem occurs with one of the controllers it should be reset by the second controller (both controllers can reset each other). This is achieved with software. The firmware in the controllers does an "alive" check of each other now and then. During normal operation, the master controller has full control of the ELMB. This means that the master controller handles the CAN communication, the ADC communication and the digital I/O line control. If the slave has control of the node (this is only recovery mode), it only handles basic CAN communication and the programming function.

The ELMB hardware has 34 digital input and/or output lines. The number of available lines for the user is dependent on the firmware in the main processor. If the standard ELMB software is used, the ELMB has 16 output lines and 8 input lines. Some of the remaining I/O lines are not used and some are used for internal ELMB communication, e.g. communication with the ADC and CAN controller (SPI). Since the ELMB hardware doesn't have any limitations other than defined input and output direction (defined in the microcontroller), it is up to the user to make proper software to implement various protocols. It should be mentioned that the ELMB has been tested to drive both I^2C and JTAG devices.

The analog part of the ELMB is build around an ADC and an analog multiplexer network. The ADC that is used has only four input channels, but with the multiplexer network the number of analog input channels is increased to 64. All channels are bipolar (unipolar settings possible through internal ADC settings), and it has a maximum input range of ±4.5V. If better resolution are required it is possible to configure the ADC in six input ranges, starting at 25mV. If the application requires a measurement of signals larger than ±4.5V some form of signal adaptation should be used. It should also be mentioned that the main processor has an internal ADC that can be used if desired. Normally the input lines for the internal ADC are used as digital input lines (PORTF). This is in principle just a mater of software (firmware) in the ATmega103 microcontroller.

ELMB analog features

- 64 bipolar/unipolar analog input channels
- 6 input ranges from ±25mV to ±4.5V
- 16-bit $\Delta\Sigma$ ADC with adjustable conversion rate from 1.88Hz to 101.1Hz
- 10-bit microcontroller on-chip ADC (firmware dependent use)
- Separate analog power for noise reduction

ELMB digital features

- Two microcontrollers for reliable operation
- Microcontrollers has on-chip EEPROM for storage of constants
- 16 input lines (firmware dependent)
- 8 output lines

- 10 general purpose I/O lines (firmware dependent)
- Real-time clock in microcontroller with external x-tall (available on ELMB board)
- In system programmable with ISP programmer and via the CAN bus with proper firmware.

ELMB CAN features

- Full CAN support, both CAN 2.0A and CAN 2.0B
- Possible to set CAN identifier with on-board switches, 6-bit identifier (firmware dependent)
- Possible to choose between 4 different baud rates (firmware dependent)

2.2.1 The ELMB motherboard

Since the ELMB is a plug-in card it can be embedded into a larger electronic system where the ELMB functionality is required. Therefore, to be able to use the ELMB you need a board with connections to two 100-pin connectors that match the ELMB connectors. The ELMB motherboard has been made to do this job. The board is primary intended to be a test board, which can be used in various prototype setups, but the board can also be used in a real application where no other electronics are required. The board has connectors for the 64 analog input channels and the digital I/O lines. In addition it is possible to add a signal adaptation network for each analog input channel. Some form of signal adaptation is normally required this is highly dependent on the application. So far four signal adapters exist for the motherboard as standard adapters. These adapters are, an adapter for an ohmic sensor connected in a four wire connection, a signal adapter for an ohmic sensor with a two-wire connection, a bipolar voltage divider and a straight resistor network for direct connection of the input connector to the ADC input. Figure 2.7 and 2.8 shows the front and backside of the motherboard. The front side of the PCB is equipped with the I/O connectors and a power terminal connector. The board can be supplied with three different voltages, one for each part of the ELMB. The CAN bus connector is a 9-pin male D-sub connector, while the other I/O signals are connected via standard header connectors. The backside holds the two 100-pin connectors for the ELMB (not shown), and sixteen 18-pin DIL sockets for the signal adapters. The picture shows a motherboard that has sixteen DIL resistor packages. With this configuration the ELMB can measure an input voltage of maximum ± 4.5V. Also a $+2.5$V reference voltage is available on each socket and on each analog input terminal (34-pin). This voltage is a derivative from the reference voltage available on the ELMB board. The reference voltage is buffered with four operational amplifiers (one for each analog input connector) to provide some current driving capability. The motherboard fits into a plastic box, which can be mounted on a standard DIN rail.

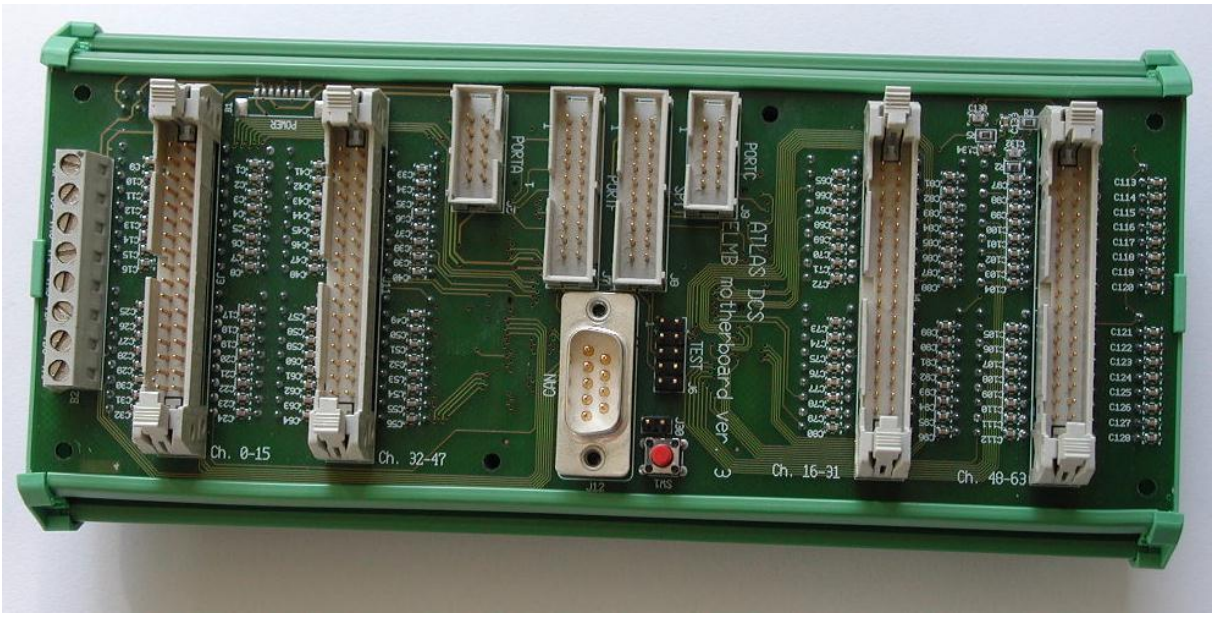

Figure 2.7: *Front side of the motherboard. The motherboard has four 34-pin connectors for the 64 analog input channels. The Digital lines are available through the four header connectors. The CAN bus is connected via a 9-pin D-sub connector. The screw connector is used to connect the power cable.*

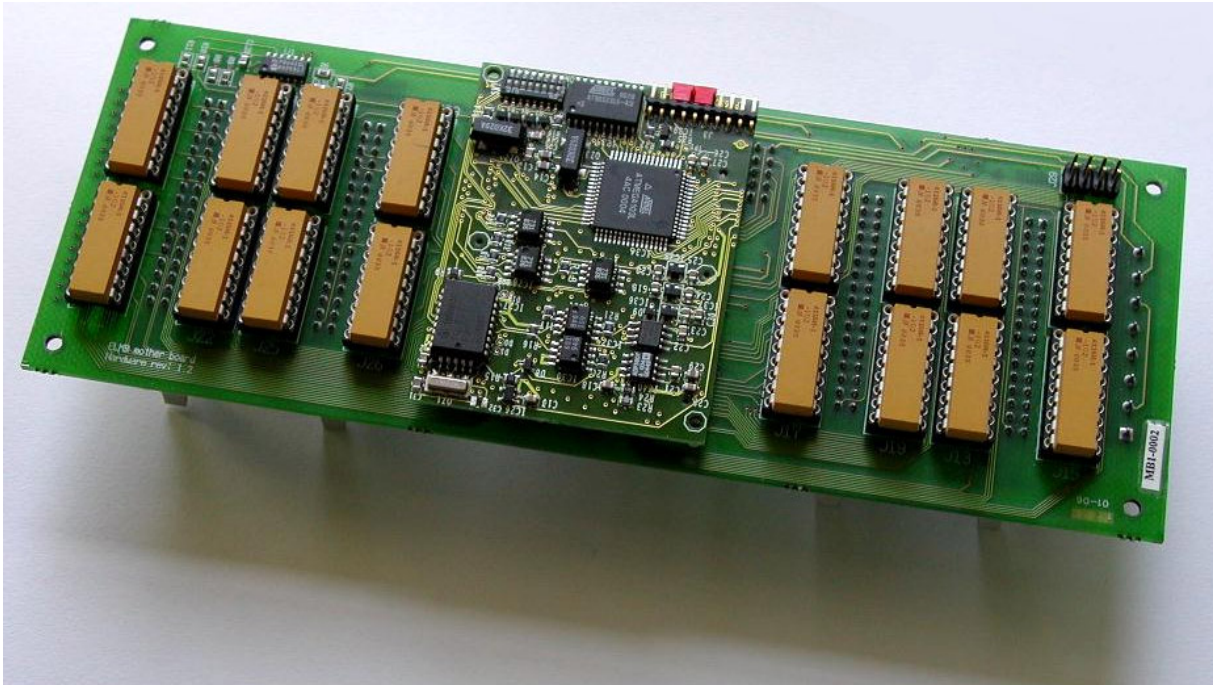

Figure 2.8: *Back side of the motherboard with the ELMB mounted. The back side of the motherboard has two 100 pin SMD connectors for the ELMB and 16 DIP sockets for signal adapters.*

2.2.2 Front-end analog part

Figure 2.9 shows a picture of the ELMB back side. As mentioned, the analog part has a $\Delta\Sigma$ ADC (IC21). This is a 16 + 7 bit ADC from Crystal semiconductors [39] CS5523AS. The ADC has a resolution of 16 bits, but since the ADC can operate in six different ranges you also have 7 bits to indicate which range you are using. This ADC has 4 bipolar input channels. These channels are increased to 64 with sixteen 4 to 1 analog multiplexers. The multiplexer which is used is the MAX4582 (IC2-5, 7-10, 12-15, 17-20) from Maxim semiconductor [35]. The ADC is fed with a +5V supply voltage, and a +2.5V reference voltage. The reference voltage is used to give a stable reference for the ADC conversion. The voltage is generated by the voltage reference circuit AD680 (IC23) from Analog devices [37]. The analog supply voltage is regulated by the low dropout voltage regulator MIC5203 (IC36) from Micrel [42]. This regulator features both current limitation and thermal limitation. This is very important since the ELMB can suffer from radiation damage that might increase the current. In addition to the +5V, the multiplexers and the ADC need to be supplied with a -5V voltage. This voltage is derived from the +5V supply via a voltage inverter. The voltage inverter is the MAX871 (IC22) from Maxim semiconductors [33].

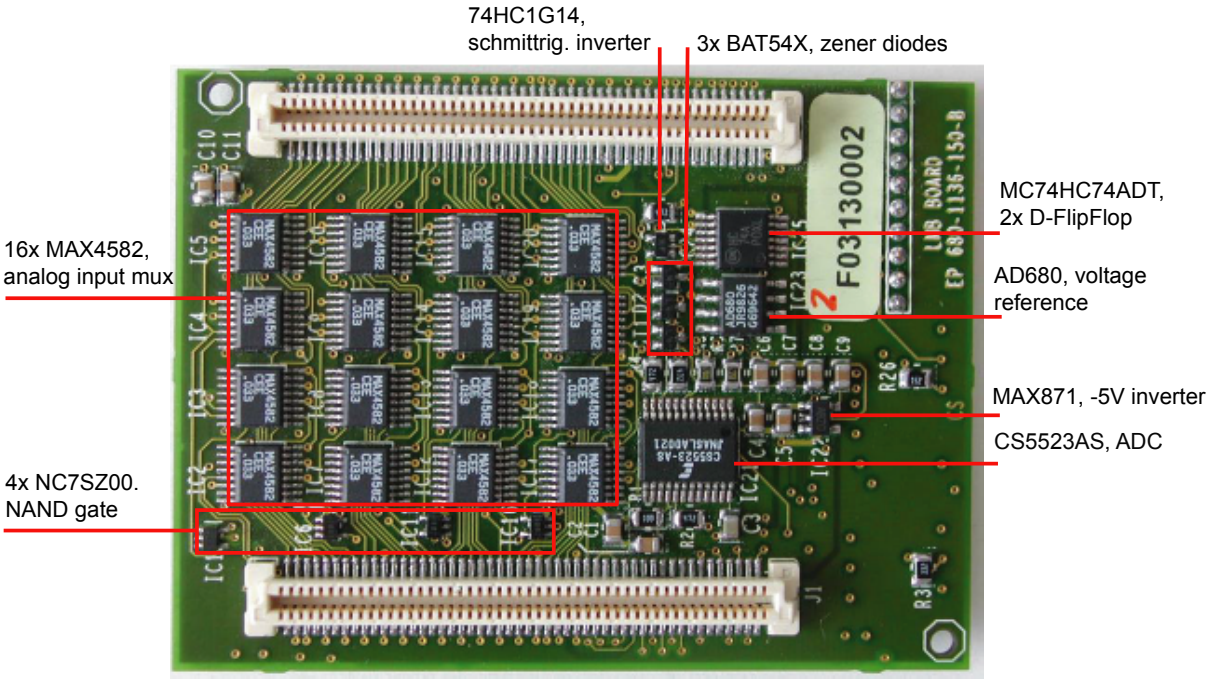

Figure 2.9: *Backside of the ELMB with the semiconductor components marked.*

The analog part does also have a few logic circuits, four NC7SZ00, which is a two input NAND gate (IC1, 6, 11, 16), a schmitt trigger inverter 74HC1G14 (IC24) and a D-Flip Flop 74HC74ADT (IC25). These components are used to control the multiplexer circuits. The last semiconductors used on the analog side are three zener diodes, BAT54W (D2, D3 and ST1).

The master controller in the digital part controls both the ADC and the multiplexer network. The communication between the microcontroller and the analog part is done via opto-couplers this ensures a galvanic separation of the two ELMB parts. The opto-coupler which is used is a general-purpose opto-coupler HCPL0731 (IC28, 29, 33).

Table 2.1 gives a summary of the semiconductors used in the analog part. The "technology" column is of special interest during analyzes of the radiation test results since various technologies react different to various sources of radiation. The ELMB schematic is included in appendix A.

Component no:	Device	Technology	Function
IC1,6,11,16	NC7SZ00	CMOS	2 input NAND
IC2-6,7-10,12-15,17-20	MAX4582	CMOS	Multiplexer
IC21	CS5523AS	CMOS	ADC
IC22	MAX871	CMOS	Voltage inverter
IC23	ADP680	Bipolar	reference voltage circuit
IC24	74HC1G14	CMOS	Schmitt trigger inverter
IC25	74HC74ADT	CMOS	2×D-FF
IC28,29,33	HCPL0731	Opto	Opto-coupler
IC36	MIC5203	CMOS	Voltage regulator
D2,D3,ST1	BAT54W	Bipolar	Zener diode

Table 2.1: Listing of the semiconductor devices and type of technology.

2.2.3 Front-end digital part and CAN part

The digital part of the ELMB is based around two AVR microcontrollers (IC34) and (IC35) from Atmel. Figure 2.10 shows the front side of the ELMB with the two microcontrollers. IC34, the ATmega130L is the main processor, also called the master processor. It has 128k bytes of Flash program memory, 4k bytes of SRAM and 4k bytes of EEPROM. The main processor is supposed to run the main program, that is, controlling the ADC and fetching data from it, reading and writing to the digital I/O lines and communicate with the CAN bus via the CAN chip (IC27). The second processor (IC35) AT90S2313, also called the slave processor is a smaller controller. It has 2k bytes of Flash program memory, 128 bytes of SRAM and 128 bytes of EEPROM. Both of these components are made with CMOS technology. Both of these components have a lot of memory and it is known that especially the SRAM is vulnerable for single event upset. This means that bit-flips in the memory can be a problem if this component is exposed to radiation with high enough energy capable of changing the state of a bit.

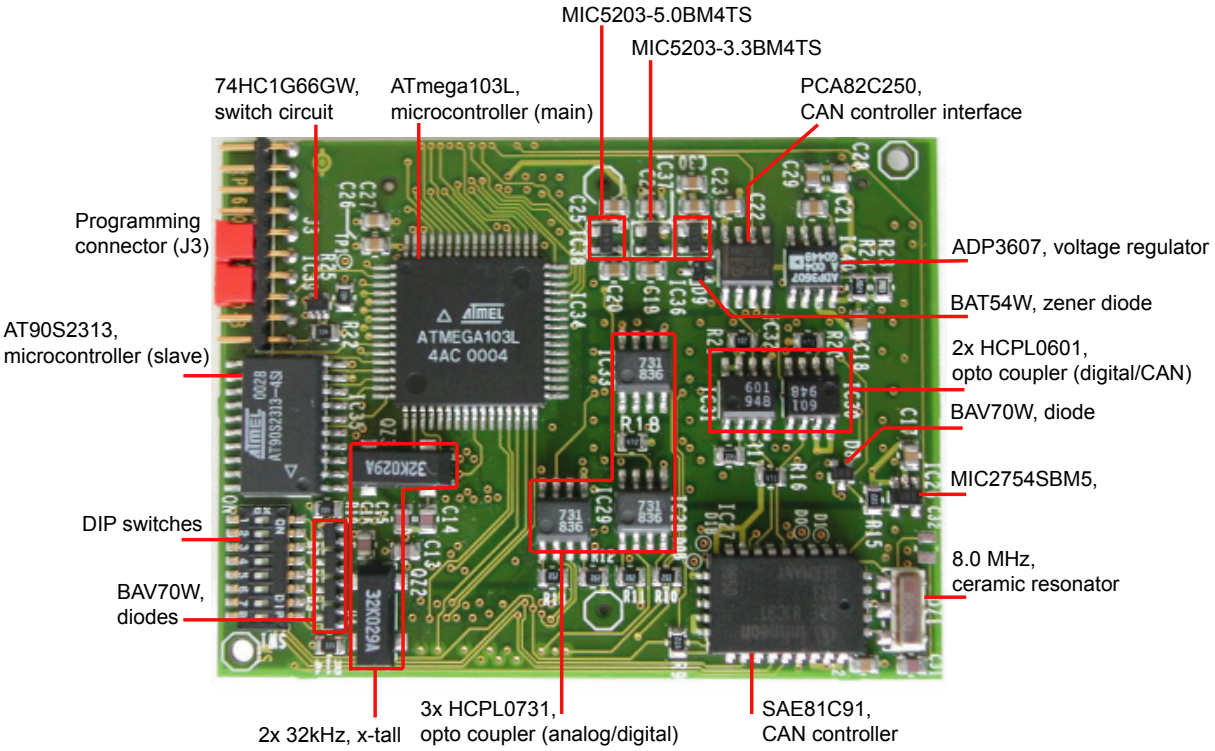

Figure 2.10: *Front side of the ELMB PCB with the semiconductor components marked.*

The digital part also have a CAN controller chip (IC27), the SAE81C91 from Infineon [34]. This chip supports the CAN communication protocol 2.0A and 2.0B. The chip is responsible for handling CAN frames to and from the CAN bus interface chip, and data to and from the microcontrollers. This chip is a CMOS device that has many registers where bit flips might occur. The ELMB is currently made as a 3.3V device and the MIC5203 (IC37) low drop voltage regulator is responsible for the voltage regulation and current limitation in the digital part. This regulator is from Micrel [42]. It should be mentioned that the first two prototype series of the ELMB was made as a 5V device. Some of these ELMBs was used during the radiation tests. Another important circuit is the reset circuit MIC2754 (IC26) from Micrel [43]. This circuit ensures proper handling of the reset signal to the microcontrollers and the CAN chip during power-up, or if the supplied voltage drops below a given threshold. The digital part is also equipped with an auxiliary power circuit. The ADP3607 (IC40) from Analog devices [36] is used to generate this auxiliary voltage. Both microcontrollers can be programmed (flash and EEPROM) via the J3 connector. In addition to the normal programming lines the connector also carries the two serial communication (RS-232) lines to/from the ATmega103L controller. These serial communication lines are very useful for software development and debugging of the software. Since the two processors are monitoring each other they must be able to reset each other. This is achieved with the double diode BAV70W (D8). The CAN baud-rate and the CAN identifier is "programmed" with the SMD mounted switch SW1.

The third part of the ELMB is the CAN part. This is a rather small part. It consists of the CAN bus interface chip PCA82C250 (IC32) from Philips [46] and two opto-couplers for galvanic separation of the digital part and the CAN part. The opto-couplers HCPL0601 (IC31 and IC 31) is from Hewlett Packard. In addition the CAN part is equipped with a voltage regulator

MIC5203 [42] from Micrel. The CAN interface chip converts the TTL/CMOS compatible input signals from the digital part to the two CAN bus signals CAN_L and CAN_H and vice-versa.

Table 2.2 show the various semiconductors which is used in the digital part and the CAN part of the ELMB. The purpose of the table is to give an overview of the components, the technology and the functionality. This is important for the radiation test since CMOS and bipolar technology responds different to various radiation, more about this in chapter 3.

Component no:	Device	Technology	Function
IC26	MIC2754	CMOS	Reset circuit
IC27	SAE81C91	CMOS	CAN controller
IC30,31	HCPL0601	Opto	Opto-coupler
IC32	PCA82C250	Biploar	CAN interface
IC34	ATmega103L	CMOS	Microcontroller
IC35	AT90S2313	CMOS	Microcontroller
IC37	MIC5203	CMOS	Voltage regulator
IC38	MIC5203	CMOS	Voltage regulator
IC49	74HC1G66	CMOS	Bilateral switch
IC40	ADP3607	CMOS	Voltage dobler
D4,5,6,7,8	BAV70W	Bipolar	Diode

Table 2.2: Listing of the semiconductors used in the digital part and the CAN part of the ELMB.

2.2.4 CAN fieldbus

A field bus is a data communication bus that is usually used in a harsh environment, e.g. an environment with a lot of electrical and magnetic noise. According to [28] the Controller Area Network (CAN) bus is one of the recommended buses for use at CERN. The CAN bus is a serial bus developed by Robert Bosch GmbH. It was originally intended as an in-vehicle network as a replacement for single cables. The CAN bus has become quite popular, and is now widely used in industry applications and for machine control.

The bus communication is based on a so-called broadcast communication mechanism. This means that each message transmitted on the network is not sent to a specific node, but as a broadcast massage to all nodes connected to the network. Instead of giving the message a destination address, the message is given an identifier that the various nodes can be programmed to receive. The identifier determines the message contents and its priority. Each node connected to the bus uses the Carrier Sense Multiple Access with Collision Detection (CSMA/CD) method to access the bus. If two nodes tries to access the bus at the same time, an arbitration of the identifier bits are done by the nodes to find out which node that gains access to the bus. The two logic levels that are used during signal transmission are called the dominant level and the rezessive level. The dominant level will overwrite a rezessive level. Figure 2.11 shows two CAN nodes that tries to access the bus at the same time. As seen an arbitration of the identifier is done, the node with dominant level wins access to the bus (node1).

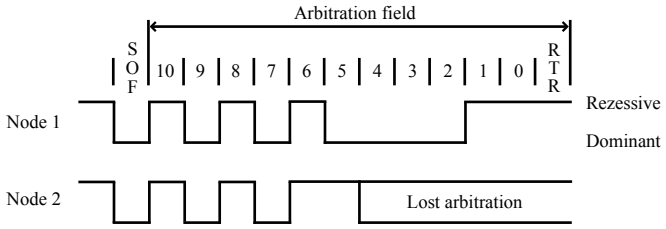

Figure 2.11: *CAN identifier arbitration.*

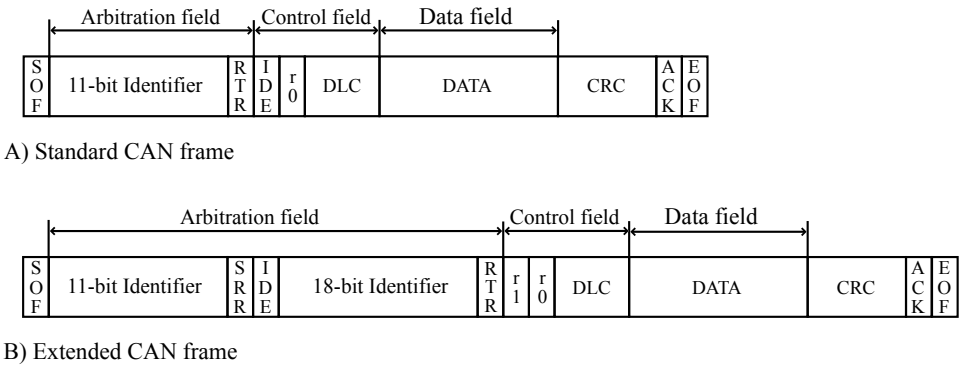

Figure 2.12: *Standard and extended CAN frame.*

To ensure a high transmission reliability several error detection mechanisms has been implemented [25]. When the message is being transmitted, acknowledge is expected from the slave nodes by the transmitter. The receiving nodes should acknowledge the message in the specific "ack" field in the CAN frame, see figure 2.12. If no acknowledge is received, the transmitter assumes that an *acknowledgement error* has occurred and aborts the transmission. A CRC value is added to the CAN frame to ensure (with some probability) that corrupted data is rejected. The CRC is calculated by the transmitter and inserted into the frame. If the receiver does not get the same CRC value after a CRC calculation a *CRC error* has occurred. Also the receivers check the frame-format. A message is expected to have a certain format. If the received message has a different format, a *form error* has been detected. As already mentioned, the transmitter monitors the bus to check whether the bit transmitted has changed or not. If an error is detected it is called a *bit error*. The CAN standard states that no more than five consecutive bits should be sent. If the bit pattern has more than five consecutive bits with the same polarity, a stuffing bit with the opposite polarity is inserted. If a conflict to this rule (six or more consecutive bits with the same polarity) is detected, a *bit stuffing error* has been detected. If any of these errors are detected in a slave node, the slave should signalize it by sending an error frame. An error frame consists of six consecutive dominant bits. The intention of this active error frame is to prevent other nodes from receiving the erroneous frame. Since the active error frame has six consecutive dominant bits, other nodes will respond with their own error frames. When the transmitting node detects the active error frame, a re-transmission of the original frame is done after a short time. Figure 2.12 shows the CAN message frame. Figure A shows the CAN 2.0A frame while B shows the CAN 2.0B frame. The difference is that CAN 2.0A has a 11-bit identifier, while CAN 2.0B has a 29-bit identifier.

2.2.5 CANopen communiction protocol

Ideally it should be possible to connect various CAN nodes from various manufacturers. If this goal should be met, the CAN nodes must "talk" the same language - they must communicate with the same protocol. The CANopen protocol is one such protocol. In addition to this protocol there exist several other protocols, but the CANopen application protocol is selected to be used at CERN. The CANopen protocol is open and a free protocol, which is a big advantage when you want to custom-build a CAN node. Figure 2.13 shows a sketch of the Open Systems Interconnection (OSI) reference model and the layers used in a CANopen compatible network node.

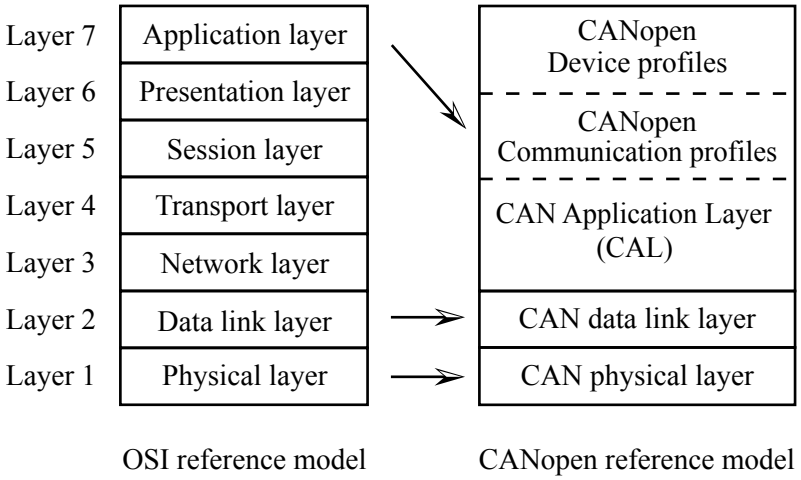

Figure 2.13: *CANopen reference model and OSI reference model.*

The two lowest layers, the physical layer and the data link layer are usually implemented in a CAN interface chip(s), while the application layer is implemented with some sort of intelligent electronics, e.g. a microprocessor. The physical layer is specified in the ISO 11898 standard. This standard specifies the bus bit timing, but not the connectors to be used and the pin connections. Only a recommendation is given. The data link layer handles the CAN frame structure. As mentioned in the previous section, there exists two CAN frame formats, CAN 2.0A and 2.0B. The CAN application layer (CAL) consists of four different parts. Each part is responsible for a specific function. The four functions are:

- **Network Management (NMT)** is used by one node (master node) to operate the network (network management). The master node controls each node and its state. This means that the NMT master can start and stop each node connected to the network.
- **Communication Object Identifier Distributor (DBT)** is used to distribute identifiers to each node. This is done by the DBT master during start of the network. When a node starts, it sends a request for an identifier.
- **Layer Management (LMT)** is used to configure the nodes connected to the network. The LMT master can configure settings like the node name, node ID and baudrate.
- **CAN Based Message Specification (CMS)** specifies a protocol for transmission of data between CAN nodes.

To organize the communication between the user application (application in the master or in the slave node) and the CAL layer, the CANopen provides an interface through a CANopen communication profile and several device profiles. The communication profile consist of a so-called *object dictionary*. The object dictionary is in principle a large registry of all parameters in a CANopen node. All data exchange between two CANopen nodes is done between entries in the object dictionary. The CANopen device profiles define how the various entries in the object dictionary should be used for different kind of nodes. E.g. the data type used for an analog input node is defined in a device profile for an analog input node.

The data exchange between the master node and the slave node usually take place in two ways. Either by use of the *Service Data Objects* (SDO) mechanism or with the *Process Data Objects* (PDO) mechanism. The SDO mechanism is a two-way communication where the master usually sends a message (SDO) to the slave and the slave responds to the message by sending a message (SDO) in return. This kind of communication is not very effective since two messages (full CAN frame, 8 bytes of data) is required. Therefore SDOs are usually only used to transfer configuration data to a node, and to read the node configuration. PDOs usually does the process data exchange between the producer nodes and the rest of the network. The PDO mechanism is based on one-way communication, no confirmation is required. This type of message transmission is based on the fact that the CAN error detection mechanism is very good and reliable. A PDO transmission can be started in several ways. This is defined in the object dictionary for the node. E.g. if a measured value increases above a limit, the measured value should be transmitted or the PDO can be triggered by a sync message (NMT) sent by the master. As mentioned in the previous section, the communication is done one broadcast basis from the nodes. Since the node can transmit different type of messages (e.g. SDO and PDO) each message needs an identifier. Such an identifier is called a Communication Object identifier COB-ID.

When a network node starts (e.g. at power up) the node will do some form of initialization, and then enter a pre-operational state. Figure 2.14 depicts a state diagram for a CANopen node. When the node is in the pre-operational state, it is not supposed to do anything else then listening for NMT messages or SDO messages. In this state it is only possible to communicate with the node by SDOs or by issuing a NMT command. The node can enter the other states by sending the proper NMT command.

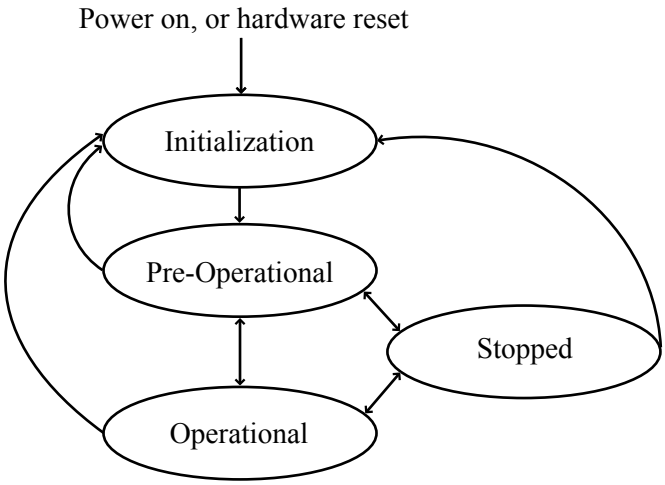

Figure 2.14: *Various states of a CANopen node.*

In addition to the standard data exchange between the nodes other message types has also been defined in the CANopen standard. One such message is the *emergency message*. This type of message is used to report error sates in a slave node. Of course only errors detected by the node can be reported this way.

Chapter 3

Effects in semiconductors due to radiation

This chapter is a theoretical study of some of the effects that can be observed in semiconductors when they are exposed to radiation. Since the ELMB was exposed to γ-rays and a proton beam it is necessary to know about the various effects caused by these two sources. The ELMB has also been tested with neutron irradiation in a reactor, but this is not part of this thesis. However, to give a complete picture of the various effects that might occur in a semiconductor used in physics experiment, a brief description of the effects caused by neutron radiation is mentioned. The γ-rays are used to test the device for the "Total Ionization Dose" (TID) effect. As the name says, this kind of radiation will ionize the material that is exposed to the radiation. In semiconductors it is usually the oxide layer in CMOS transistors that is sensitive to ionization. This kind of radiation will change the electrical parameters to the device under test. The TID test will give an indication of the total integrated dose that the device can withstand without failure. In addition to the ionization of the oxide layer, high-energy particles can cause upsets in memories. This means that a particle that passes through a chip can change the logic-state in a memory cell. High-energy particles can also damage the circuit by destroying the transistors directly or indirectly (current increase can cause the part to fail). This kind of memory upsets and chip failure are called "Single Event Effects" (SEE). To find out if the circuit under test is sensitive to SEE, it should be irradiated with high-energy particles. The ELMB was irradiated with a 60MeV proton-beam. The last test is the "Non Ionization Energy Loss" (NIEL) test. The intention of this test is to find out if the device is sensitive to displacement effects. The NIEL test is done by irradiating the circuit with a radiation beam capable of destroying the silicon lattice. This destruction is referred to as displacement damage. Displacement damage will change the electrical parameters of the circuit. The NIEL test is done by irradiating the circuit with neutrons. The TID, SEE and NIEL test procedures are described in chapter 4.

3.1 Ionizing radiation

Ionizing radiation can cause charge to be accumulated in CMOS transistors. The charge is usually deposited in the silicon dioxide layer between the gate and the silicon bulk in a CMOS transistor [1]. Ionization damage in bipolar transistors are not considered to be a major problem [1]. The charge accumulation effect is usually a slow degrading effect that is dependent of the absorbed dose, the irradiation time, the dose-rate and the process used to fabricate the transistor. The ionization will often change the electrical parameters of a CMOS transistor, and the functionality of the circuit will be altered. The accumulated charge in the oxide layer can cause change in the threshold voltage, which can lead to leakage currents in the circuit. In addition, the channel mobility in the CMOS transistor tends to decrease. This will have impact on the circuit timing parameters. A degradation of the timing parameters might influence the maximum operating frequency of a circuit. Also changes in the V_{IL} and V_{IH} voltages has been observed (change in the circuit noise margin) [2]. The ELMB has a comprehensive analog multiplexer network between the analog input pins and the ADC. It should therefore be mentioned that the R_{ON} resistance in the multiplexers can increase due to the ionization [2]. The accuracy of the ADC can also be degraded [2]. A more detailed description of the degrading effects caused by ionization is given in the following sections.

3.1.1 Gamma-ray interaction with CMOS devices

When γ photons passes through matter they will lose some of or all of its energy. The γ photon loses energy in three possible ways.

- **Photo electric effect**: The photon interacts with a bounded electron. All photon energy is used to disengage an electron and to give it a kinetic energy. This absorption mechanism is the most important absorption process for energies below 100keV [49].
- **Compton scattering**: This effect is evident when a γ photon hits a free or weakly bounded electron. Some of the photon energy is transferred to the electron as kinetic energy, while some of the energy reminds in the photon. The collision between the photon and the electron causes the electron and the photon to diverge in two directions with an angle between the two paths. The Compton scattering is the most important absorption mechanism for interaction between a γ photon and matter when the photon has an energy between 100keV and 10MeV [49].
- **Pair production**: All of the photon energy is used to create an electron and a positron. The energy must be higher than 1.02MeV for a pair production. This absorption mechanism is significant when the incoming photon has an energy over 10MeV [49].

In the following I will study the attenuation of the γ photon through matter. When the photon passes through a material, it loses energy as described. The attenuation of the intensity or the fluence is dependent on the distance the photon travels in a specific material. The intensity of the photon at position x

$$I(x) = I(0)e^{-\mu x} \tag{3.1}$$

where $I(0)$ is the initial photon intensity and μ is the linear attenuation coefficient. This constant is given in unites of cm^{-1}. The linear attenuation coefficient is in some cases renamed to the

mass absorption coefficient $\kappa = \mu/\rho$. This coefficient is given in cm^2 per gram. The intensity equation with the mass attenuation coefficient is given in equation 3.2

$$I(x) = I(0)e^{-\kappa\rho x} \tag{3.2}$$

Both of these equations are based on the fact that all energy from the γ photon is absorbed. As mentioned the photon can lose energy by the Compton scattering effect. When we are dealing with the Compton effect, the photon is not completely absorbed and the photon is still present, but due to the scattering (the photon is not traveling in the direction it used to move) it is considered to be a good approximation [1].

The loss of photon energy is proportional to the average quantity of electrons in the material. The photon stopping power is given as

$$-\frac{dE}{\rho dx} \sim \frac{N_0 Z}{A} \tag{3.3}$$

where N_0 is the Avogadro's number, Z is the atomic number and A is the mass number of the material that the photons are passing or are stopped by. The higher the atomic number (Z), the larger stopping power. Lead has an atomic number of 82 and is often used as a shielding material.

Dosimetry

When a material is exposed to ionizing radiation some energy will be deposited in the material. The amount of energy that is deposited is called the absorbed dose or the integrated dose. The dose is given the letter D. Dose is the term used to define the energy deposited per unit mass. The dose is defined as

$$D = \frac{dE}{dm} \tag{3.4}$$

where dE/dm is the deposited energy per unit mass, and D is the dose. The SI unit for the dose is called *Gray* (Gy). The definition of the Gray is: 1 Gy = 1 Joule/kg. The Gray unit is closely connected to the unit *rad* which is also used for the absorbed dose: 1 Gy = 100 rad. When one of these units are used, the material where the energy was absorbed should always be mentioned e.g. Gy(Si) for the dose absorbed in the silicon or, Gy(SIO_2) for the dose absorbed in the silicon dioxide layer. In the following chapters only the Gray unit will be used for the absorbed dose.

The dose-rate is the rate of change in the absorbed dose. The dose-rate is given as the dose per time unit, e.g. Gy/hour. The relation between the radiation intensity I(x), and the dose rate is

$$\frac{dD}{dt} = I\frac{\mu}{\rho} \tag{3.5}$$

The exposure rate is a measure of the radioactivity per unit time that can be measured at certain location. The exposure rate is larger close to the radioactive source than a few meters away. The exposure rate is given as

$$\text{Exposure rate} = \Gamma\frac{\mathcal{A}}{d^2} \tag{3.6}$$

where Γ is a specific γ-ray constant, $\mathcal{A}$ is the source activity and d is the distance from the source. The exposure rate is measured in Roentgen/hour (R/h). The source activity is given in Becquerel (Bq) or Curie (Ci) depending of the Γ constant. Becquerel is the number of disintegrations per second in the radionuclide. The relation between Curie and Becquerel is: 1 Ci = 3.7×10^{10} Bq. The Γ constant describes the γ-ray emission for each radionuclide, and is often given in $(R/h)/(Ci/cm^2)$ [16].

The radiation safety aspect should also be mentioned. When we are talking about safety issues and deposition of energy in the human body we use the unit *equivalent dose*. The equivalent dose is measured in *Sivert* (Sv) and is a weighted number. The relation between the *absorbed dose* in Gy and the equivalent dose in Sv is: Sv = Gy$\times w_R$ (J/kg). The factor w_R is a weighting factor. This factor is dependent on the type of radiation and the energy [16].

During the radiation tests (γ-ray test) of the ELMBs, the absorbed dose was measured with L-alanine dosimeters.

3.1.2 Proton particle interaction with CMOS devices

Protons are used to test if a circuit is sensitive to *upsets*. An upset is a term used to describe a situation where the circuit under test enters a condition where the circuit, or a part of the circuit does not function as intended [1]. Section 3.2 gives a description of the various errors that might occur in a device which is exposed to high energy protons. In the following, I will give a short description of the effects that is expected in a circuit, and must be considered when a circuit or an electronic system is designed, e.g. like current limitation.

One important upset is the *Latch-up*. A latch-up occurs when a device enters an incorrect state where the device no longer responds to input signals. An example of such upset is the triggering of a silicon-controlled rectifier (SCR) in a CMOS inverter. The SCR consist of two parasitic bipolar transistors. Figure 3.1 A depict a CMOS inverter where such SCR can be triggered, and 3.1 B shows the SCR.

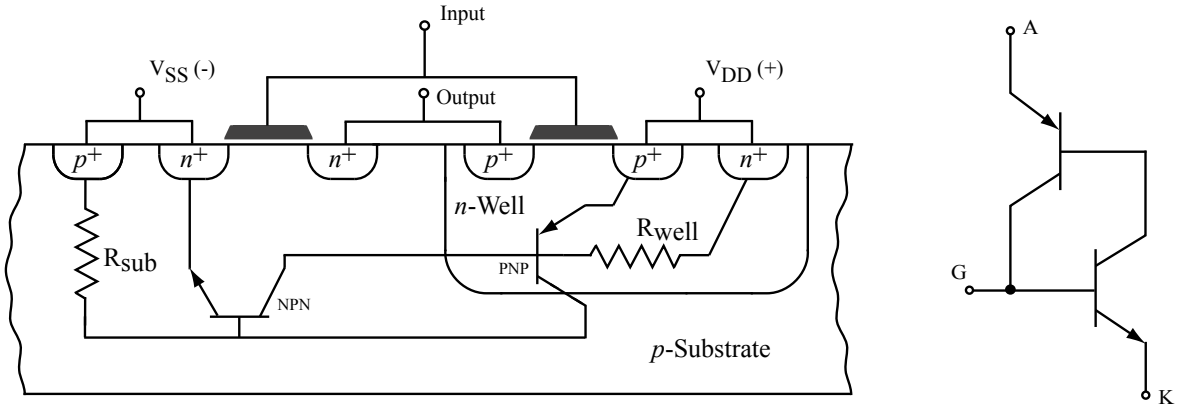

A) CMOS inverter in latch-up state B) Parasitic SCR

Figure 3.1: *CMOS inverted in latch-up state (SEL).*

If an incident proton creates a large enough positive charge in the p-substrate region, a small current will flow in the pn junction between the p-substrate and the n^+ NMOS source terminal.

The small current (base-emitter) triggers a current flow from the positive voltage supply (V_{DD}) through the n-well resistance and the NPN transistor to the negative source terminal (V_{SS}) (NMOS). The collector current (NPN) will create a voltage drop over the R_{well} resistor. If this voltage drop is large enough, a second parasitic transistor (PNP) pn-junction will conduct (base-emitter). This will again lead to a current flow from the positive voltage supply (V_{DD}), to (V_{SS}) through the PNP transistor, and the substrate resistance, R_{sub}. A current drop over the substrate resistance will make sure that the NPN transistor is turned "on". The SCR are now turned on. When a latch-up of this type is created it is only possible to turn the SCR "off" by removing the voltage across the SCR. It should also be mentioned that if the current is not limited in this circuit, it will eventually be burnt [1].

The upset can be created by an energetic ion traversing the silicon lattice. One such incident is referred to as funneling. When a high-energy ion traverses the silicon lattice, the ion leaves behind a wake of electrons and ions. Figure 3.2 shows the wake created by the ion. The incident ion will destroy the depletion layer and create a large electric field between the surface and the bottom of the wake. The electric field will propel the electrons back up the funnel to the depletion layer and the holes down into the silicon. This results in a large increase in negative charge over the funnel. If this charge is large enough, an upset can be triggered (the base-emitter pn-junction of a NPN transistor conducts when the emitter is negative compared to the base ($\sim$0.6 V)).

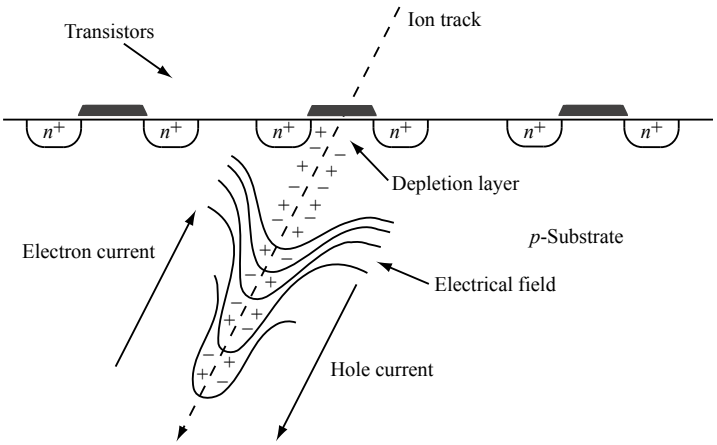

Figure 3.2: *Funneling in a NMOS semiconductor created by a traversing ion.*

3.1.3 Charge generation and recombination

When a high energetic hadron or photon traverses through the silicon chip some of the energy is deposited in the silicon along the path. A γ photon loses energy as already described, and a high energy hadron or a proton as will be used during the ELMB testing, loses energy by creating electron-hole pairs along the particle track. The oxide-insulating layer in a CMOS transistor is usually most sensitive to ionizing radiation. The energy deposited in the oxide layer creates free electrons and holes along the path. During the first few pico-seconds after the electrons and holes was created some of them will recombine close to where they was created. The remaining free electrons will (since they are very mobile - compared to the holes) be attracted by the positive voltage on the gate (n-type transistor) and sweped out of the oxide layer. The remaining holes are still in the oxide layer (they do not move as fast as the electrons). After some time, and a

rather complex stochastic process they will move (electric field between the gate and the silicon) from their location and towards the negative charged silicon (bulk). The holes will be trapped at the Si/SiO_2 interface. The positive charge will attract electrons in the silicon and cause a current leakage. Trapped positive charge in the oxide will cause an electrical field in the same way as when a voltage is supplied to the gate electrode. This creates a negative threshold voltage shift. A negative voltage shift means that the transistor is already conducting. Other effects caused by the trapped positive charge and the interface traps is reduced operating frequency (the circuit is slower than an unirradiated circuit) and reduced noise margins [2]. Figure 3.3 show a drawing of the gate, the oxide layer and the silicon interface with the trapped charge.

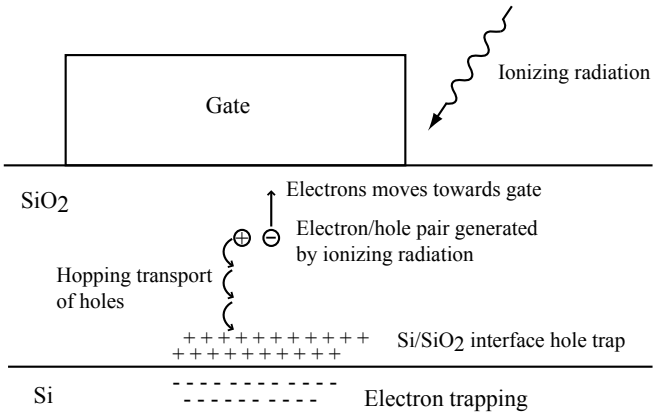

Figure 3.3: *Charge trapping in the Si/SiO_2 interface layer in a NMOS transistor.*

Most of the chip area is covered with an oxide layer. This means that there is potentially a large area for positive charge trapping. Charge trapping at various locations in the chip can cause leakage currents. The positive charged hole that is trapped in the oxide layer is not stable. Some of or all of the trapped charges can be removed. This process is called annealing and is described in the following section.

3.1.4 Annealing effects

Annealing effects are changes that are observed in the MOS device after the irradiation has been stopped. The trapped positive holes in the silicon dioxide layer are in reality not trapped there forever. The holes might disappear over time. This process is called annealing. In principle there are two different annealing processes [2]. The first take place when the device is biased and operated under normal operating temperatures. This annealing is described as the tunnel annealing. The tunnel annealing can be caused by two effects, the first effect happens in the electron tunnel close to the Si/SiO_2 interface. Some of the electrons in this tunnel will recombine with some of holes in the SiO_2. The probability for a recombination is exponentially decreasing with the distance from the Si/SiO_2 interface into the dioxide. This means that charge trapped further inside the oxide layer does not anneal right away. The holes must first move closer to the Si/SiO_2 interface. In addition to this Si/SiO_2 interface annealing, there is also a similar tunneling effect at the gate-oxide interface. This last effect becomes significant when the gate oxide is thin [2].

Trapped holes in the oxide layer can also be removed by thermal annealing. Thermal annealing is

done by increasing the temperature of the circuit under test. Most of the recovery of the circuit is achieved when the temperature is between 150 °C and 300 °C [2].

3.1.5 Dose-rate effects

The functionality of the circuit which has been irradiated is not just dependent on the total dose absorbed, but also of the rate at which the dose was absorbed, the dose-rate. According to [2] dose-rate experiments has been performed on circuits by changing the dose-rate and by comparing speed changes of circuits irradiated with both high and low dose-rate. The results showed that circuits irradiated with the lowest dose-rate did show a large change (degrading). Another test confirmed this. The circuits that were exposed for a low dose-rate irradiation showed an increase in the number of interface traps compared to circuits irradiated with a higher dose-rate. Experiments has shown that the total number of interface traps for a device irradiated with a high dose-rate and annealed for a time equivalent to the irradiation time for the circuit irradiated at a low dose-rate is the same [2]. This is the dose-rate effect. This means that the circuit can get worse after the irradiation has been stopped [2].

3.2 Single event errors

In addition to the charge cumulative degrading TID effect, circuits can also be susceptive to random single incidents. These incidents are referred to as Single Event Effects (SEE). In many cases it is just referred to as an upset or a single event upset. A SEE can be caused directly by a heavy ion or indirectly by a hadron which creates a nuclear reaction, which in turn is responsible for the SEE [51]. Since protons are used in the ELMB test, only protons are discussed in the following. A proton must have sufficient stopping power to deposit energy equal or larger than the critical charge required for a SEE upset. The stopping power is defined as the energy deposited per unit track length, dE/dx, also referred to as the Linear Energy Transfer (LET). The critical charge is the amount of charge that is required to change the state of a circuit.

The SEE is not measured like the TID as the total absorbed dose or as the dose per time. The device is characterized by its cross-section

$$\sigma = \frac{N}{\Psi_p} \tag{3.7}$$

where σ is the cross-section, N is the number of errors that are observed during the test, and Ψ_p is the proton fluence, protons/cm^2. If the number of bit-flips is counted during a SEE test, the cross-section can be given as cm^2/bit.

SEE errors are normally observed as a bit-flip in a memory cell, in a flip-flop, in an I/O port or as a change in some logic function. SEE errors can also affect analog circuits by creating transients in the circuit. The error is categorized by its effect in the device.

- **Single Event Upset (SEU)** is a general description of an incident in a circuit. The change can be in an analog circuit, digital circuit or in an optical component. In addition, changes in the surrounding circuitry are also referred to as a SEU.

- **Single Event Functional Interrupt (SEFI)** is an error that impacts the functionality of the device under test. This is a non-destructive soft error. The functionality is recovered by resetting the circuit or by doing a power off-on cycle.
- **Single Event Latch-up (SEL)** triggers a parasitic component in the circuit. This can lead to a rapid current increase, which can cause a malfunction of the device if the current is not limited. This error can be a destructive error if the current is not limited. If the current increase does not damage the circuit, the SEL error can be removed by doing a power off-on cycle.
- **Single Hard Error (SHE)** is an error that causes a permanent damage to the circuit. Like a stuck bit in a memory cell. This is indeed a destructive error and the circuit is damaged.
- **Single Event Burnout (SEB)** is an incident where the drain-source channel suffers from a burnout. This is also a destructive error.
- **Single Event Gate Rapture (SEGR)** is an error where the gate insulator suffers a burnout. This is also a destructive error.

3.3 Displacement effects

Displacement damage in a semiconductor is usually caused by neutron radiation. This is because the neutron is quite heavy - 1840 times heavier than an electron. When a high-energy neutron collide with a semiconductor, the neutron will dislodge and displace atoms in the semiconductor lattice, creating a "hole" in the semiconductor lattice. This is called a *vacancy*. This causes disruption and disorientation in the lattice structure. If the incident neutron has high enough energy, it can transfer some of its energy to an atom, which in turn can displace other atoms in the lattice. Since neutrons are electrically neutral, they can not ionize atoms directly. However, neutrons can ionize atoms indirectly. A neutron can produce recoil atoms or ions, which can cause ionization. If the neutron excites an atom, the atom can de-excite by emitting a γ-ray, which in turn can ionize the semiconductor. The third possibility is that the neutron is completely absorbed by the targeted atom. This can cause formation of a new atom in the silicon lattice. In this process an α-particle or a proton is usually created, which in turn can ionize the semiconductor [1]. It should be mentioned that the semiconductor, which is exposed to neutron radiation, would be radioactive even after the irradiation, and a de-activation time is needed.

In addition to the ionization created by the secondary neutron effects, the electrical properties of the semiconductors are degraded. These effects are caused by creation of new atoms. This can cause increased resistivity in the material and minority carrier lifetime reduction [1]. Neutron induced displacement degradation are most evident in bipolar semiconductors. Some of the vacancies created by the incident neutron will anneal after a short period of time. This is a so-called unstable displacement effect. In addition to the unstable effect, there are also some stable defects in the lattice. These can lead to a degradation of the semiconductor and its electrical properties.

Chapter 4

Radiation test procedures

This chapter gives a description of the rules that should be used when COTS semiconductors are tested for radiation tolerance.

The chapter does also give a detailed description of the test procedures, the test locations and the test setup equipment including the software that was used in the various tests.

4.1 ATLAS radiation policy

To ensure a safe operation of the ATLAS detector and to preserve the safety of the personnel working at the detector, specific rules has been prepared. The "ATLAS Policy on Radiation Tolerant Electronics" [14] has been formed to give the ATLAS sub-system groups specific rules concerning testing and qualifying of radiation tolerant electronics. The electronic components are divided into two different types, Application Specific Integrated Circuits (ASIC) and Commercial Of The Shelf (COTS). In the following I will only talk about COTS since the ELMB only consists of COTS components.

To qualify an electronic component there are several steps one should follow. The first step in the process is to do a pre-selection test of the components. This test is done to investigate and see if the components can be used in a radiation environment. The second step is to do a qualification of the selected components. This thesis is based on the pre-selection test. The qualification tests has not jet been done.

First of all one must determine the radiation level where the part will be located. The radiation levels for various parts of the detector are listed in [14], these are the simulated radiation levels. The table lists three different radiation levels for each location. The first is a simulated radiation level (SRL) for the Total Ionizing Dose (TID), the next is the level for the Non-Ionizing Energy Loss (NIEL) and the last is levels for the Single Event Effects (SEE). This means that three different tests must be done on each component to qualify it. In addition to the simulated radiation levels one must also add a safety factor (SF) to get the total radiation level that the component must be qualified for. The calculation of this level is referred to as the "Radiation Tolerance Criteria" (RTC). The RTC for the TID and the NIEL are calculated like this

$$\mathrm{RTC_{TID}} = \mathrm{SRL_{TID}} \times \mathrm{SF_{sim}} \times \mathrm{SF_{ldr}} \times \mathrm{SF_{lot}}\ [\mathrm{Gy}] \tag{4.1}$$

$$\mathrm{RTC_{NIEL}} = \mathrm{SRL_{NIEL}} \times \mathrm{SF_{sim}} \times \mathrm{SF_{ldr}} \times \mathrm{SF_{lot}}\ [\mathrm{neutron/cm^2}] \tag{4.2}$$

where $\mathrm{SF_{sim}}$ is the safety factor for the simulation, $\mathrm{SF_{ldr}}$ is the safety factor for the low dose-rate effects and $\mathrm{SF_{lot}}$ is a safety factor for variation from component to component inside a lot and from lot to lot.

The RTC for the SEE is not calculated like the two previous RTCs, but the SEE RTC is defined by each system in the detector. This is dependent of how many SEE errors you can allow in your system. To determine if a component will satisfy your requirement the SEE is divided into three different types of SEE. The first is the so-called soft SEE, also known as soft SEU (single event upset). If you have a "not permanent" bit-flip that corrupts your data in a register or memory cell, but can be restored they are called soft SEU. If the bit-flip is permanent (not possible to change the bit by writing to the register/memory cell or resetting the system) you have a hard SEE, also known as hard SEU. The last possibility is a SEE that is destructive. This means that there is a permanent short circuit in the component. The Soft SEU rate is given as

$$\text{Soft SEU}_\mathrm{f} = \left(\frac{\text{Soft SEU}_\mathrm{m}}{\mathrm{ARL}}\right)\left(\frac{\mathrm{SRL_{SEE}}}{10^8}\right)\mathrm{SF_{sim}} \tag{4.3}$$

where Soft $\mathrm{SEU_f}$ is the estimated rate of soft SEU, Soft $\mathrm{SEU_m}$ is the total number of soft SEU measured during the SEE test, ARL is the applied radiation level (the particle fluence used during the test, hadrons/$\mathrm{cm^2}$), $\mathrm{SRL_{SEE}}$ is the simulated radiation level (hadrons/$\mathrm{cm^2}$) and $\mathrm{SF_{sim}}$ is the safety factor for simulation uncertainty. The number 10^8 is a estimate of beam time in seconds during ten years of operation. Calculation of the hard and the destructive SEU is done the same way as for the soft SEU. To be able to qualify the component for the specific location in ATLAS all of these three equations must be satisfied:

$$\text{Soft SEE}_\mathrm{f} < \mathrm{RTC_{SEE,soft}} \tag{4.4}$$

$$\text{Hard SEE}_\mathrm{f} < \mathrm{RTC_{SEE,hard}} \tag{4.5}$$

$$\text{Destructive SEE}_\mathrm{f} < \mathrm{RTC_{SEE,destructive}} \tag{4.6}$$

The safety factors can in some cases be significant and you might end up with a RTC that is not possible to achieve. In some cases the safety factors can be reduced.

For instance if an accelerated aging test is done after the TID test, and the component is still working properly, the $\mathrm{SF_{ldr}}$ safety factor can be reduced to 1. If it is possible to obtain a homogeneous batch of devices, the $\mathrm{SF_{lot}}$ safety factor can also be reduced to 1.

4.1.1 Total Ionizing Dose test method

To qualify the electronic device for the TID, the component must be exposed to γ or x-ray radiation. The device should be exposed until the total integrated dose in the device equals the RTC calculated for the component. Reference [14] gives a detailed description of how this should be done.

The radiation test can be performed in two possible ways, the simplified version or the extended version. The simplified version gives a safety factor, SF_{ldr}, of 5 and the extended version gives a safety factor of 1. The only difference between the two methods is accelerated aging testing after the irradiation. Here is a short description on how the TID qualification is done. This is not a complete list, a complete step by step list can be found in [14]. The list summarizes the important topics for the TID test.

- During the test 11 (10 + 1 ref.) devices should be used if each device is from the same lot (homogeneous lot). If not, 22 (20 + 2 ref.) devices should be used instead.
- All important parameters should be measured at room temperature before the irradiation is started.
- In total 10 or 20 devices (depending of homogeneous lot or not) should be irradiated under room temperature while they are powered. The remaining device(s) should be kept as a reference device.
- After irradiation the devices should be annealed in room temperature while the devices are powered.
- Accelerated aging test should be done if the extended procedure is chosen.
- If any of the devices fails the lot should be rejected.

4.1.2 Non-Ionizing Energy Loss test method

Non-Ionizing Energy Loss (NIEL) testing of devices is done with neutrons with an energy of 1 MeV. The neutron radiation can create displacement damage in the semiconductor. As mentioned in chapter 3, CMOS devices is normally not affected by displacement damage. Therefore, CMOS devices do not need to undergo the NIEL test. The following list is a summary of the rules describes for NIEL testing in [14].

- As with the TID test, 11 or 22 devices depending of homogenous batch or not should be chosen for the test.
- Electrical parameters should be measured in room temperature before the irradiation.
- 10 or 20 of the devices should be irradiated up to the required RTC_{NIEL} and one/two devices should be kept as a reference device.
- The devices should be irradiated to the required RTC_{NIEL} in one go, or in smaller steps.
- Measurement of the devices can be done on line or after the irradiation. If one of the devices is outside its specification the batch is rejected.

4.1.3 Single Event Effect test method

The Single Event Effect (SEE) test can be done with either proton or neutron radiation of the device under test. To be able to create a SEE in the device it is important that the energy of the particle is large enough. Protons with energy around 60MeV can create soft SEE, but the

energy is too small to create hard and destructive SEE [14]. The normal procedure is to use a proton source with energy between 60MeV and 200MeV. This will only create soft SEE. If there is necessary to test the device for hard or destructive SEE, the protons must have energy larger than 500MeV. The following list shows the main topics from the original description [14] describing the SEE test procedure.

- The SEE test requires 4 devices to be tested.
- All important parameters should be measured before the irradiation is started.
- The irradiation of the devices should be done with a constant proton flux until the total fluence is large enough to create enough SEE for accurate statistics.
- On line measurements and recording of data should be done one the devices during irradiation.

4.1.4 Radiation requirements for the ELMB

The ELMB is intended to be used in the ATLAS underground cavern. As a starting point for the radiation testing, the location of the muon MDT detectors has been chosen. According to the simulated radiation levels presented in [14], the end-cap 1 area has the highest radiation levels and is selected as the worst location for the ELMB. During 10 years of operation the muon MDT end-cap 1 will receive these radiation levels (SRL):

- TID : 6.38 Gy
- NIEL: 2.94×10^{11} neutrons/cm^2, energy = 1 MeV
- SEE : 4.83×10^{10} hadrons/cm^{2}10y, energy $>$ 20 MeV

When the simulated radiation levels is known, it is possible to determine the RTC required for the qualification for the ELMB in the muon MDT end-cap 1 area. In the following, two different values for the RTC are calculated. The first is a "worst-case" calculation. The RTC for the TID and the NIEL has been calculated with the absolute "worst-case" safety factors as shown in table 4.1. The second calculation is done with the safety factors shown in table 4.2. These factors apply when an extended test method with accelerated aging test is performed, and homogeneous component batches are used.

Test	**SRL$_{sim}$**	**SRL$_{ldr}$**	**SRL$_{lot}$**
TID	$\times$ 3.5	$\times$ 5.0	$\times$ 4.0
NIEL	$\times$ 5.0	$\times$ 1.0	$\times$ 4.0

Table 4.1: Worst case safety factors in the muon MDT end-cap 1 area.

Worst-case RTC:

- RTC$_{TID}$ = 450 Gy
- RTC$_{NIEL}$ = 6×10^{12} neutrons/cm^2

Test	**SRL$_{sim}$**	**SRL$_{ldr}$**	**SRL$_{lot}$**
TID	$\times$ 3.5	$\times$ 1.0	$\times$ 1.0
NIEL	$\times$ 5.0	$\times$ 1.0	$\times$ 1.0

Table 4.2: These safety factors can be used when the extended qualification test is performed, and homogeneous component batches are used in the ELMB.

Best-case RTC:

- $RTC_{TID} = 22$ Gy
- $RTC_{NIEL} = 1.5 \times 10^{12}$ neutrons/cm^2

To be able to say anything about the SRL_{SEE} for the ELMB it is necessary to know the system where the ELMB is intended to be used, and the maximum allowed number of errors must be known.

The ELMB is intended to be used in the ATLAS-DCS system and the system will consist of about 3000 ELMBs. These are distributed in many CAN networks, or branches. One such branch will include 64 ELMBs at most. Table 4.3 gives a list of the SEU requirements in the ATLAS-DCS system. The error acceptance is highly dependent on the system and type of error. As seen in the table, there are a higher acceptance for the number of errors, which does not need an external intervention, than for errors that requires an external intervention, like a reset, or a power off/on cycle.

SEU category/Symptoms	**Recovery**	**Maximum allowed error rate**
Soft SEU/Data read-out erros	Automatic	1 every 10 minutes per CAN branch
Soft SEU/CAN node hang	CANopen reset	1 every 24 hours per CAN node
Soft SEU/CAN branch hang	Power cycling	1 every 24 hours per CAN branch
Hard SEU/Permanent error	Replace ELMB	1 every 2 month per 3000 ELMB
Destructive SEU/Damage	Power limitation	Not allowed

Table 4.3: Listing of the maximum SEU requirements in the ATLAS-DCS system.

- **Soft SEU/Data read-out errors:** Errors in this category is handled by the ELMB software. This error could be a bit-flip in some part of the ELMB which influences the data value read. During the next read cycle the error is removed. E.g. if there is an error in the ADC, a calibration of the ADC could solve the problem.
- **Soft SEU/CAN node hang:** Errors in this category can not be detected by the node itself, and an external node reset is required. The reset should be a software reset, e.g. by sending a CANopen command "reset node" or a "reset communication" command.
- **Soft SEU/CAN branch hang:** This kind of error influences all network nodes connected to one CAN branch. The erroneous node blocks the bus that makes it impossible for other nodes to gain access to the bus. The error can be removed by doing a power off/on cycle.
- **Hard SEU/Permanent error:** A permanent error is where the ELMB hardware is damaged. This could be a stuck bit, which influences the operation of the affected ELMB.

Table 4.4 shows the maximum allowed error rate for one ELMB in the ATLAS-DCS system with a beam time of 10^8 seconds. This is the expected beam time during ten years of operation of the detector.

SEU category/Symptoms	**Requirements per ELMB**
Soft SEU/Data read-out erros	2604
Soft SEU/CAN node hang	1157
Soft SEU/CAN branch hang	18
Hard SEU/Permanent error	0.006

Table 4.4: The SEU requirements for various types of SEU in the ATLAS-DCS system. This is the number of error for one ELMB during 10^8 seconds of beam time.

The simulated hadron fluence in the muon MDT end-cap 1 area given in [14], must be multiplied with two safety factors to get the RTC_{SEE}. Table 4.5 shows the safety factors used for both pre-selection and qualification of components. In the following chapter, the pre-selection fluence is used in the calculations.

Selection	$\mathbf{SF_{sim}}$	$\mathbf{SF_{lot}}$	**Fluence**, Ψ_h
Pre-selection	$\times$ 5	$\times$ 2	4.83×11^{11} hadrons/cm^2
Qualification	$\times$ 5	$\times$ 1	2.42×11^{11} hadrons/cm^2

Table 4.5: Safety factors used for pre-selection and qualification of components in the SEE test. The rightmost column shows the resulting fluence.

4.2 Total Ionization Dose test

The TID test performed on the ELMB is not done according to the method described in section 4.1.1. The reason for this was that this test was not meant to be any pre-selection test, or in any way a qualification of the ELMB, but a simple test of the ELMB. The test would also give us experience with the radiation test routines, and we would get an indication of the radiation tolerance of the ELMB. It should also be mentioned that the ELMB has been tested as a complete working system and not in separate components. The reason for this kind of test is to gain experience with the complete system while under irradiation and to reduce the amount of work required when testing individual components.

In total three different TID tests with γ-ray radiation has been performed. The first test was done at the PAGURE radiation facility at CIS bio international[1]. Section 4.2.1 gives a detailed description of the PAGURE facility. In this test two ELMBs were irradiated. The first ELMB known as ELMB1, and the motherboard was from the first prototype production of five ELMBs. Due to this it had many PCB wiring errors. Some of the wiring modifications were needed to be made by hand on the PCB. One of the errors was missing power lines. This was modified by connecting the analog and the digital power lines together at the input of the regulators (analog and digital supply through the same cable). A second error was missing wiring of the reference voltage into the 100-pin connector and down to the motherboard. There were no wires

[1]CIS bio international has several irradaition facilities where it is possible to test various electronics. CIS bio international is located outside Paris, France [48].

on the PCB motherboard for the reference voltage. Therefore the analog supply voltage was used instead, this was available on the board. It should be pointed out that the analog supply voltage is +5V and not +2.5V as the reference voltage, this is visible on the measurement of the ADC in chapter 5. The third difference between ELMB1 and ELMB2 was the opto-couplers between the CAN part and the digital part. These opto-couplers was exchanged with a new type of magnetic coupler from Analog devices [38]. The magnetic coupler (ADuM1100) had significant lower power consumption than the opto-coupler. This is the reason why we wanted to test the component (if this could be used, the power consumtion of the ELMB would be reduced further). The ELMB2 is from the first pre-series production of ELMBs and motherboards. It was made twenty pieces of both the motherboard and the ELMB in this production. The ELMB2 had correct wiring of the power distribution on the PCB, and the reference voltage was available on the motherboard. It should also be mentioned that the reference voltage was distributed on the motherboard via four operational amplifiers. One amplifier for each sixteen channels. This was done to reduce the load on the reference circuit. The ELMBs were placed at a distance of 114cm from the source inside the PAGURE radiation facility. At this distance the dose rate was measured to be 77 Gy(Si)/h ±6%. First the ELMB1 was tested, when this ceased to work properly, it was exchanged with the ELMB2.

As described in chapter 3 the γ-ray radiation will ionize the Si/SiO_2 and contribute to a charge buildup in the Si/SiO_2 interface. The charge buildup can cause current leakage. Due to this it is important to measure the currents during operation. In the PAGURE test the CAN current and the sum of the analog and the digital currents was measured. In addition, the analog input channels were measured. This was done to see if the radiation caused any change in the analog multiplexer circuits, or in the ADC itself. These measurements were achieved with an online measurement system. The setup, and the online measurement system is further described in section 4.2.3 and section 4.2.5.

Due to the high dose rate offered by the PAGURE facility, and the rapid current increase in the ELMBs during the first test, it was decided to do a second test with lower dose-rate. According to a test done by Temic [29], the dose-rate could have significant effect on the current leakage. Figure 4.1 shows the results from a test done by Temic. It is clearly shown that the dose-rate has a significant effect on the current increase. This is oposite to the observations mentioned in section 3.1.5.

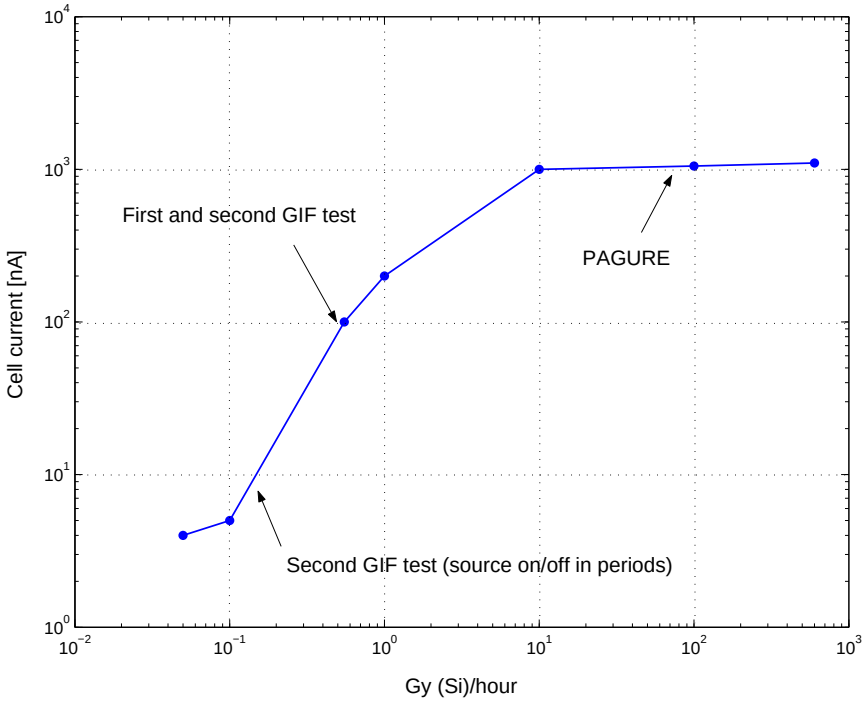

Figure 4.1: *Plot of the leakage current in a memory cell versus the dose rate. The figure is plotted with data from a test done by Temic [29].*

The second TID test was done at the Gamma Irradiation Facility (GIF) [21] at CERN. At this facility it was possible to do a test with dose-rates at least 160 times lower than the PAGURE dose-rate. The dose-rate was chosen to be 0.5Gy(Si)/h. This was the highest dose-rate available in the GIF (the dose-rate could have been selected lower, but due to time limitations the highest dose-rate was chosen). After the irradiation the dose-rate was measured to be 0.48 Gy(Si)/h ±15%. A detailed description of this facility is given in section 4.2.2. The ELMB used in this test was given the label ELMB3. This ELMB and the motherboard were from the same series production as the ELMB2.

In addition to the parameters measured in the PAGURE test we also wanted to measure the analog and the digital currents separately. A description of the setup and the monitoring software used in this test is given in section 4.2.3 and 4.2.5.

As mentioned earlier in this chapter, an accelerated aging test can eliminate the low dose-rate safety factor, SF_{ldr}. Based on the fact that the ELMB was a bit sensitive to the γ-ray irradiation it was decided that we needed to do an accelerated aging test to possibly rule out the mentioned safety factor. In addition to this, it would also be interesting to test the reliability of the ELMB. The accelerated aging test was done with two ELMBs, one that had undergone a period with radiation, and one unirradiated. The unirradiated ELMB was labeled ELMB4. The accelerated aging test is further described in section 4.2.6.

During the two first TID tests the programming function of the two microcontrollers was lost. This could be a problem if you needed to upgrade the ELMB software during the lifetime of the ATLAS detector. It was therefore of great interest to find out at which total integrated dose the programming function ceased to work. To find out this, it was necessary to do a third TID test. This test was also done at the GIF, but the ELMB and the motherboard that was used was a

bit different from the previous tests. The ELMB and the motherboard are from the first series production of the 300 pieces of the ELMB. This ELMB, which is referred to as ELMB5 was a 3.3V version, while the preceding four has all been 5V versions. These changes only involve the digital part of the ELMB. The components have been changed to 3.3V compliant components.

Since the purpose of this test was to find the total integrated dose where the programming function of the microcontrollers was lost it was important to measure the currents to see if there was any correlation with the increased current and the loss of the programming function. The measurement setup used in this test is described in section 4.2.3. Another important matter in this test is the dose-rate, and the on/off time of the radioactive source. The dose-rate in this test was set to 0.45Gy(Si)/h (theoretical), but the source was not on all around the clock. The source was switched on and off in periods during the test. The purpose was to investigate and see if there could be observed any annealing effect during the "off" period. The test was performed by switching the source on in the morning, and leave it on for about ten hours. When the source was switched off, a test of the programming function was done. The programming functions were tested by uploading a different software version to the master controller, and then check the software version with the CAN analyzer. If the programming function was found to be working, the master controller was reprogrammed with the original software and left to anneal for about fourteen hours. Since the ELMB was located inside the radiation zone, it was not practical to remove it each time the programming function should be checked. Therefore, the programming of the master controller was done via the CAN bus through the slave controller.

The following is tested in the TID tests:

- The three ELMB supply currents is measured online.
- The analog input channels is read-out during irradiation.
- The digital I/O line check program checks the I/O lines during irradiation.
- The programming function of the microcontrollers is checked.
- The three regulated supply voltages (regulator output) is measured before and after the test.

4.2.1 Cobalt-60 source

Figure 4.2 shows a picture from the PAGURE radiation facility [48]. The facility is quite big, it consists of a room that is 5×5×5m, and it is surrounded by thick concrete. The source is located in a shielded room under the floor. The radiation is stared by elevating the source with the use of the control panel shown in picture B.

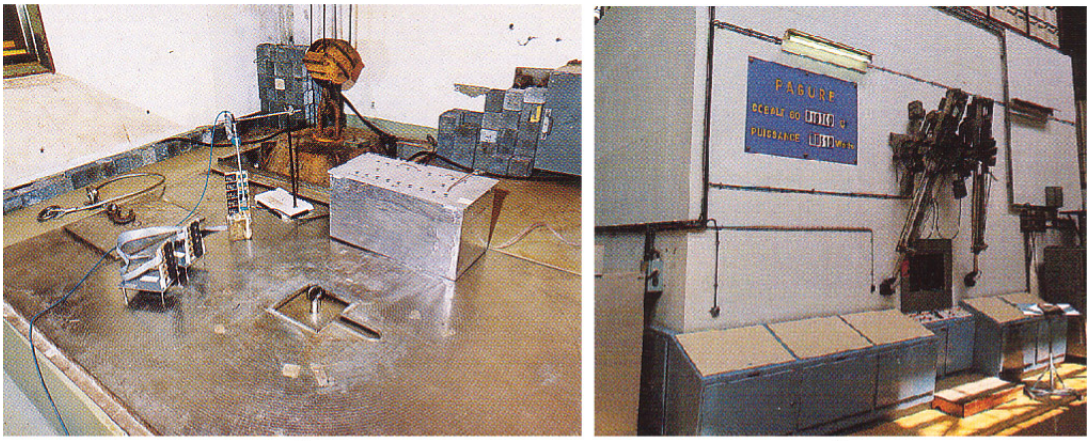

Figure 4.2: *A) shows a picture from the inside of the PAGURE facility. B) shows a picture of the outside of the PAGURE facility. Both pictures are taken from [48].*

The radioactive source used at the PAGURE facility consists of 10 rods of the ^{60}Co isotope. The ^{60}Co source decays in three steps down to a stable ^{60}Ni isotope. Figure 4.3 shows how the ^{60}Co isotope decays. Each atom disintegrates to Nickel and emits one β particle with an energy of 0.31MeV and two γ photons with an energy of 1.17MeV and 1.33MeV. In our calculations only the γ photon is of interest. The mean energy of the γ photon is 1.25MeV, this energy is used in our calculations. The 10 ^{60}Co rods had an activity of 4.4×10^{14} Bq. The half-life for this source is 5.271 years.

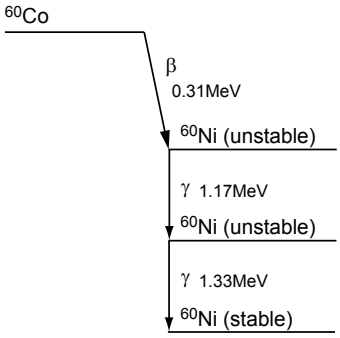

Figure 4.3: *Cobalt-60 decay.*

4.2.2 Cesium-137 source

The Gamma Irradiation Facility (GIF) is a local test facility at CERN. This is the "end-station" of the X5 beam, which is a muon beam. This beam is used for prototype testing of parts to the detectors that is under construction for the new LHC accelerator [21]. In addition to the X5 beam there is also a ^{137}Cs radioactive source in the GIF. The purpose of this source is to give a radiation level similar to the background radiation in the LHC accelerator. Figure 4.4 shows a drawing of the GIF. A concrete wall surrounds the source, which are 8m high and 80cm thick. The source is located inside a lead container 5m from the wall facing the X5 beam. As seen on the picture, the source has two different radiation beams. The large beam, called the main beam

has an opening angle of 74 degrees, while the second beam, called the side beam, has an opening angle of 22 degrees. In addition, the side beam has a shutter function that can be used to stop the radiation in the side beam, while the radiation is still on in the main beam [21]. The source is activated by elevating the source from the lead container and opening the shutter (if the side beam is used). All this is done from a control room where you have access to radiation monitors, and a monitor that shows the inside of the radiation zone.

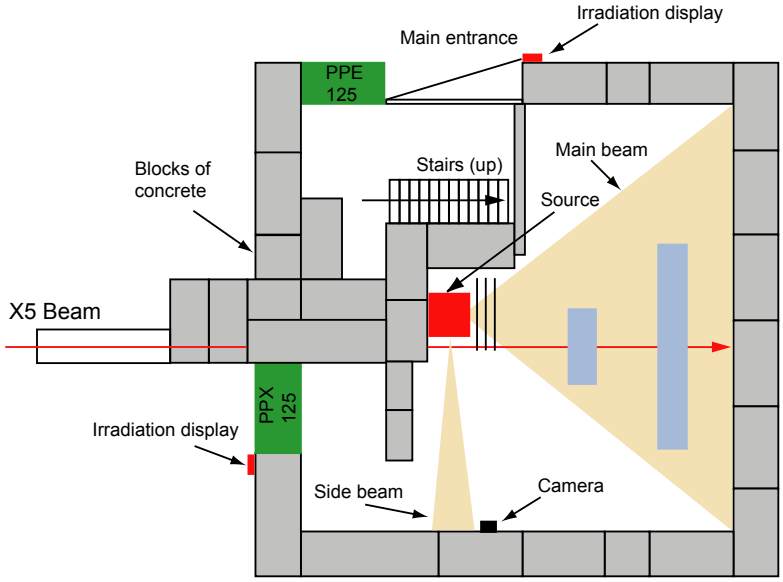

Figure 4.4: *The Gamma Irradiation Facility at CERN.*

The radioactive isotope ^{137}Cs used at the GIF can decay down-to the stable isotope ^{137}Ba in two different ways. Figure 4.5 shows a diagram of the two possible ways the source can decay. 5.4% of all disintegration's creates a β particle with an energy of 1.172MeV. In the remaining 94.6% of the time the source decays by emitting a β particle with an energy of 0.512MeV and then emitting a γ photon with an energy of 0.662MeV. The source has an activity of 740×10^9 Bq and the half-life for the ^{137}Cs source is 30 years.

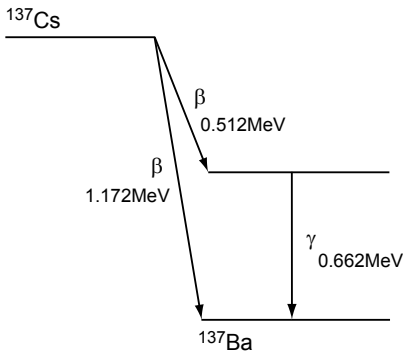

Figure 4.5: *Cesium-137 decay.*

4.2.3 Measurement setup used in the Total Ionizing Dose test

As described in chapter 3, γ-ray irradiation can cause trapping of charges in CMOS transistors, thus the drain-source current in the transistor might increase. Therefore the current drawn by the ELMB must be measured.

Since we are testing the complete setup of the ELMB, and not just components, the ELMB should be operated, as it would be in the ATLAS detector. The ELMB was remotely controlled and powered via the CAN bus. The control system that was used was the PVSS II SCADA[2] system. The SCADA software is described in section 4.2.5.

Since the ELMB was tested as a complete system it was necessary to test as much as possible. During the test both the ADC and the digital I/O lines were tested. The I/O lines was tested by connecting them together in a specific pattern and let the processor write and read the various lines. The I/O test and the connection of the I/O ports is further described in [30].

The ADC was tested by reading all 64 channels quite often. If this read-out should give any useful results it was necessary to apply a voltage on each analog input channel. Each of the analog input channels was supplied with a small voltage derived from the reference voltage. The reference voltage that was used was buffered through the operational amplifiers on the motherboard. Figure 4.6 shows a sketch of the resistor network used to generate the different voltages. The resistor network was mounted on a small piece of "veroboard" PCB and connected to the motherboard with a flat cable. It should be mentioned that each of the analog input channel connectors (34-pin) carries the buffered reference voltage and an analog ground connection.

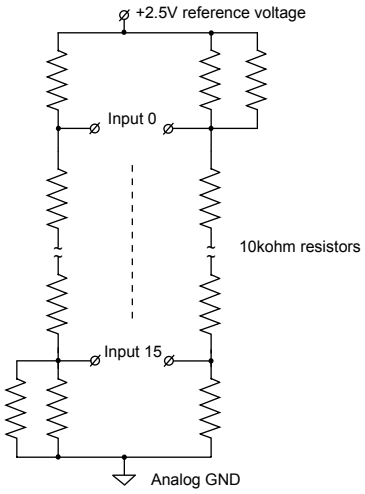

Figure 4.6: *Analog input channel voltage divider.*

The currents drawn by the ELMB was measured online with the same SCADA system that was used to control the ELMB. It should also be mentioned that the ambient temperature was also measured during irradiation. The currents and the temperature were measured with a LMB, the former front-end CAN node. The LMB was connected to the same CAN bus as the ELMB. The advantage of this is that only one CAN cable is required. On the other side, this could also be a

[2]PVSS II has been chosen to be the SCADA system used in the ATLAS community. This system is made by the Austrian company ETM, www.pvss.at

drawback since problems with the ELMB could affect the CAN communication with the LMB.

The PAGURE test

Figure 4.7 shows a sketch of the test setup used during the TID test at the PAGURE. The motherboard with the ELMB was mounted vertical on a piece of wood and placed 114cm from the source. The distance of 114cm was chosen too reach a total integrated dose of 350Gy in 6 hours (included setup). At the time when this test was done we used a dose of 0.5Gy(Si)/year as the maximum dose that the ELMB should withstand. This gives a total dose (RTC) of 350 Gy(Si) with the worst-case safety factors.

Each of the analog input connectors on the motherboard was connected to the voltage divider circuit as shown in figure 4.6, also the four digital I/O connectors was connected together in the mentioned pattern with pull-up and pull-down resistors. The ELMB was remotely powered through a 30m long cable, the same cable as used for the CAN bus. The power was injected via a distribution box. This box had connections to the power supplies, the CAN interface to the ELMB, the CAN interface to the LMB and to the computers. In this test the analog and the digital part of the ELMB was supplied with power through the same cable. Due to this, it was only possible to measure the sum of the analog and the digital currents. The LMB was also connected to the box with a flat cable, where the currents were read. The currents were read with an ADC module connected to the LMB main module. The readings were simply a voltage drop across a resistor in the power-line. In addition to the currents, the temperature was also read-out for two different locations. The temperature measurement was done with two PT-100 sensors. One of the sensors was located inside the distribution box, while the second was connected on a 5m cable. Unfortunately the cable was not long enough to reach the ELMB board, but long enough to measure the temperature inside the PAGURE.

The test was done with two portable computers. The SCADA system was running on one computer, while the second computer was used as a CAN analyzer tool. The CAN analyzer[3] is simply a program that monitors the CAN bus and displays all the activity on the bus. In addition to monitoring the bus, the program can also send CAN messages to the bus. The analyzer is a very powerful tool and was used to monitor the traffic on the CAN bus during the irradiation to see if there was any unusual activity. It is also very useful when debugging problems with the setup. Figure 4.7 depicts the setup used in the PAGURE test.

[3]The CAN analyzer from Vector Informatik was used in this test. www.vector-informatik.de

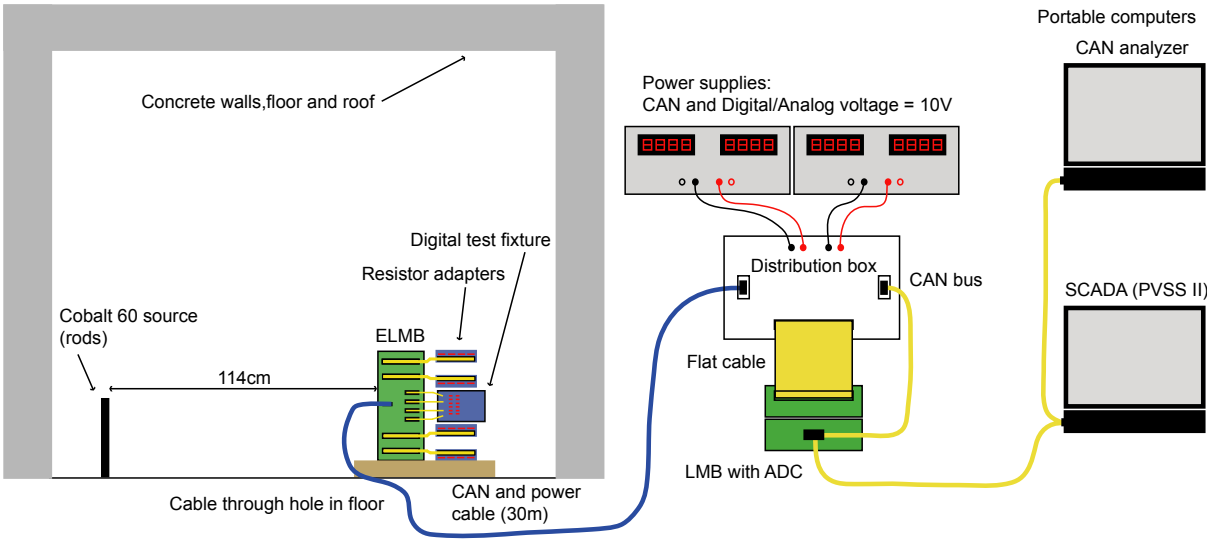

Figure 4.7: *Measurement setup used at the PAGURE radiation facility.*

The first GIF test

The second TID test was done at the GIF located at CERN. Figure 4.8 shows a sketch of the GIF, and a picture of the setup inside the GIF. The motherboard with the ELMB was placed 5 cm from the source enclosure in the side beam area. This corresponds to a dose-rate of 0.45Gy(Si)/h (distance is of about 25cm from the source). In this test only one of the reference voltage divider adapters was used. This adapter was used for all channels. The adapter was connected to the four input connectors with one cable. This means that four input channels were connected in parallel for each input voltage. Since the four connectors was connected in parallel with a flat cable also the buffered reference voltages will be connected in parallel. To avoid this one should cut the cable between these outputs and feed the adapter with a reference voltage from the connector closest to the adapter. However, this was not the case in this test, the cable was not cut, and the operational amplifier outputs were connected in parallel. This was an error. A second difference between the PAGURE setup and this setup was the separation of the analog and the digital power lines. In this setup a separate cable for the analog power was added. Also the cable for the PT-100 temperature sensor was increased in length. This made it possible to measure all three currents and the temperature where the ELMB was located. The power distribution was done with the same distribution box as in the first test, the currents was measured in the same way, but the two computers was exchanged with a desktop computer running only the SCADA application. The irradiation of the ELMB was in principle constant, the source was only stopped for a few minutes every day when personnel needed to enter the GIF radiation zone.

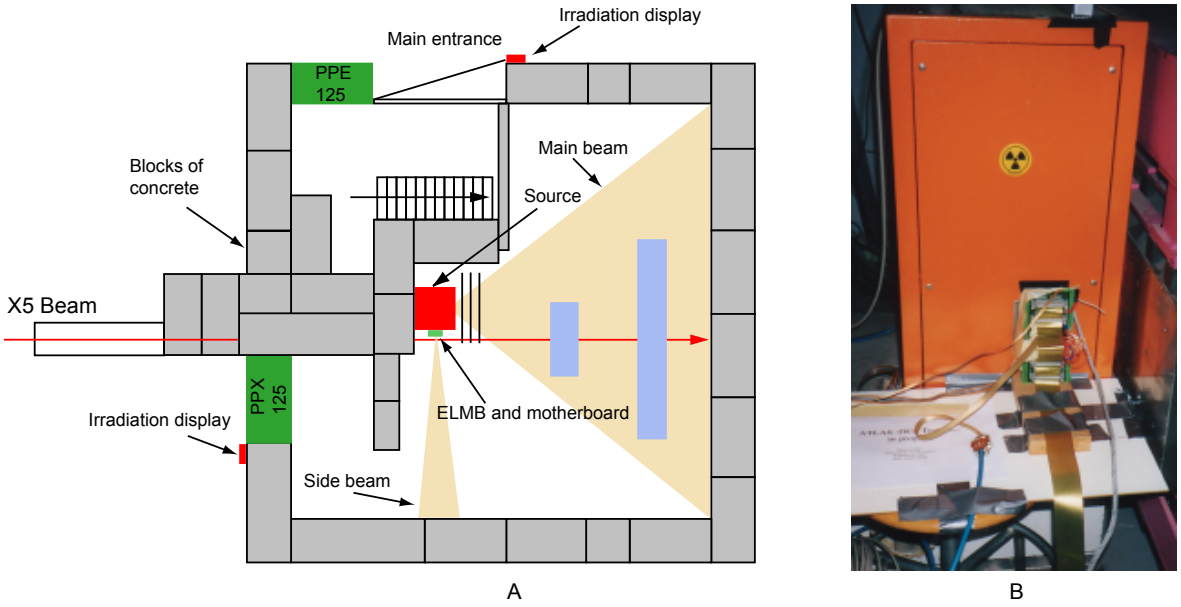

Figure 4.8: *A) shows a drawing of the Gamma Irradiation Facility at CERN. B) shows a picture from the first ELMB setup.*

The second GIF test

The third TID test was also done at the GIF. Also in this test the ELMB was placed at a distance of about 25cm from the source, but the source was not on all the time. The idea was to create an annealing effect between each irradiation period, and see if this changed the current drawn by the ELMB. The analog input channels was connected to the same voltage divider fixture as in the first GIF test, but now only the outermost buffered reference voltage was used. Also the PT-100 temperature sensor was placed close to the ELMB board. In this test the distribution box was not used. Instead a new box was created. The idea of this box was that is should be easy and fast to install the measuring equipment (the box was intended to be used in the later SEE test). Also, it would be good to decrease the length of the cables from the current measuring LMB to the ELMB. The box has a CAN bus input connector, a CAN bus output connector and two power connectors for connection of two ELMBs. The LMB is also integrated into the box. The power is fed to the box via the CAN cable (one CAN power supply and a second supply for the analog/digital power). The box were placed inside the GIF radiation zone, but behind a block of concrete. The cable from the box (after the LMB) was now reduced from 30m down-to 3m. With this setup it was possible to measure six different currents and two temperatures (PT-100 sensors, 4-wire connection). In our setup the three currents and the ambient temperature inside the GIF was measured. The same desktop computer was used in this test, but the SCADA software was changed a bit. The computer had a network connection, and every second hour the application extracted the current measurement data and stored them in a file accessible through the web, for easy access to the measurement data.

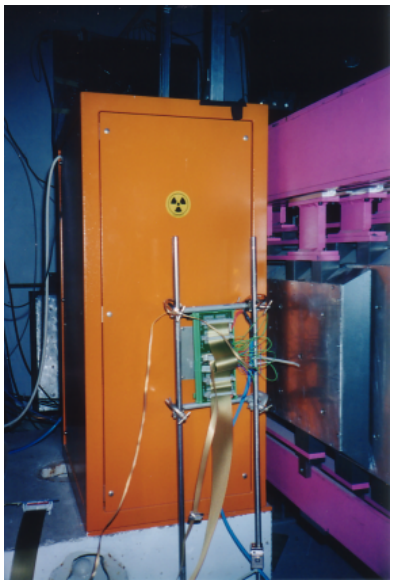

Figure 4.9: *Picture of the ELMB setup used at the second GIF test.*

4.2.4 Measurement equipment

Figure 4.10 depicts the principle of the temperature measurement and how ELMB currents was measured.

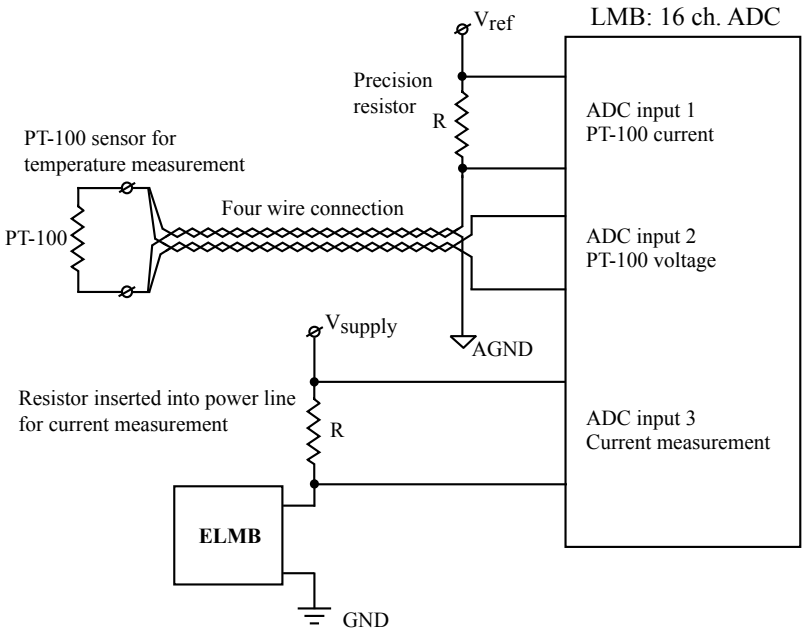

Figure 4.10: *Principle of temperature measurement and current measurement. The temperature measurement is done with a PT-100 sensor connected in a four wire fashion. The current measurement is done by measuring the voltage drop over a resistor inserted into the power line. The figure shows only one such resistor. It is necessary to use three similar circuits to measure all three currents drawn by the ELMB.*

The currents were measured as a voltage drop across a resistor. The voltage drop was measured with a LMB with an ADC module. The resistor which was inserted into the power supply lines was 10Ω±1%. This setup was used in the PAGURE test, in the first GIF test and in the accelerated aging test.

The second GIF (also the SEE) test was done with a different measurement box than the box that was used in the previous TID test. In this box the currents was measured as a voltage drop over a voltage divider (several resistors) inserted into the power supply lines. This was done to reduce the voltage into the LMB ADC. This would give a larger margin before the LMB ADC would overflow.

The LMB read-out was calibrated with the use of a separate ampere meter. This was done (during the analysis of the data) by shifting the ADC raw values that was collected during the test so that the data gave the same value as the value measured with the ampere meter.

4.2.5 Monitoring software

Both the LMB and the ELMB which was connected to the CAN network was controlled with the PVSS II SCADA system. The SCADA system is a high level control and data acquisition system. The SCADA system is very flexible and it is possible to get data into the system in many different ways. E.g. the system can be connected to the hardware through a dedicated driver or through an OPC (OLE for Process Control) server. In our setup the latter alternative was used. The communication between the CAN hardware interface, and the SCADA software was done with a CANopen compliant OPC server. This means that the server was able to send and receive CANopen messages. The OPC server used was made by the St. Petersburg Nuclear Physics Institute (PNPI) for the ATLAS DCS group.

An OPC server is a concept developed by Microsoft, and the Microsoft COM technology is used. This implies that the OPC server must run on a Windows computer, but the SCADA system does not, it can run on a computer with e.g. a Linux operating system. If this is the case, the SCADA system can be connected to the Windows computer via a network connection (LAN).

The SCADA system used for the three TID test was running on a Windows NT system. In addition to the SCADA system the OPC server was also running on the same computer. The CAN bus was connected to this computer via a CAN card from National instruments. The CAN card used for the desktop computer was a two port (possible with two different CAN network) PCI card (PCI-CAN/2) and the card used for the portable computer was a two port PCMCIA card (PCMCIA-CAN/2). The second portable computer used a PCMCIA card from Vector Informatik with the CANopen analyzer tool (CANalyzer) also from Vector Informatik.

The SCADA application used in the three TID tests was in principle the same application there were only small differences in the functionality between each test. The application consisted of three parts, a configuration part, a monitoring part and a data extraction part. With the configuration part is was possible to send configuration data and commands to the ELMB and the LMB. Before any data could be collected from the LMB and the ELMB it was necessary to configure the ADCs with the correct parameters (input range, conversion frequency etc). This was done by issuing SDO messages with configuration data. After configuration of the nodes they was in principle ready for data acquisition and they could be put into operational state (after power-up they are in the pre-operational state as described in chapter 2), this was done by sending a "start node" NMT command. The nodes were configured (object dictionary entry) to do data acquisition when it received a sync message from the network master (the computer).

The SCADA system was the network master, and it had a feature were it was possible to adjust the synch period. In the PAGURE test, and the second GIF test the sync interval was set to one minute, while the sync period was set to ten minutes in the first GIF test.

The data that was returned from the LMB and the ELMB after the sync command was transmitted via PDO messages. The PDO messages were received by the monitoring part of the application where it was decoded and displayed. The 64 analog input channels were displayed with 64 curves. This made it easy to see if there was any drift in the ADC readings. The analog configuration byte that is included in the PDO was displayed in a column with the corresponding channel number. This byte holds information of the current configuration for that particular channel and there is also a bit that indicates if the measurement is valid, e.g. if there is an ADC overflow. This made it easy to see if there was any error with the ADC configuration and the reading.

The digital I/O line test was also triggered by the sync command. The result from this test was returned as a 32-bit number. The number was decoded into four bytes representing the four ports, and displayed as a decimal number. If a logic "1" was returned at one of the bit locations in the byte, it was an indication that there was something wrong with this bit in the corresponding port.

The current and the temperature readings from the LMB were also displayed graphically with curves. This made it easy to see any current change. Also the configuration of the ADC was displayed for the LMB. It was displayed in the same way as for the ELMB. The reason for using the SCADA system was in principle not the graphical interface, well - of course it was nice to display the data as curves, but the main advantage was that is was possible to store the received data in a SQL database. The data was stored together with a timestamp indicating when the data was received. With the last part of the SCADA application you could extract the data of interest from the database and save this to an ASCII file for further analysis.

4.2.6 Accelerated aging test

The purpose of the accelerated aging test was too investigate and see if there was any annealing effect in the ELMB. By increasing the temperature the annealing effect will increase, and the currents should in theory decrease much faster [2]. In addition it would be interesting to find out how the ELMB responds to the increased temperature. To investigate this, a second ELMB (ELMB4) was tested together with the irradiated ELMB3.

According to [2] the CMOS components can suffer from low dose-rate effects. This means that the electrical properties of the semiconductors can get worse after the irradiation is finished. To simulate the low dose-rate effect, the device should be biased and heated for some time. According to the "ATLAS Policy on Radiation Tolerant Electronics" [14], the component under test should be annealed for 168 hours at 100 °C while under bias. If the electrical parameters does not get worse in this test and the components is still functional, it is not susceptible to low dose-rate effects, and the mentioned safety factor SF_{ldr} could be eliminated.

Since this was the first accelerated aging test, it was decided to go a bit slowly on the temperature increase. The two ELMBs was placed inside a temperature chamber and connected to a PC via a CAN network. Before the test, the programming function of the ELMB3 was tested (master processor). The programming function had failed, and the program was lost. Due to this, only the ELMB4 was working normal during the accelerated aging test (the slave processor in the ELMB3 was still operational and was in control of the node). During the test, the ADC was

read out from ELMB4, in addition, the three currents for each ELMB were read out. Also a PT-100 temperature sensor was connected to the LMB read-out node. This was done to keep track of the temperature with a timestamp that could be related to data for the currents.

The data acquisition software used during the accelerated aging test was done with the same kind of PVSS II SCADA system as used during the first GIF test. The values for the currents, the temperature and the ELMB4 ADC were read-out every tenth minute and stored in the SCADA database. The six currents and the temperature were read-out with the LMB. The currents was read-out as a voltage drop across a resistor placed in the power feeding cable for each part of the ELMBs.

4.3 Single Event Effect test

The purpose of the SEE test was to find out if the ELMB was susceptible to SEE. The test was done according to the pre-selection rules described for SEE testing in [14]. The test was done at the LOuvain-la-NEue Cyclone, this is located at the Université Catholique de Louvain in Belgium. At this facility it was possible to test the ELMB with a proton beam with an energy of 60MeV.

The simulated hadron fluence at the muon MDT end-cap 1 location is 4.83×10^{10} hadrons/cm^{2}10y [14]. To have a sufficient margin to this fluence, and to be able to provide some statistics, it was decided to irradiate the ELMB with a fluence, Ψ_p, of 3×10^{11} protons/cm^2. According to [14] the SEE test should be done on at least four ELMBs. A fluence of 10^{11} protons/cm^2 gives a total integrated dose of 140Gy(Si) [24]. Since the protons are positive charged they will in addition to the SEE also contribute to a TID effect. The TID effect is the limiting parameter in this test. The analysis of the TID tests showed that the total integrated dose should not exceed 35-40Gy(Si), otherwise the digital current would increase too much, and the current limitation feature integrated into the voltage regulators would be activated. To achieve this, the total fluence needed to be distributed on at least ten ELMBs. It was decided that the ELMBs should receive a fluence of about 3×10^{10} protons/cm^2, this corresponds to an integrated dose of 42Gy(Si). During the test eleven ELMBs was irradiated.

In order to detect and record the SEE which would be created it was chosen to use a flux, Φ_p, of 2.5×10^7 protons/cm^{2}s. With this flux, each ELMB needed to be irradiated for about 1200 seconds. Due to time limitations at the radiation facility, only the first five ELMBs was irradiated with this flux. The last six ELMBs was irradiated with a higher flux, the flux was set to 5×10^7 protons/cm^{2}s.

The proton flux is expected to create bit-flips in memory cells and registers. Thus, components with registers and memory were of special interest to monitor. This involves the two microcontrollers (ATmega103 and AT90S2313), the CAN controller (SAE81C91) and the ADC (CS5523). In addition, the multiplexer (MAX4582) and the components controlling the multiplexer were of interest to monitor. To be able to test this, an on-line measurement system was required. In addition to the individual results for the components, it would be very interesting to see how the ELMB and the ELMB firmware would handle the proton irradiation.

The idea of the test was to let the master processor do all the testing and report the test results to the computers via the CAN bus. During the test, the master processor would perform seven different tests of the involved components. This also includes read-out of the analog input channels. This way it is possible to test the complete data acquisition chain, from the input

channels to the SCADA system. In our measurement setup, three computers were used for data acquisition. This is described further in section 4.3.1. One computer was running the SCADA system, while the two other computers were running a CAN bus monitoring program. The reason for using the CAN bus monitor was to find out if there were any communication errors. E.g. if a proton changed something in the CAN interface chip (PCA82C250) or any of the opto-couplers in between this chip and the CAN controller. Due to problems with getting all the data from the ELMB through the OPC server, it was decided to use the CAN bus monitor as the main data acquisition system in this test.

4.3.1 Setup used in the Single Event Effect test

Figure 4.11 shows a drawing of the setup used during the SEE test and figure 4.12 shows a picture of the ELMB and the motherboard mounted in front of the proton beam pipe. The motherboard with the ELMB was mounted inside the radiation facility 1m from the proton beam pipe, and fixated with a few lead blocks. With this setup, only the ELMB was changed, the motherboard was used for all eleven ELMBs. Since the ELMB would suffer from TID effects and there was a risk for a SEL during the test, the currents needed to be measured. Also the temperature was measured. The temperature sensor was placed close to the ELMB board, as seen on the picture. The three currents and the temperature (PT-100 sensor connected to the LMB ADC in a four wire connection) was measured with the same "measurement box" as used at the second GIF test. The box was placed together with the ELMB inside the radiation facility, this kept the length of the cables to the temperature sensor and the power cables short. In addition to the current measurement done with the LMB and the SCADA system, two multi-meters were used. The multi-meters served as a backup system and as a system to verify that the currents were normal. These multi-meters was not connected to any computer, they was just read manually now and then. The measurement box, and the ELMB inside the radiation facility was supplied with power and a CAN bus through a 40m cable. The CAN cable was also connected to three portable computers used as the data acquisition system for the test. The data acquisition system is further described in section 4.3.3

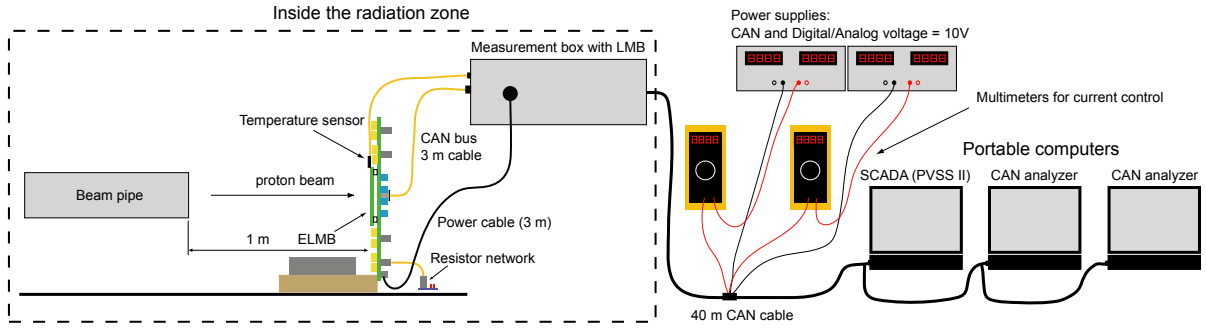

Figure 4.11: *Drawing of the measurement setup used during the SEE test.*

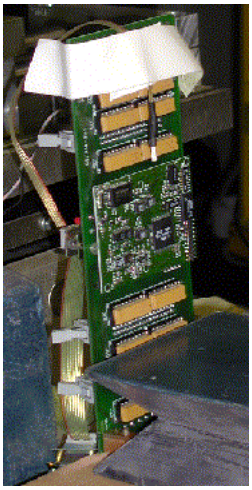

Figure 4.12: *Picture of the ELMB and the motherboard in front of the proton beam pipe. The PT-100 sensor can be seen just above the ELMB board.*

The ADC functionality was also tested during the irradiation. The analog input connector for the 16 lowest channels were connected to the voltage divider network described in section 4.2.3.

4.3.2 ELMB software

The firmware used in the master processor (ATmega103L) during the SEE test was an extended version of the standard software version (the master processor was programmed with the ELflash2.hex software, and the slave was programmed with the ELMBmon14 software version). In addition to the normal functionality, the program performed various self-tests. Each of these tests was repeated every fifth second and reported to the computers via the CAN bus (PDO messages). The additional test procedure used during the SEE test is described in [30]. The test sequence that was done is listed below.

- **ADC read-out**. During each test cycle, the first four analog input channels were read out.
- **Test of the SRAM**. When the test program was started, a test pattern was programmed into 2k bytes of the SRAM. During each test cycle, the SRAM was tested. If an error was found, the error was corrected and reported.
- **Test of the EEPROM contents**. When the master processor firmware was uploaded to the ELMB with the In System Programmer (ISP) the EEPROM was also filled with a bit-pattern. During the test, 3.5k bytes of the EEPROM was tested. If an error were found in the EEPROM memory it would not be repaired only reported. This means that an error would be reported several times during the test.
- **Test of the flash program memory**. The test was done by programming bit patterns (0xAA) in the unused program area, and to check this value. In total 64k byte of the flash memory was checked each time this test was performed. In addition to this on-line check, a complete check (128k byte) was done after the irradiation.

- **Test of the CAN controller**. During start-up of the program, some of the CAN controller registers were filled with proper values and tested in the same way as the SRAM. In total 40 bytes was tested in each test cycle. If an error were found the register would be updated with a correct value and an error would be reported.
- **Test of the ADC**. The ADC was also programmed with the proper values during start-up of the program. In this test 33 bytes of data in the ADC registers were tested in each test cycle. Like the CAN controller, the registers was corrected and an error was reported if found.
- **CRC test of the program memory**. A CRC value was calculated for the program and programmed in the two last byte locations in the flash memory. In this test a CRC value was calculated from the program contents and checked with the CRC value that was stored in the flash memory. Errors in this test would be reported, but not corrected.

During each test cycle, the ELMB returned ten CAN frames if no errors were found. If errors were found, more messages would be sent. Figure 4.13 shows the message format that was used for the SEE test. The ADC read-out is returned as it would in the normal firmware. The ADC read-out is reported with a PDO message with the COB-ID 0x2BF. The SEE test results is reported with the COB-ID 0x3FF. In total, eight errors can be reported for each element tested in one test cycle. This means that you can receive 48 frames with error messages from one test cycle.

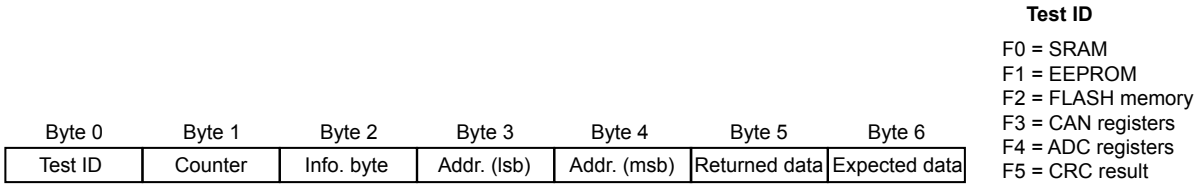

Figure 4.13: *CANopen message returned from the ELMB during the SEE test.*

The test ID is used to identify the message. The counter is simply an 8-bit counter value that is changing for each cycle. The reason for this was that we wanted to have a byte that was changing in the message from one test cycle to the next. The next byte is used to indicate if the message is an error message (byte = 0x01) or a summary message (byte = 0x00) of the number of errors that was found. If it's a summary message, the number of errors will be indicated in the next byte (addr. (lsb)). The next two bytes return the address where the error was found. The reason for returning the address was that it would be interesting to see if there were any errors in the same address area. For instance if a proton could contribute to bit-flips in neighboring address locations. To find out how many bits that was changed, and if the bit-flips was from "1" to "0" or from "0" to "1" the read and the expected bytes was returned in the two last bytes.

4.3.3 Monitoring software

As mentioned, the data acquisition system used at the SEE test consisted of three portable computers. One computer was running the PVSS II SCADA system, while the other computers were running a CAN bus monitoring program. The SCADA software was in principle supposed

to be the main data acquisition software during this test. But, due to time limitations to finish the application and problems to get all data from the ELMB through the OPC server, it was decided to use a CAN bus monitor to store all CAN bus activity. As a backup solution, two computers were used (to make sure that all data was collected). This turned out to be a good solution because there was a problem with one of the analyzers and some data was not stored. A second reason for using the CAN bus monitor was that erroneous communication could be detected, e.g. if a data frame on the bus was corrupted. The SCADA application was used to collect and store the currents and temperature measurement data from the LMB and to display the data. With a graphical presentation of the data it was easy to observe if there were any trending in the current drawn by the ELMB. The SCADA application did also display the four analog input channels that were read. The CAN bus monitors saved all the bus traffic to ascii files for further analyses.

Figure 4.14 shows a listing from two test cycles with actual data from the SEE test. The listing shows that it was found and reported two kind of faults during the two cycles shown in the list. Several SRAM errors and one CAN register error were reported.

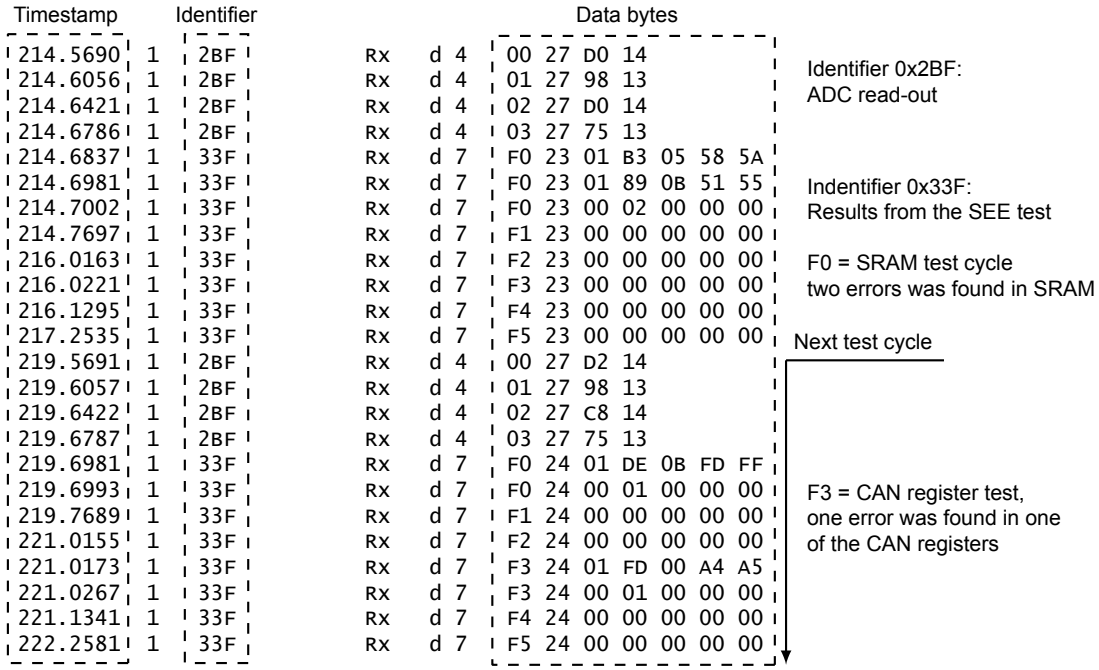

Figure 4.14: *Listing from the CAN monitor during the SEE test.*

The test sequence of the ELMB was stared by sending the CANopen command "start node". After this command was sent the ELMB would do the five seconds loop forever until an error interrupted the test loop. In addition to the test loop it was also of interest to test as much as possible of the ELMB functionality. The CAN message receive functionality was tested by sending a SDO message to the ELMB from the CAN analyzer on a regular basis. If everything were working as normal the ELMB would receive this SDO, and answer with a SDO message.

Chapter 5

Results from the radiation tests

This chapter present the results gained from the three TID tests, the accelerated aging test and the SEE test. The measurement setup used during these tests is described in chapter 4

A summary of the results has been presented at the "7th Workshop on Electronics for LHC Experiments", Stockholm, Sweden, 10 to 14 September, 2001 [5]. The results are also described in the ATLAS DCS internal working notes [6], [7], [8] and [9]. The ATLAS DCS internal working note [8] which describes the results from the third TID test has been written by me. This paper is included in appendix B together with the paper presented at the "7th Workshop on Electronics for LHC Experiments".

5.1 Total ionization dose test results

This section gives a detailed description of the results gained from the three TID tests. In addition results from the SEE test that is related to the TID effect is described. At the end of the section the results are summarized, and the key results are presented in some detail.

5.1.1 Total ionization dose test done at the PAGURE

As mentioned in section 4.2.3 the analog and the digital power cables was connected together at the ELMB side. Since the currents was measured at the cable end where the power supplies were connected, it was not possible to measure more than two currents. The CAN current and the sum of the analog and digital currents were measured. However, due to problems with the ADC channel (LMB) that was used for the CAN current it was not possible to get credible measurements from this channel. The ELMB1 and ELMB2 were placed inside the PAGURE radiation facility at a distance of 114cm from the source. The dose received by the ELMBs was measured with L-alanine dosimeters placed on the ELMB. The dose-rate was found to be 1.28Gy/min $\pm$ 6%.

ELMB1

After 43 minutes (total integrated dose equals 55Gy(Si)) of continuous operation, the communication with the ELMB1 was interrupted. The CAN bus monitor indicated that there were some problems with the communication (error frames could be observed). After the error frames had been seen, the CAN bus became blocked, and it was not possible to contact either the

ELMB1 or the LMB (not possible to measure the currents). The irradiation of the ELMB was not stopped immediately when the ELMB failed to work properly. The reason for this was that other peoples were also using the PAGURE facility, and the operator needed to be contacted. When the irradiation stopped, the ELMB1 had received a total integrated dose of 85Gy(Si) (66 min). During the irradiation, the sum of the digital and the analog currents had increased by a factor of three. Figure 5.1 shows a plot of the sum of the analog and digital currents. This large current increase caused the LMB ADC to overflow (the ADC was configured to measure the current in the middle of the ADC range, which was set to 1V (the current was measured as a voltage drop over a 10Ω resistor)). The ADC overflow happed almost at the same time as the ELMB1 stopped working (the current was only sampled every minute, so these events seems to be correlated on the figure, but they are not).

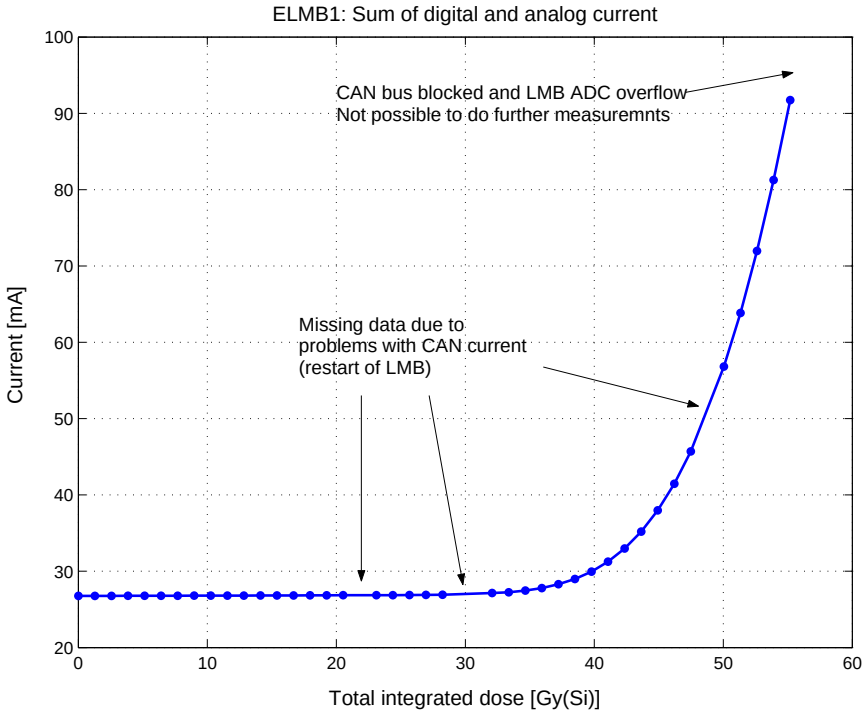

Figure 5.1: *Sum of the analog and digital currents for the ELMB1 .*

During the test we experienced some problems with one of the input channels on the LMB. The affected channel was used to measure the CAN current. Due to this, it was not possible to get any data for this current. It was only possible to measure the current after the irradiation. In addition, the CAN current and the sum of the analog and the digital current were re-measured 48 hours after the test. Table 5.1 shows the currents measured before, during and after the irradiation. As seen, the CAN current had increased by a factor two during the irradiation, while the analog and digital current had increased almost by a factor five. Due to the large increase in the analog/digital current, the voltage regulator built in current limitation was activated. To be able to measure the analog/digital currents it was necessary to bypass the voltage regulators (the output voltage pin on the regulators was lifted from the PCB). The currents were measured by injecting a +5V voltage directly into the ELMB after the voltage regulators.

Current	Before	After [55Gy(Si)]	End of test [85Gy(Si)]	After 48 hours
CAN	14 mA	n/a	28 mA	32 mA
Analog/Digital	27 mA	93 mA	130 mA	126 mA

Table 5.1: *Measurement of the CAN current, and the sum of the analog and the digital currents before, during and after the irradiation.*

During the irradiation all analog input channels (64 channels) were read-out. Figure 5.2 shows the raw values from the ELMB1 ADC. The plots clearly show a drift in the values for all channels. The drift can be explained by the fact that the ELMB1 did not have any reference voltage available for the voltage divider network, instead the analog supply voltage was used. During this test, the ELMB ADC was configured with an input range of 1V, unipolar mode and with a 1.88Hz conversion rate. The average drift of the channels is 0.8mV. This corresponds to about 0.5% drift of the measured input voltage. The average drift for all analog input channels is shown in figure 5.3.

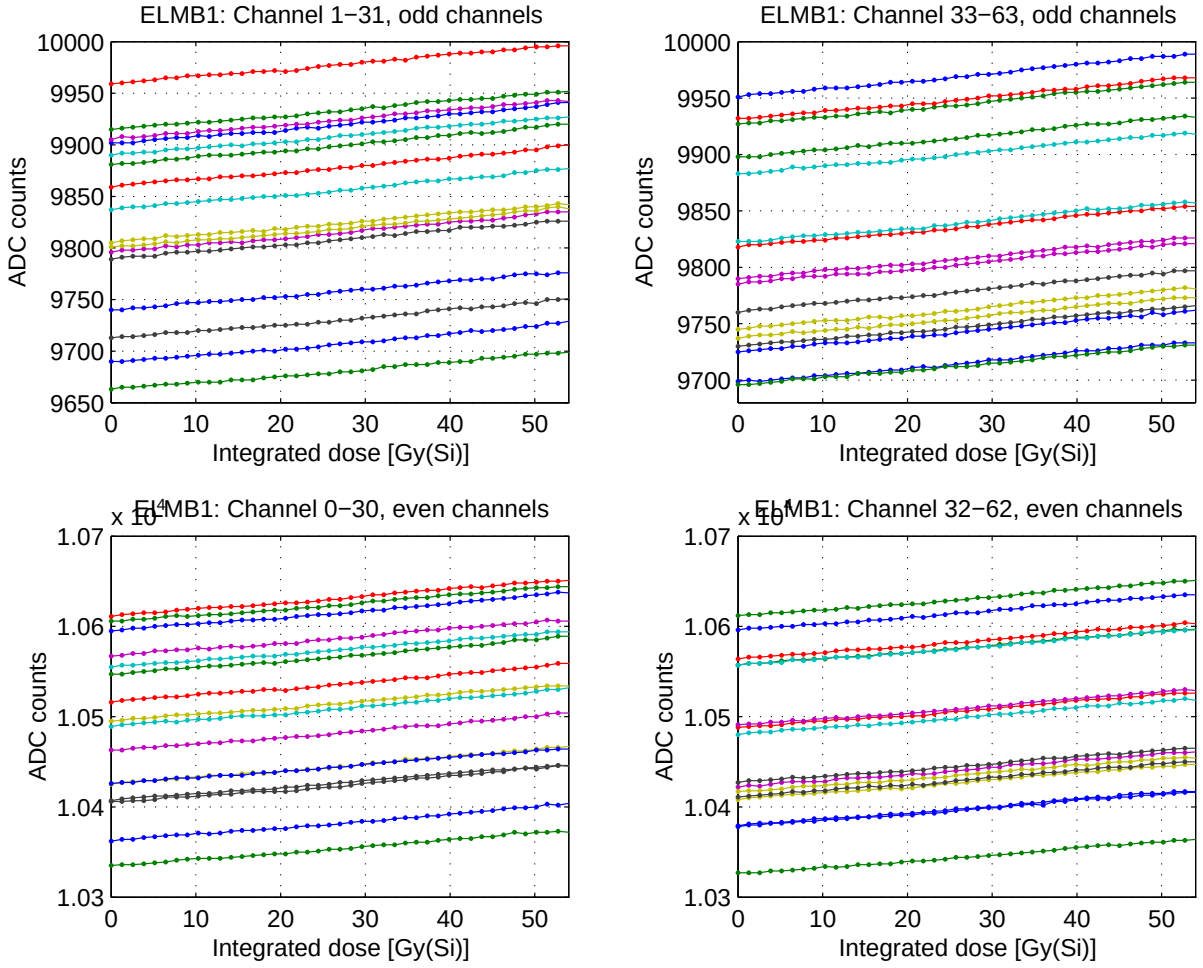

Figure 5.2: *Plot of the ADC raw values from ELMB1 during irradiation.*

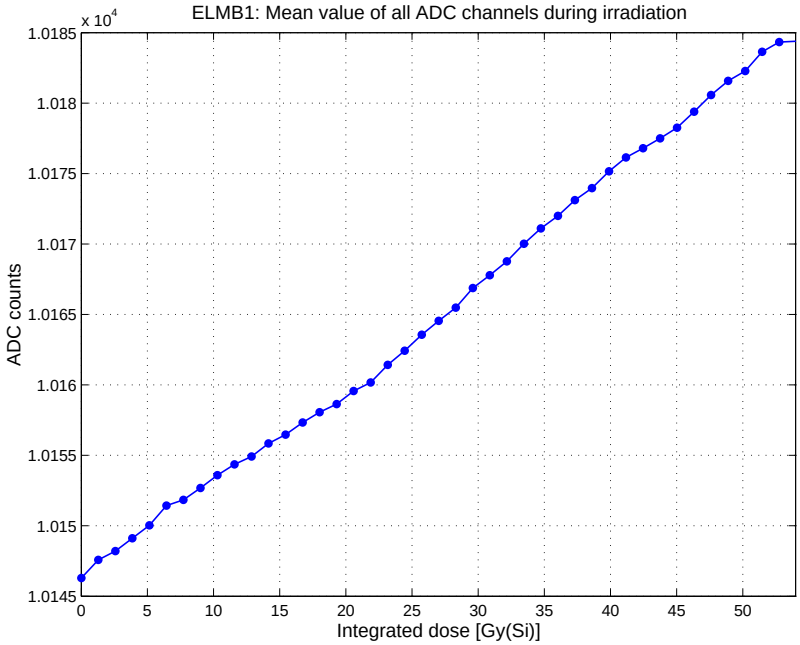

Figure 5.3: *Plot of the mean value for all analog input channels from ELMB1 during irradiation.*

After the irradiation (48 hours after irradiation), the ELMB1 was taken apart step by step. This was done by lifting the power supply pins on the components one by one. It was found that the three most complex integrated circuits (CMOS) were affected by the irradiation. This was the two microcontrollers (ATmega103 and AT90S2313) and the CAN controller (SAE81C91). Table 5.2 shows the current values for these components. Both the +5V voltage regulators MIC5203 (IC36, analog and IC 38, CAN) showed a voltage change smaller than the 0.3%. This is well within the voltage output accuracy which is 3% [42]. The third regulator (IC 37, digital) could not be measured due to a damaged pin on the package. The reference voltage circuit (IC23, AD680) was also found to be well within the +2.5V ±10mV specification [37].

Device	Typical value	After irradiation [85Gy(Si)]
ATmega103 (IC 34)	7 mA	70 mA
AT90S2313 (IC 35)	4 mA	22 mA
SAE81C91 (IC 27)	5 mA	24 mA
Other digital circuitry	5 mA	5 mA
Analog circuitry	7 mA	7 mA
Total current	28 mA	128 mA

Table 5.2: *Summation of the currents in the analog and the digital parts of the ELMB1.*

After the components was tested, the magnetic couplers ADuM1100 between the digital part and the CAN part (IC30 and IC31) was exchanged with two HCPL-0601 opto-couplers, the same type that was intended to be used in the ELMB in the first place. The ELMB was then connected to the same measurement setup and tested. The ELMB1 was found to be working as a normal ELMB, except that the digital current had increased more than five times the typical value. It should be mentioned that the digital voltage regulator was bypassed during this.

ELMB2

When the ELMB1 test ended, it was replaced with the ELMB2. The ELMB2 was placed at the same distance as ELMB1, so the dose-rate was the same. The ELMB was operated in the same way as ELMB1. When the ELMB2 had received a total integrated dose of 60Gy(Si) (47 min), the operation was interrupted. At this point, the sum of the analog and the digital currents had increased by a factor three. Figure 5.4 shows a plot of the sum of the analog and the digital currents. Also in this test, the LMB ADC went into overflow during the current measurement. As seen in the plot, the sum of the currents is a bit higher than for the ELMB1. This is because the opto-coupler HCPL-0601 between the digital part and the CAN part draws more current than the magnetic coupler ADuM1100 which was used in the ELMB1. Also in this test, the source was not stopped immediately after the ELMB failed. The source was stopped after 73 minutes this corresponds to an integrated dose of 94Gy(Si).

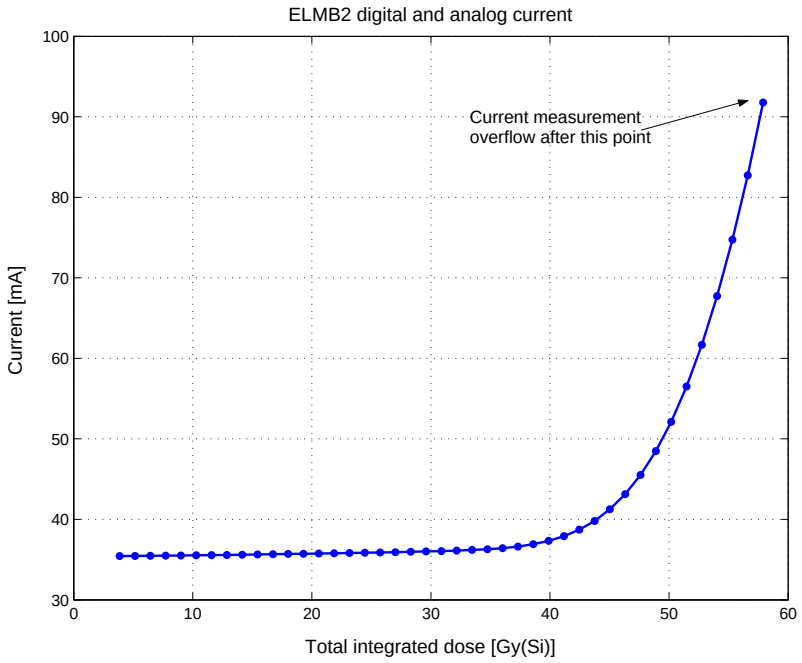

Figure 5.4: *Sum of the analog and digital currents for the ELMB2 .*

The analog input channels on ELMB2 was measured in the same way as the ELMB1, the only difference was the voltage supply to the voltage divider network. In this test, it was supplied with a +2.5V (reference voltage), instead of the +5V analog supply voltage. This is clearly seen in figure 5.5 where the ADC raw value drift is much smaller than the ADC drift for ELMB1. Figure 5.6 shows a plot of the mean value for all analog input channels during the irradiation. The total mean drift for all channels is +3.031 counts. This corresponds to 46μV drift (0.0046%), (ELMB ADC configuration: 1V range, unipolar and 1.88Hz conversion rate). Another distinct difference between the ADC read-out from the two ELMBs is that the ELMB2 raw value is about half the value that was measured with ELMB1. This is because the +2.5V reference voltage was used to feed the resistor network instead of the +5V supply.

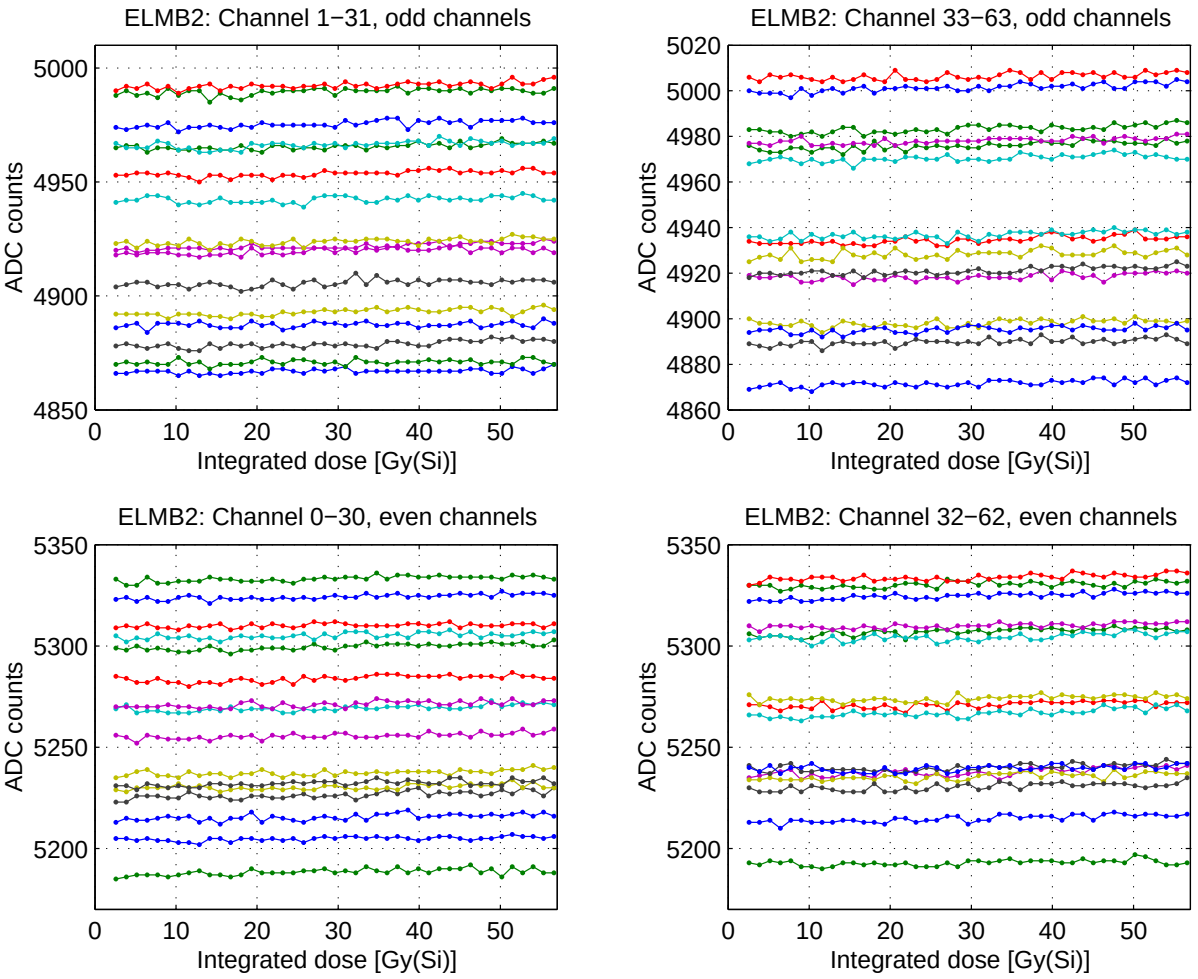

Figure 5.5: *Plot of the ADC raw values from the ELMB2 during irradiation.*

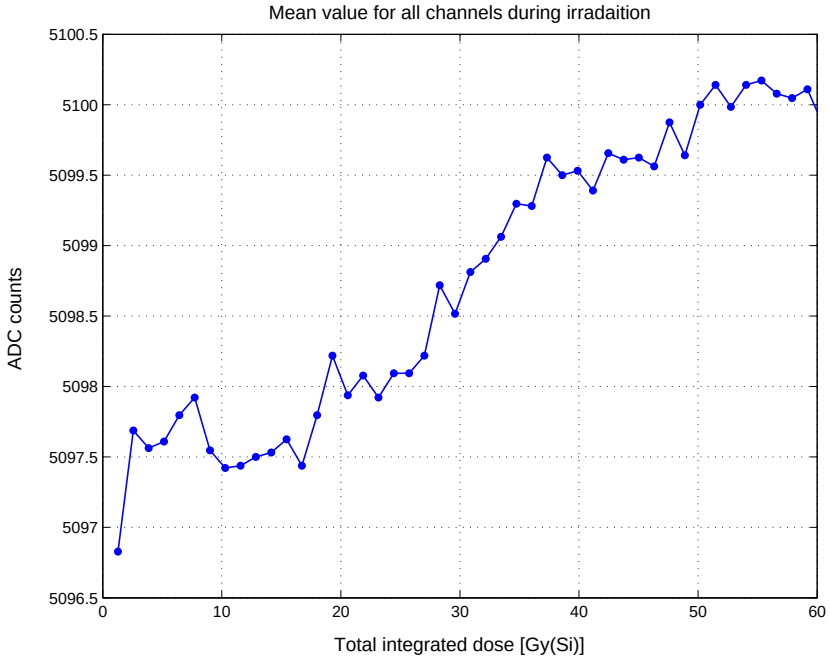

Figure 5.6: *Plot of the mean value for all analog channels from ELMB2 during irradiation.*

After the irradiation the three supply currents were measured. The currents were also re-measured after 48 hours. Table 5.3 shows the measured currents. It is evident that the digital part was influenced by the γ-ray irradiation. The digital current increased almost by a factor 4, but the CAN current and the analog current did not change noticeable during the test. It should be noted that the CAN current and the digital currents are a bit higher for ELMB2 than for ELMB1. This is because the two opto-couplers (HCPL-0601) between the digital and the CAN part draws more current then the magnetic-couplers (ADuM1100). Also in this ELMB, the increased current was traced to the same circuits as found in the ELMB1. The two microcontrollers, (ATmega103 and AT90S2313) and the CAN controller (SAE81C91). The table shows that the digital current has decreased a bit after 48 hours. This is probably because there is an annealing effect in some of the affected components (the components that contributed to the increased current).

Current	Before test	End of test [94Gy(Si)]	After 48 hours
CAN	19 mA	19 mA	19 mA
Analog	9 mA	10 mA	9 mA
Digital	35 mA	130 mA	118 mA

Table 5.3: *Measurement of the CAN, analog and digital currents for ELMB2 before the test, at the end of the test and 48 hours after the test.*

5.1.2 First total ionization dose test done at the GIF

The purpose of this TID test was to find out if a lower dose-rate would have any influence on the TID acceptance on the two microcontrollers and the CAN controller. As mentioned in chapter 4 the dose-rate could have major impact on the dose acceptance. In addition an accelerated aging test was also done. The results from the accelerated aging test is presented in section 5.1.5. The ELMB that was tested is referred to as ELMB3. This was placed at 25cm from the source. The dose-rate was measured with L-alanine dosimeters and the total integrated dose was found to be 43Gy(Si) ±15%. The test lasted for 90.25 hours this corresponds to a dose-rate of 0.48Gy(Si)/h. Also in this test the digital current showed a rapid increase after the ELMB had received a total integrated dose of about 35Gy(Si). The test was ended after the ELMB had received an integrated dose of 43Gy(Si). The reason for stopping the irradiation was that further irradiation would not give any more information and the current would increase until the voltage regulator limited it. If the current was allowed to be limited, the digital voltage would be reduced (onboard) and the ELMB would cease to work. Figure 5.7 shows the three currents during irradiation.

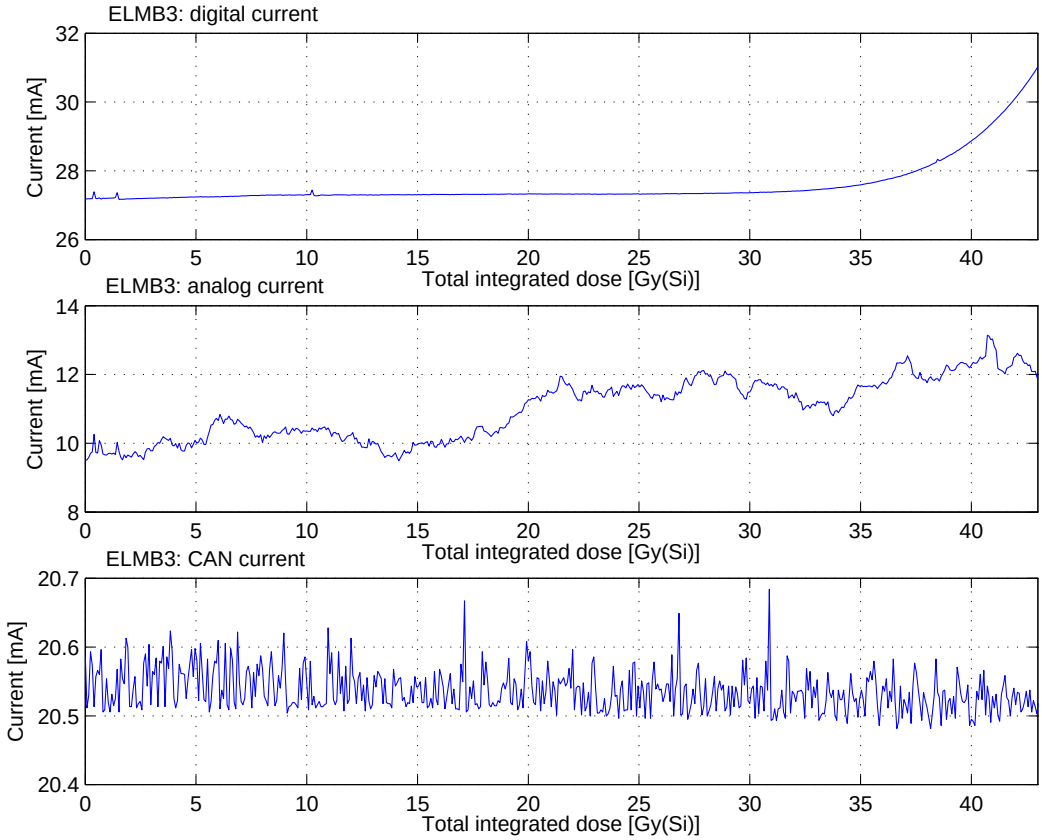

Figure 5.7: *Plot of the analog, digital and the CAN currents for ELMB3 during irradiation.*

The analog current did show an increase. It increased from about 9.5mA to about 12mA, but the current was not stable at all. As seen, the analog current seemed to be changing randomly around a linear increase. This random behavior was only present when the source and the shutter were on. Figure 5.8 shows the analog current versus the time the ELMB3 was in the GIF. In this figure it is clearly shown that the random analog current behavior was dependent on the γ-ray

radiation. The reason for this behavior is not known, but this could be related to a photoelectric effect or a Compton effect in some of the analog circuits. The CAN current shown in figure 5.7 also seems a bit random, but it should be noted that the scale is in mA, this leaves the change very small. This current behavior can be caused by several reasons. The LMB ADC (16-bit) used for the current measurement was configured in unipolar mode, 1V input range and with 15Hz conversion rate. With this configuration the ADC LSB is 15μV. This means that random current behavior most likely has a noise component. Another possibility is that it is the actual current that is measured, but the current is changing because the ELMB3 CAN part is operational (receiving or sending messages during the current measurement). The currents measured before the test and after the test is summarized in table 5.4.

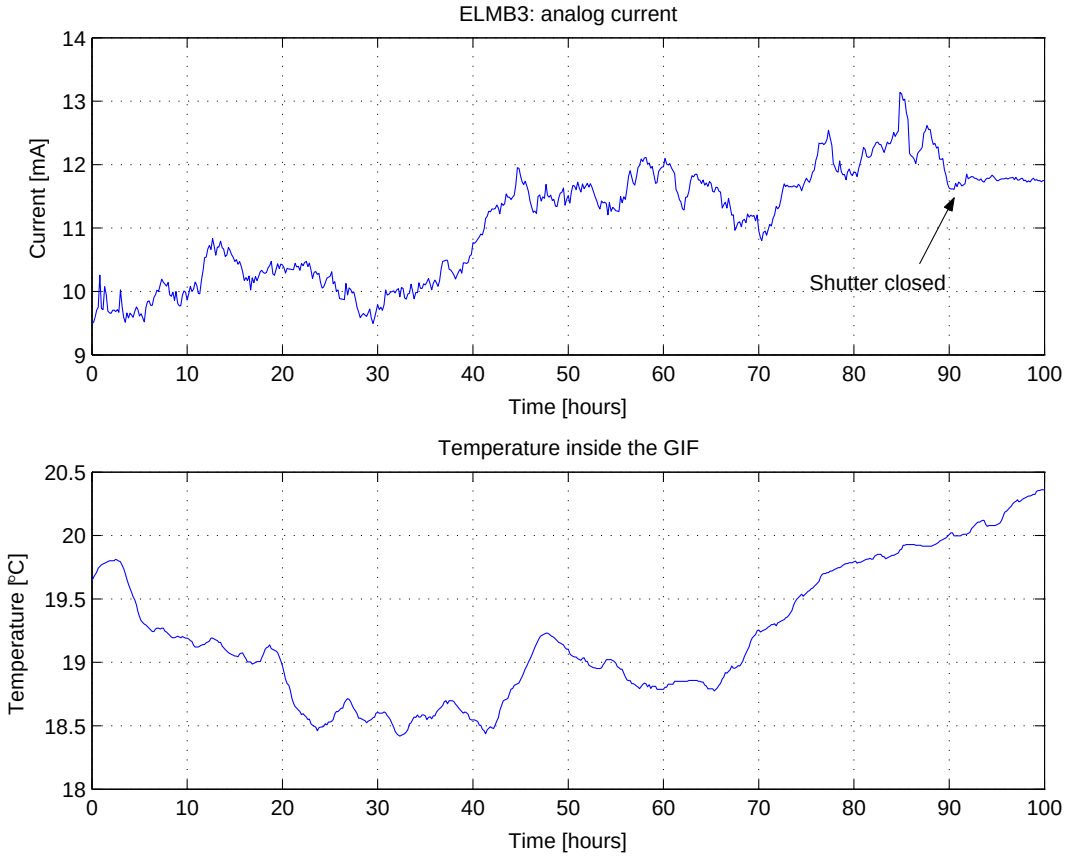

Figure 5.8: *Plot of the analog current and the temperature inside the GIF versus time.*

Current	Before radiation	After 43Gy(Si)
Digital	27.2 mA	32.4 mA
Analog	9.6 mA	11.8 mA
CAN	20.5 mA	20.5 mA

Table 5.4: *Summary of the currents measured during the ELMB3 test.*

To verify the stability of the voltage regulators, and the reference voltage, the voltages was measured before and after the irradiation. Table 5.5 shows the values that was measured. During

the irradiation all voltages increased a bit, but the voltage regulators MIC5203 had the largest voltage change. The worst case voltage change was about 33mV. The voltage output accuracy of this regulator is 3% or 150mV. The worst case change is well within the specification for this regulator. The voltage reference circuit AD680 only changed 100μV. However, the operational amplifier that is used to distribute the reference voltage on the motherboard had changed a bit more, the worst case change was 3.2mV. It should be mentioned that the operational amplifier has been tested before, and found to be not radiation tolerant. This information was not known when the motherboard was equipped with the operational amplifier [31].

DC voltages measured	Before	End [43Gy(Si)]	Change
Voltage regulator MIC5203 CAN (IC 38)	4984.6 mV	5004.0 mV	19.4 mV
Voltage regulator MIC5203 Digital (IC 37)	4942.2 mV	4961.5 mV	19.3 mV
Voltage regulator MIC5203 Analog (IC 36)	4969.8 mV	5003.1 mV	33.3 mV
Reference voltage circuit AD680 (IC 23)	2488.9 mV	2489.0 mV	0.1 mV
Op-Amp LMC6084 ch0-15 (motherboard)	2489.7 mV	2492.8 mV	3.1 mV
Op-Amp LMC6084 ch16-31 (motherboard)	2489.3 mV	2492.5 mV	3.2 mV
Op-Amp LMC6084 ch32-47 (motherboard)	2489.5 mV	2491.6 mV	2.1 mV
Op-Amp LMC6084 ch48-63 (motherboard)	2490.0 mV	2493.2 mV	3.2 mV

Table 5.5: *Voltage measurements of the voltage regulators, the voltage reference circuit and the operational amplifier buffered reference voltage before and after the irradiation.*

The programming function of the two microcontrollers was also tested after the radiation test. This test was done with the ISP programmer made especially for the ELMB ISP connector J3. With this programmer it is possible to program the microcontrollers (one at a time). The advantage of the ISP programming feature is that it is possible to program the chips when they are mounted on the PCB. The ISP programmer was controlled with the ISP software from Kanda-Systems[1]. With this software you have access to all memory locations that is possible to read and program. The first step in the test was to read the program memory and check that the contents were unchanged. The second test was to erase the memory and to do a re-program cycle. This was done for the flash memory and the EEPROM in both microcontrollers. Table 5.6 shows the results from the test. It shows that the programming function for both the flash and the EEPROM in the master controller was destroyed during the γ-ray irradiation. The programming functions in the slave controller were working as normal.

Device	Prog. check	Flash erase	Flash prog	EE erase	EE prog.
ATmega103	Pass	Pass	Failed	Pass	Failed
AT90S2313	Pass	Pass	Pass	Pass	Pass

Table 5.6: *Test of the programming function of the two microcontrollers.*

The analog input channels was also read-out during the test. In this test only one voltage divider circuit was used. This was connected in parallel to all four connectors. In this test an error was made, the last connector closest to the divider network was supposed to deliver the reference voltage, but by a mistake the wires between the four connectors was never cut. With this cable all operational amplifier outputs was connected in parallel. Figure 5.9 shows the read-out from

[1] AVR ISP software from www.kanda.com

the 64 analog input channels during irradiation, and figure 5.10 shows the drift of the ADC read-out. During the test which lasted for 90.25 minutes (corresponding to a total integrated dose of 43Gy(Si)) the ADC read-out showed an average drift of 6.5 counts this corresponds to a drift of 99μV or 0.01%.

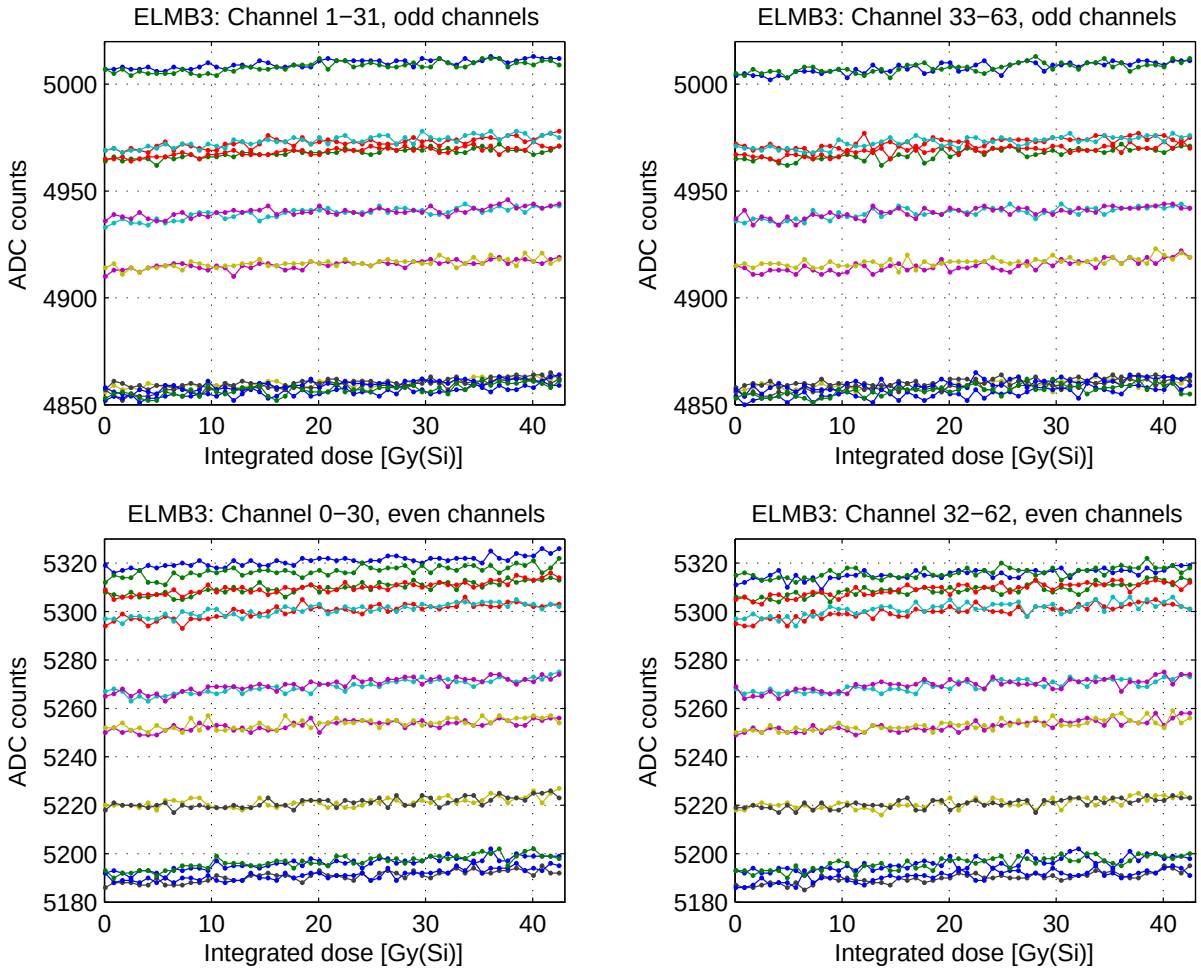

Figure 5.9: *Plot of the 64 analog input channels for ELMB3.*

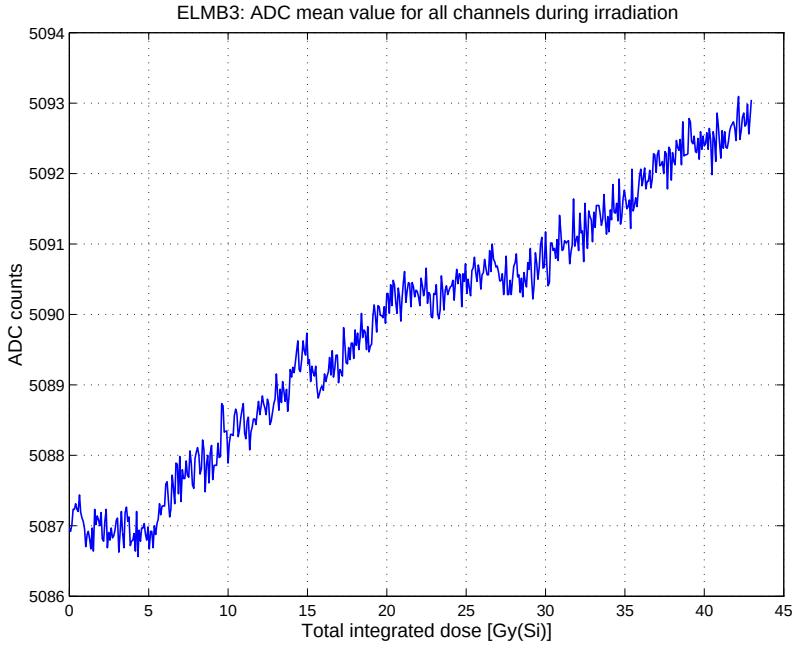

Figure 5.10: *Plot of the mean value for all analog input channels during irradiation.*

5.1.3 Second total ionization dose test done at the GIF

As mentioned in section 4.2, the second GIF test was done to investigate the loss of the programming function of the microcontrollers, especially the master controller was of interest since the program in this might be changed during the ATLAS lifetime.

The ELMB5 was placed at a distance of 25cm from the source. At this distance the dose-rate is 0.45Gy(Si)/h (theoretical - not measured in this test), but since the source was on for about 10 hours and off for about 14 hours the effective dose-rate during 24 hours is 0.17Gy/h (in the first part of the test). After each irradiation period the programming function was tested. In total eight successful reprogramming cycles was done. The function failed on the ninth reprogramming attempt. Table 5.7 shows the integrated dose, and the digital current during each reprogramming cycle. The reprogramming function ceased to work somewhere between a total integrated dose of 33.8Gy(Si) and 37.9Gy(Si). Figure 5.11 shows a plot of the digital current versus the time up till the point where the programming function failed. Each test is indicated with a number. After each reprogramming the digital current changed a little bit and there is also a small decrease in the current. When the reprogramming function failed it was decided to leave the source on to see if the digital current started to increase as it had in the previous tests. When the source was stopped the ELMB had received a total integrated dose of 80.3Gy(Si).

Period	Digital current	Integrated dose
1	14.100 mA	0.5 Gy(Si)
2	14.109 mA	7.9 Gy(Si)
3	14.111 mA	12.2 Gy(Si)
4	14.112 mA	16.3 Gy(Si)
5	14.105 mA	20.8 Gy(Si)
6	14.103 mA	25.2 Gy(Si)
7	14.083 mA	29.4 Gy(Si)
8	14.045 mA	33.8 Gy(Si)
9 (failed)	13.999 mA	37.9 Gy(Si)
End of test	39.622 mA	80.3 Gy(Si)

Table 5.7: *Current and integrated dose for ELMB5 when the programming function was tested.*

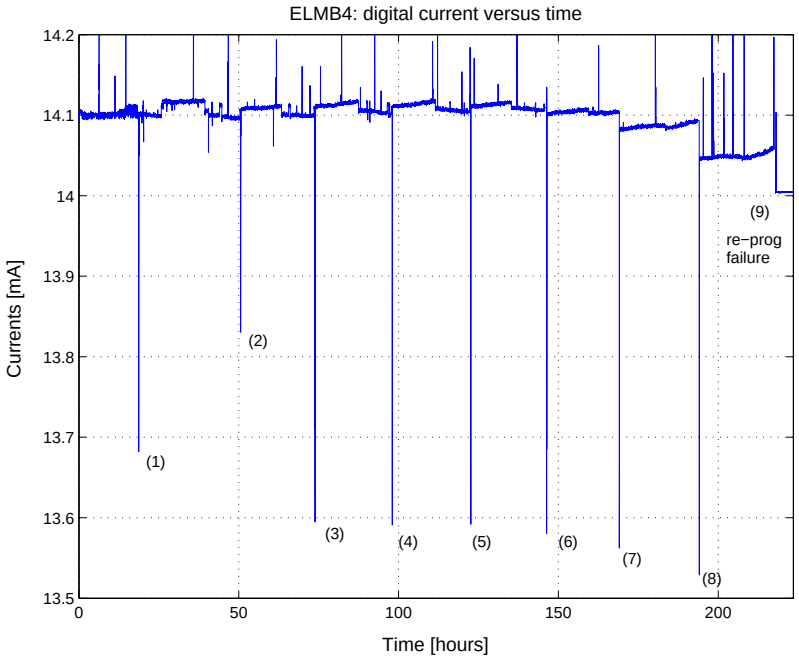

Figure 5.11: *Plot of the digital current versus time for ELMB5. The figure shows when the programming function was tested and when it failed.*

Figure 5.12 shows the analog and the digital currents versus time. The photo current effect is clearly visible on the analog current in the first part where the current is jumping up and down when the shutter is opened and closed. In addition, there is a clear linear increase in the analog current. However, this current increase is very small, just around 75μV. When the programming function failed the master processor was erased (this is part of the programming sequence) and the ADC could not be put into operation again. This would explain the current decrease shown in the analog current in figure 5.12. The jump back up is probably because of the photocurrent (source was on all the time at this point). Shortly after the reprogramming function ceased to work a rapid increase in the digital current was observed. After about 300 hours of testing the analog current started to decrease. This decrease could also be observed on the CAN current shown in figure 5.13. It is believed that this current decrease is correlated with the increased

temperature on the PCB caused by the increased digital current (the voltage regulator gets hot). The three voltage regulators are located side by side on the PCB, and the heat from the digital voltage regulator is likely to be transferred to the neighboring circuits.

After about 330 hours the shutter was closed, and the ELMB was left to anneal in room temperature for about 170 hours. It is clearly visible that there is an annealing effect in the components, which contributes to the increased digital current. Figure 5.13 does also show the temperature inside the GIF during the test. The curve shaped form on the three currents is believed to be caused by variations in the ambient temperature. The figure clearly shows the day/night temperature variations.

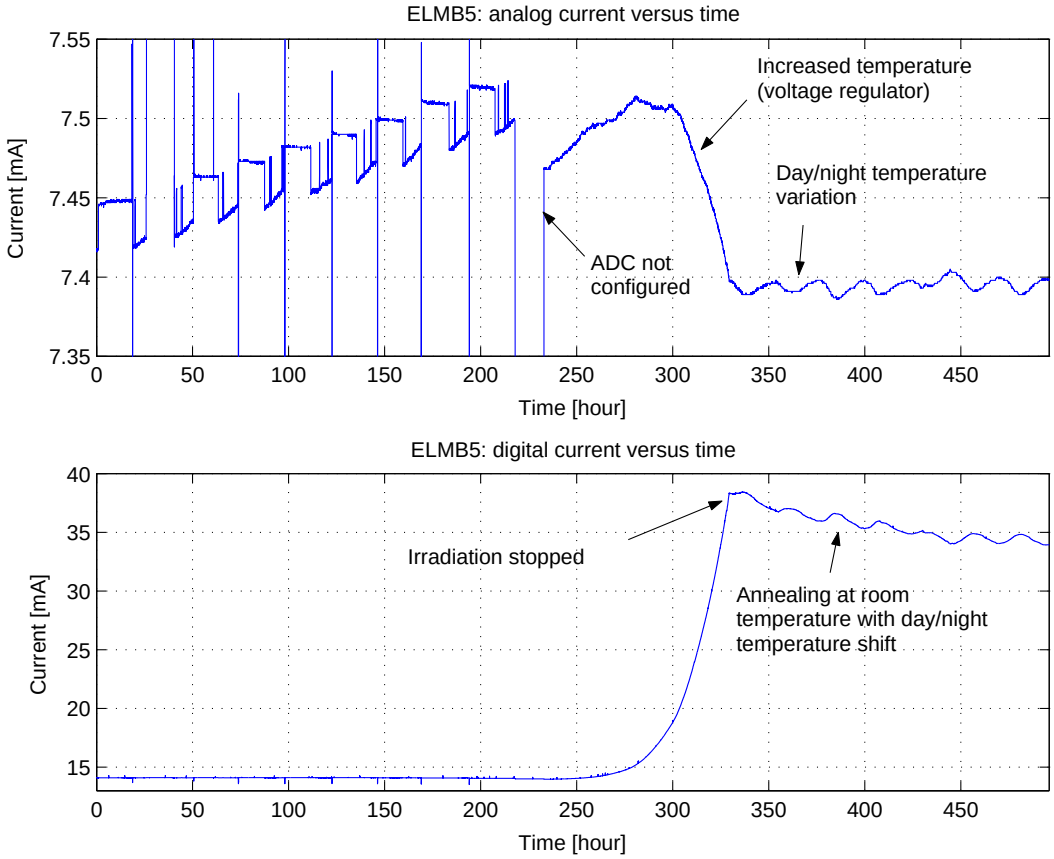

Figure 5.12: *Plot of the analog and the digital current versus time for ELMB5.*

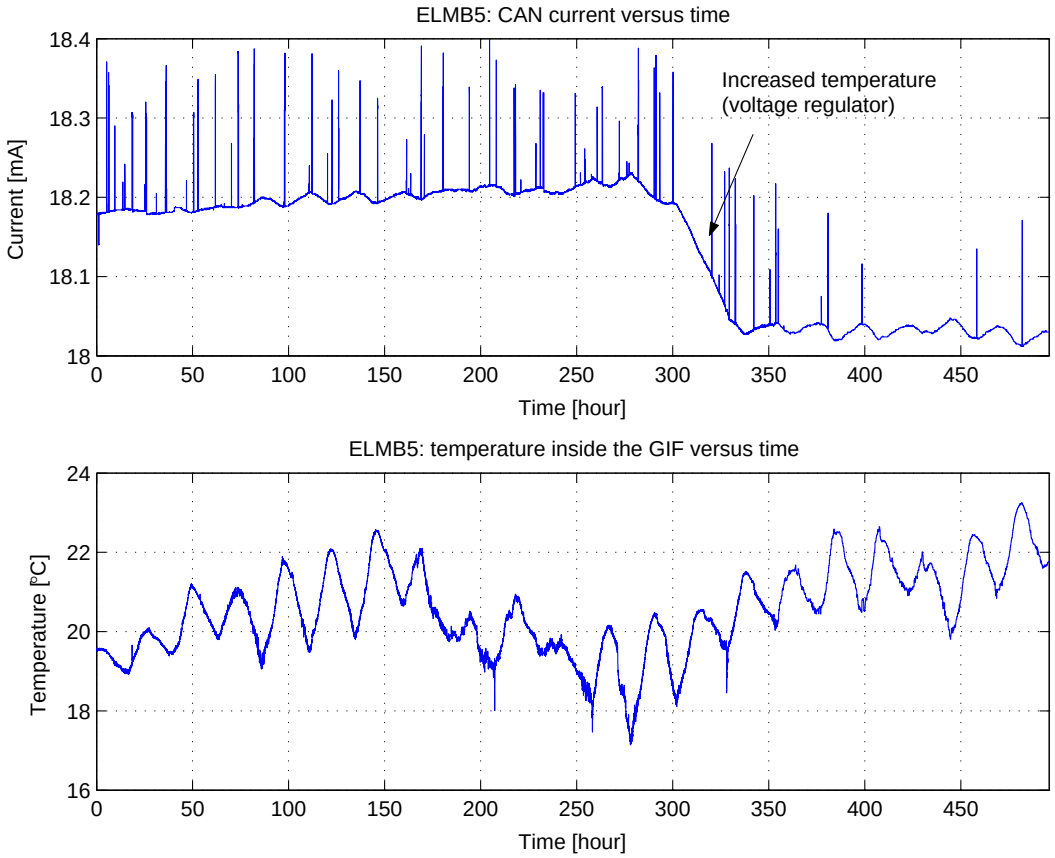

Figure 5.13: *Plot of the CAN current and the temperature inside the GIF during the ELMB5 test.*

Figure 5.14, 5.15 and 5.16 shows the analog, digital and the CAN currents versus the total integrated dose. The analog current shows a linear increase of about 75μV. The digital current showed a somewhat strange behavior. As seen, the current made a jump after each reprogramming sequence. Since this current jump does not happen in the analog current measurement it is not caused by the measurement equipment. Since the jumps appear after each reprogramming sequence it could be related to the flash programming circuitry. The flash memory needs a higher voltage then the +5V voltage supplied to the microcontroller for programming. This voltage is generated on-chip. The current jumps can be related to stress on this circuit or stress on the flash memory itself (the flash memory can only be programmed 1000 times according to the datasheet [40]).

The CAN current also shows a tendency to increase after each reprogramming/non-irradiation period. The current decreases while the source is on, but jumps when the reprogramming sequence is performed. This jump can be related to some internal reset or a similar function since the ELMB is reset when the programming is performed. It should also be noted that the change is rather small.

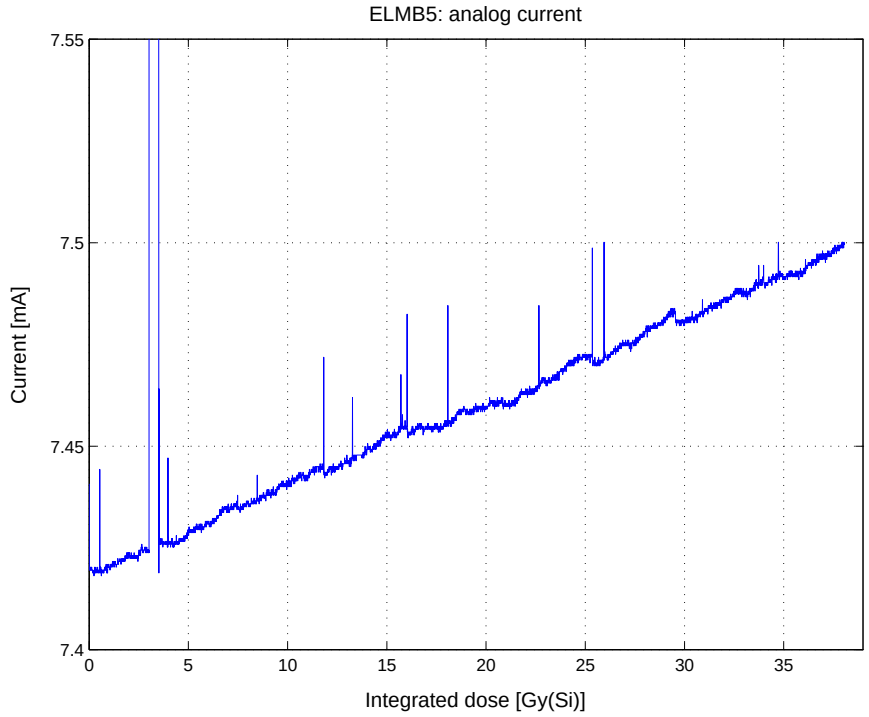

Figure 5.14: *Plot of the analog current versus the integrated dose for ELMB5.*

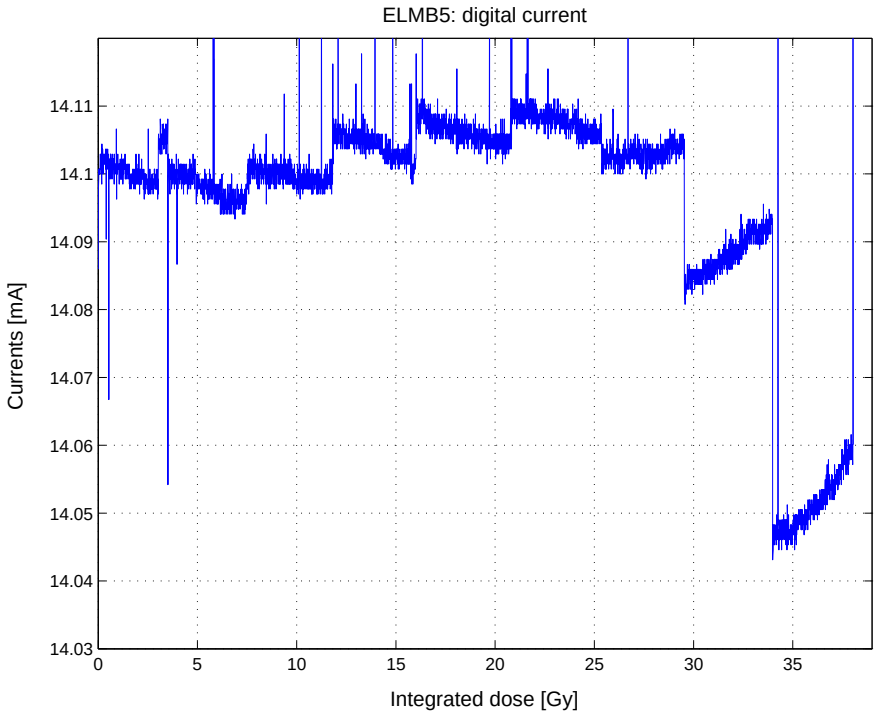

Figure 5.15: *Plot of the digital current versus the integrated dose for ELMB5.*

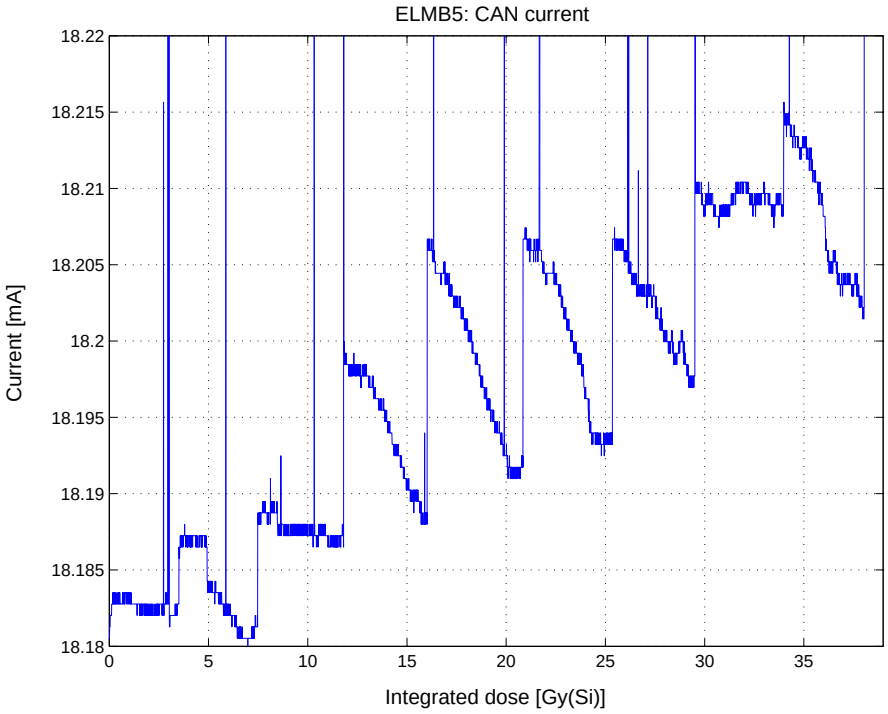

Figure 5.16: *Plot of the CAN current versus the integrated dose for ELMB5.*

Also in this test the 64 analog input channels was read-out when the shutter was both open and closed. Figure 5.17 shows the ADC raw values during the ELMB5 irradiation. During a short period of time, the ADC was operated with a wrong configuration. This was a user fault the right configuration was not loaded into the ELMB after the reprogramming sequence. This is clearly shown in the figure where the read-out values are higher than the normal expected value. The plots also show a second jump in the ADC read-out. This error happened during the test. The cause of this error is not known. This fault was corrected by resetting the ELMB and by loading new configuration data to the ADC via SDO messages. Figure 5.18 shows the mean value for all analog input channels during the irradiation, the values from the read-out when the ADC was run with a wrong configuration is omitted in this figure. The figure shows a drift of about 1.4 counts during the irradiation. It should be noted that the ADC was loaded with new configuration data and calibrated after each reprogramming (this feature is part of the current ELMB firmware). This is probably the reason for the small ADC drift compared to the previous tests. It should also be pointed out that the ADC input range was 1V, which corresponds to an ADC LSB of only 15μV. This gives a drift of about 20μV.

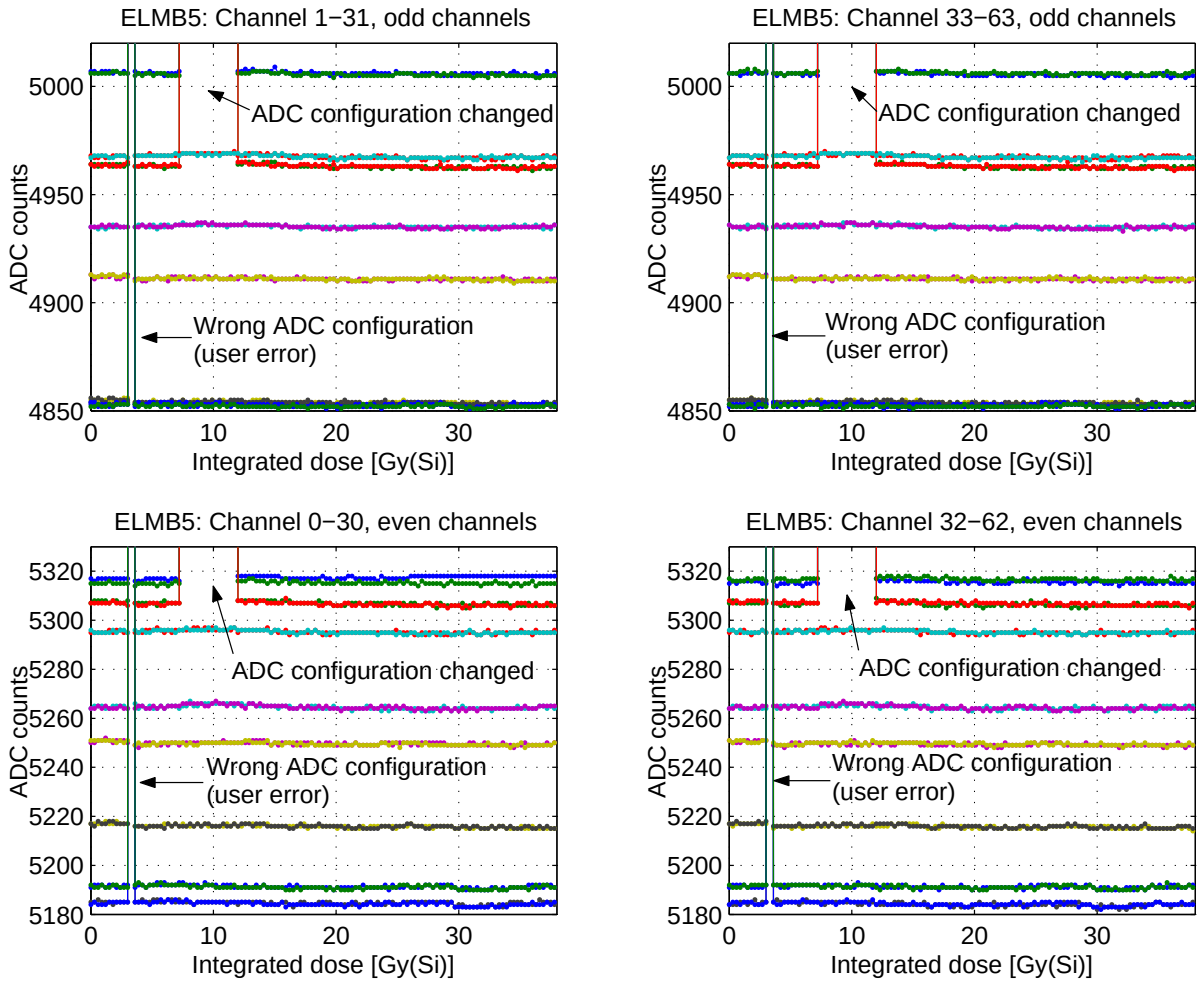

Figure 5.17: *Plot of raw values from the analog input channels on ELMB5.*

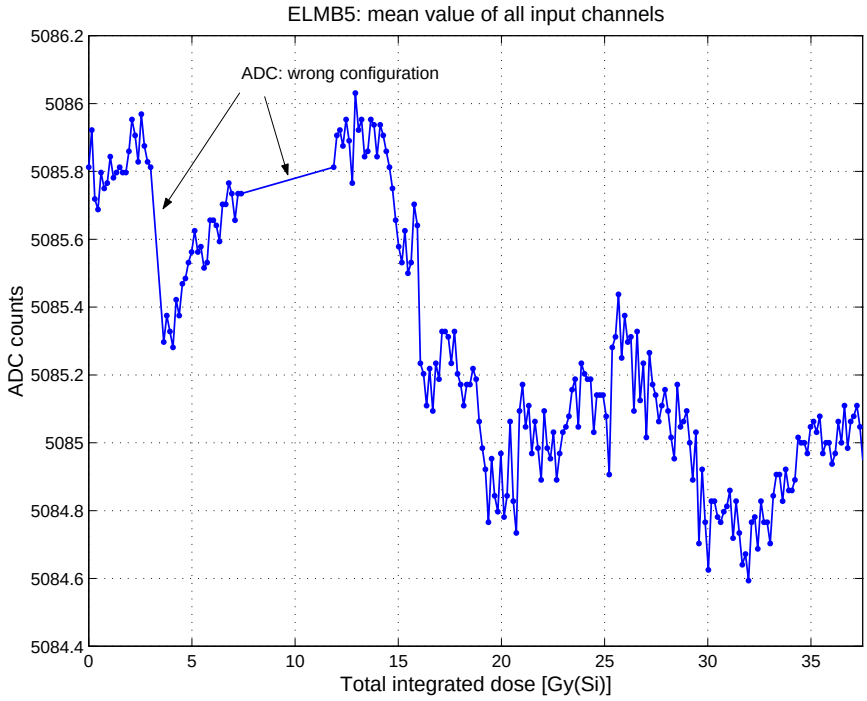

Figure 5.18: *Plot of the mean value for all analog input channels during irradaition.*

After the irradiation of the ELMB the DC voltages on the three voltage regulators, the reference voltage and the buffered reference voltages (operational amplifier output) were measured. The results is shown in table 5.8. All voltages are found to be within the specification. Also the programming function of the two microcontrollers was tested after the irradiation. This test was not done via the CAN programming function, which was used during the reprogramming sequence, but with the ISP programming connector where it is possible to access both the flash and the EEPROM directly. Table 5.9 shows the results from the test. When the master processor (ATmega103) was checked it was found that the entire flash memory was erased to 0xFF except one memory location (byte). After a new programming cycle (erase is done first in this cycle), the entire memory was erased, but it was not possible to program the flash memory. However, it was possible to program the EEPROM (both 0x00 and 0xFF), but it was not possible to erase the EEPROM with the erase command. The erase function seems to be destroyed. The smaller slave processor (AT90S2313) was not tested during the irradiation. It was only tested after the radiation test. The program memory (flash) was read-out and compared with the original program, and no changes were found. The program memory was then erased with an erase command, This command worked, the memory was erased to 0xFF in all memory locations, but it was not possible to reprogram the memory. The programming function was destroyed. The EEPROM erase and reprogramming function worked as normal.

DC voltages measured	Voltage
Voltage regulator MIC5203 CAN (IC 38)	5.013 V
Voltage regulator MIC5203 Digital (IC 37)	3.327 V
Voltage regulator MIC5203 Analog (IC 36)	5.064 V
Reference voltage circuit AD680 (IC 23)	2.498 V
Op-Amp LMC6084 ch0-15 (on motherboard)	2.499 V
Op-Amp LMC6084 ch16-31 (on motherboard)	2.500 V
Op-Amp LMC6084 ch32-47 (on motherboard)	2.503 V
Op-Amp LMC6084 ch48-63 (on motherboard)	2.503 V

Table 5.8: *Voltage measurements of the voltage regulators, the voltage reference circuit and the operational amplifier buffered reference voltage after the irradiation.*

Device	Prog. check	Flash erase	Flash prog	EE erase	EE prog.
ATmega103	-	Pass	Failed	Pass	Failed
AT90S2313	Pass	Pass	Failed	Pass	Pass

Table 5.9: *Test of the programming function of the two microcontrollers on ELMB5.*

5.1.4 Total ionization dose results from the SEE test

The results presented in this section is from the SEE test, but since the positive charged protons creates a TID effect it was natural to present the results in this section.

Device	Integrated dose
ELMB61	43 Gy(Si)
ELMB62	42 Gy(Si)
ELMB63	48 Gy(Si)
ELMB64	43 Gy(Si)
ELMB65	43 Gy(Si)
ELMB66	56 Gy(Si)
ELMB67	53 Gy(Si)
ELMB69	44 Gy(Si)
ELMB70	50 Gy(Si)
ELMB71	41 Gy(Si)
ELMB72	44 Gy(Si)
Average	**46** Gy(Si)

Table 5.10: *The total integrated dose for each ELMB used in the SEE test. It should be noted that the value has been calculated with the total fluence,* Ψ_{tot}.

The setup used in the SEE test is described in detail in section 4.3.1. During the test the three currents was measured for each ELMB. It was two reasons for this, the most important one was to see if the protons had created a SEL. A SEL would cause a rapid current increase in the component that was effected. The second reason was to study the current, to see if any TID effects were created. Experience from the previous TID test has shown that the three most

complex digital circuits (two microcontrollers and the CAN controller) were affected (increased digital current). The currents are presented in figure 5.19, 5.20, 5.21 and 5.22. The ELMB61 shows a rapid current increase in the digital current. This current increase is believed to be caused by a SEL. This is further discussed in section 5.2.1. To get back to the normal current, the ELMB needed to be switched off/on. The ELMB63 shows a rapid current increase in the CAN current, this is caused by extremely high CAN bus activity. Also in this case, the ELMB was switched off/on to regain normal operation. In addition to this abnormal current behavior all currents has some small jumps now and then. This is probably caused by charge deposition in a part of the circuit where the deposition creates an increased current leakage. In total none of the currents that was measured showed any significant increase as the previous TID tests had shown for the digital current. Table 5.10 shows the total integrated dose that each ELMB received during the SEE test. The table shows that all the ELMBs received a larger total integrated dose (average 46Gy(Si)), than the dose which caused the current increase in the previous TID tests. It should be mentioned that the dose has been calculated with the total received fluence, Ψ_{tot}.

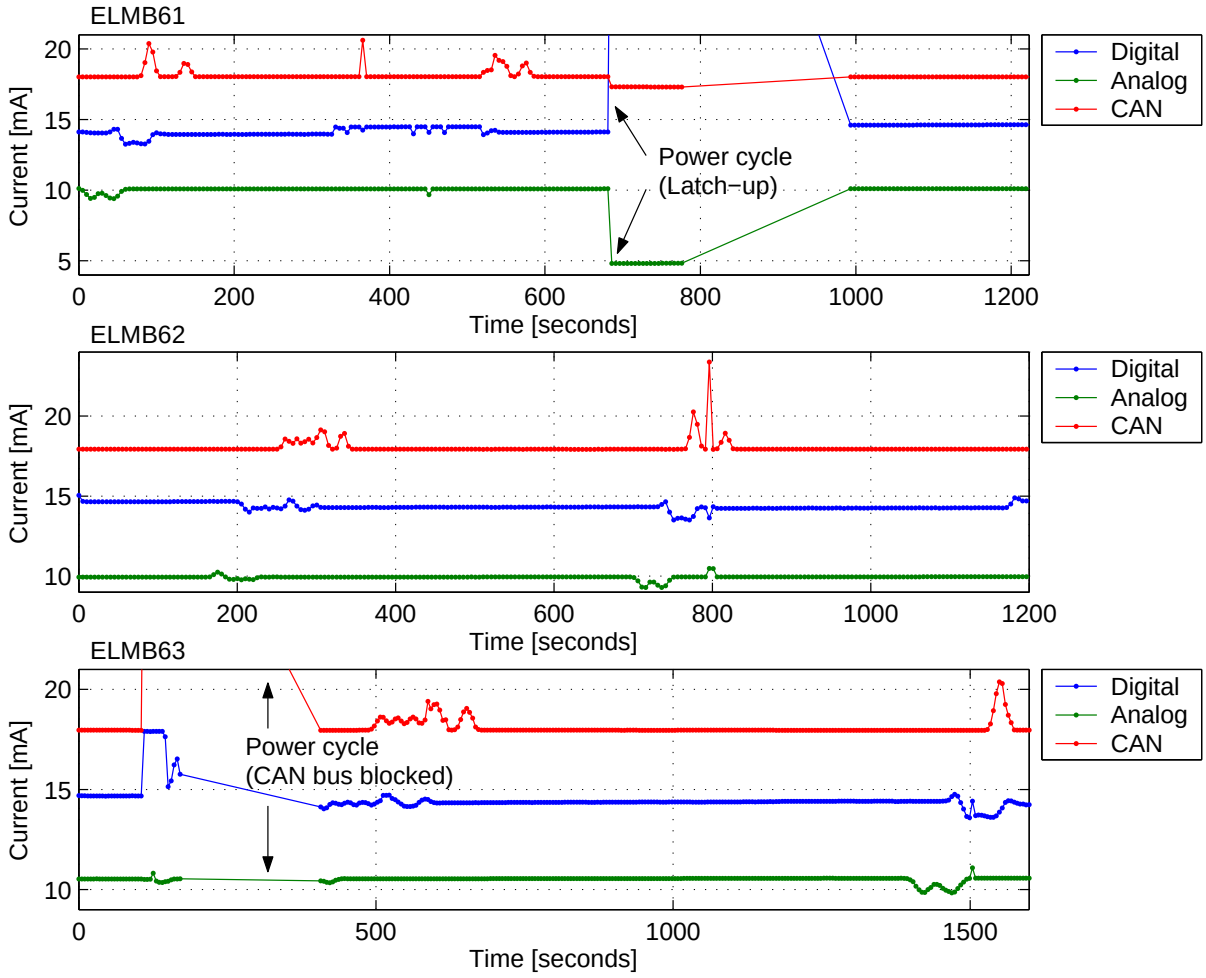

Figure 5.19: *Plot of the analog, digital and the CAN currents for ELMB 61-63 during the SEE test.*

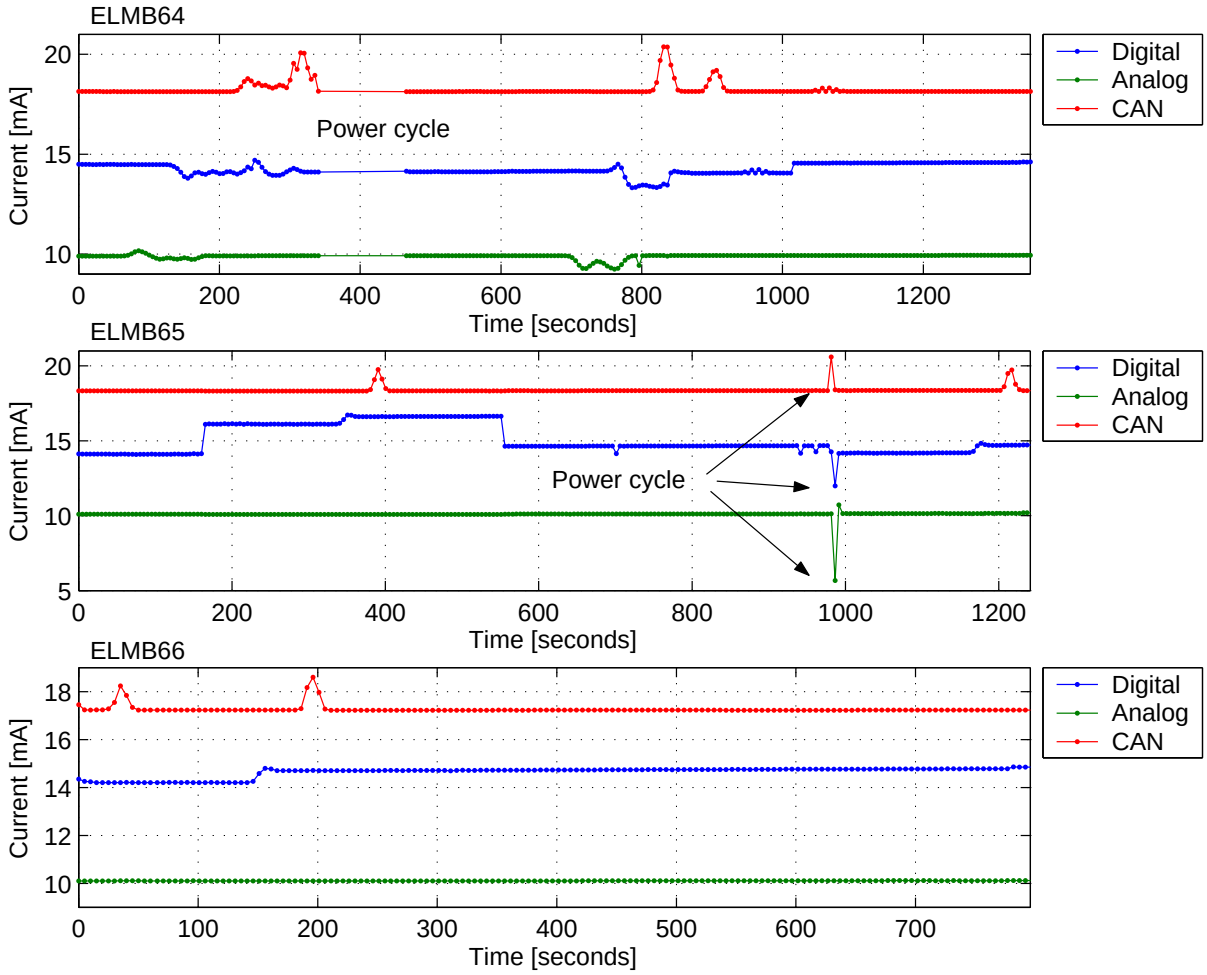

Figure 5.20: *Plot of the analog, digital and the CAN currents for ELMB 64-66 during the SEE test.*

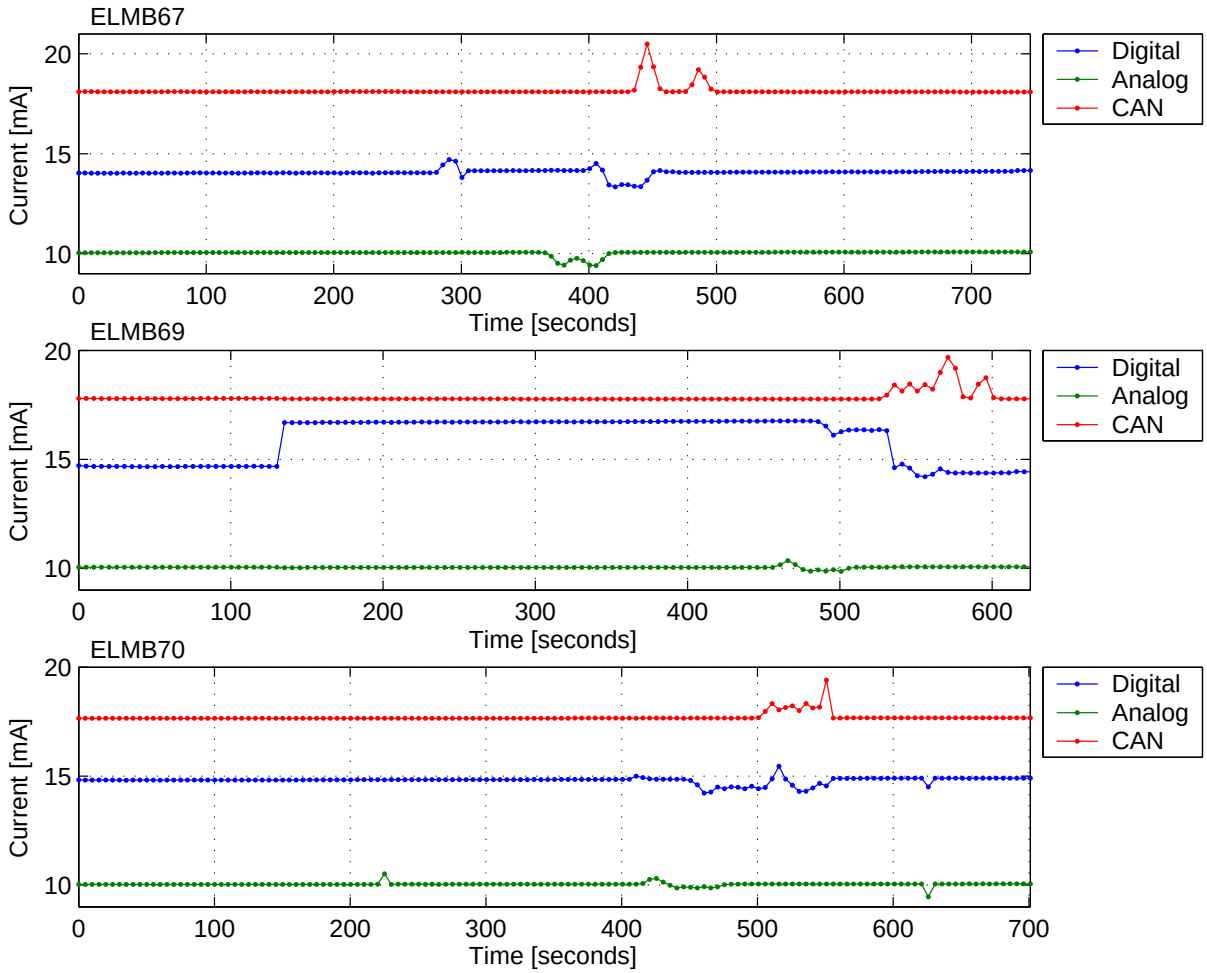

Figure 5.21: *Plot of the analog, digital and the CAN currents for ELMB 68,69,70 during the SEE test.*

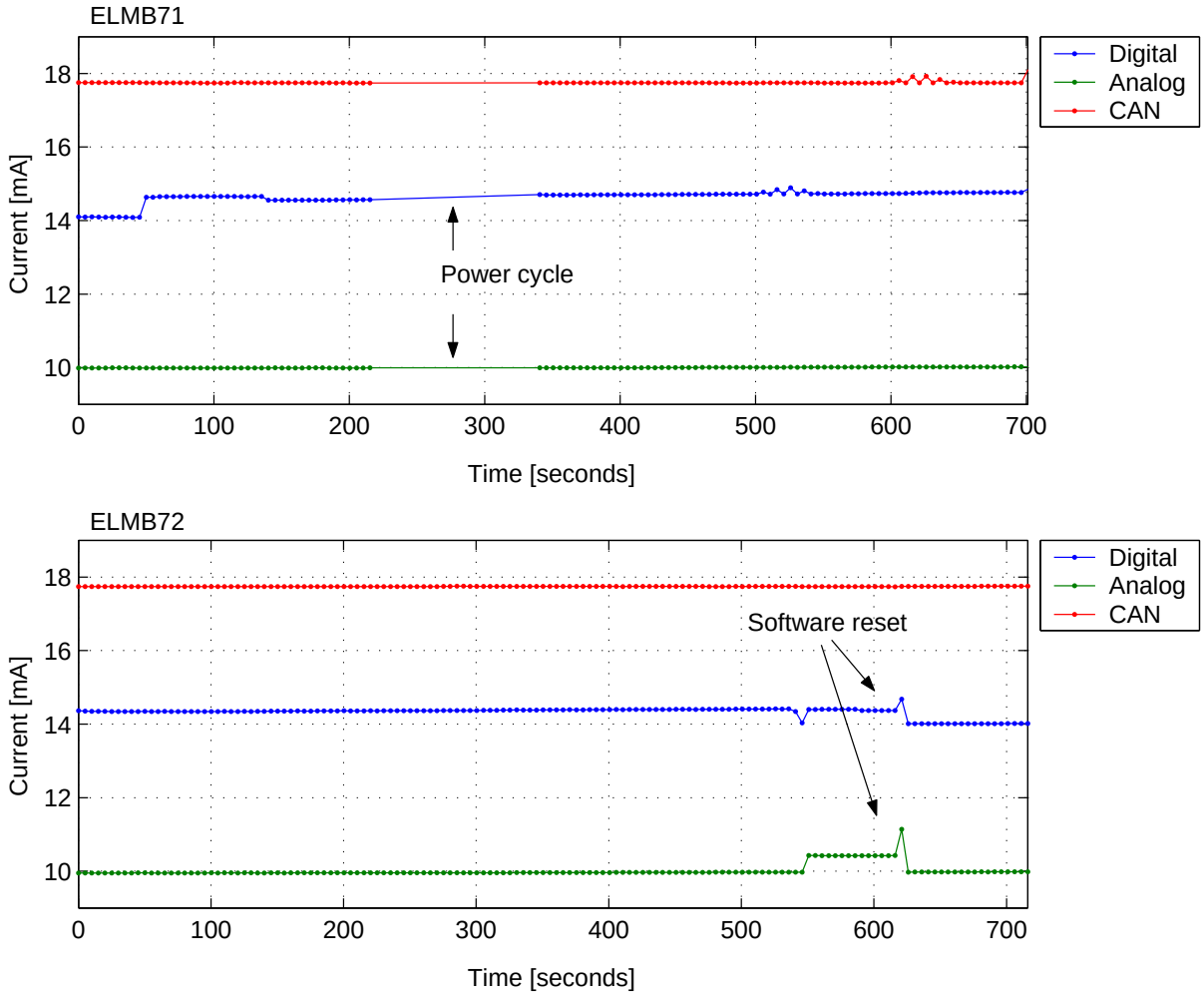

Figure 5.22: *Plot of the analog, digital and the CAN currents for ELMB 71-72 during the SEE test.*

After the irradiation and de-activation of the ELMBs, the three supply voltages and the reference voltage was measured. The buffered reference voltage (output of the operational amplifier) was not measured during this test. The reason for this was that the operational amplifier was not directly irradiated and the operational amplifier used on the motherboard had been tested before, and found not to be radiation tolerant. The measured voltages are summarized in table 5.11, 5.12, 5.13 and 5.14, where the values are compared with the values measured before the irradiation. The reference voltage (AD680JR) is very stable the largest change was 1.7mV, which corresponds to 0.07%. The initial accuracy of this circuit is +2.5V ±10mV, or ±0.4%. The change is well within the specifications for the initial voltage. The largest change found in the voltage regulators (MIC5203) was in the CAN part of ELMB70. The change was 15.3mV, or 0.31%. The absolute output voltage accuracy is specified to be +5V (or +3.3V for the digital part) ±3%. The line and load regulation is specified to be 0.3%. Since the ELMB is designed with the output voltage accuracy of the regulator as the important parameter, the small 0.31% change is considered to be insignificant. In addition to the voltage measurement the programming function on all microcontrollers was tested. All devices passed the test (average integrated dose = 46Gy(Si)).

Device	Before (MIC5203)	After	Change	Change %
ELMB61	4965.9 mV	4974.8 mV	8.9 mV	0.18
ELMB62	4941.0 mV	4945.3 mV	4.3 mV	0.09
ELMB63	5013.3 mV	5024.8 mV	11.5 mV	0.23
ELMB64	4965.3 mV	4972.0 mV	6.7 mV	0.13
ELMB65	4989.5 mV	4998.4 mV	8.9 mV	0.18
ELMB66	4974.4 mV	4982.8 mV	8.4 mV	0.17
ELMB67	4988.6 mV	4993.9 mV	5.3 mV	0.11
ELMB69	5019.8 mV	5026.6 mV	6.8 mV	0.14
ELMB70	5013.3 mV	5024.8 mV	5.0 mV	0.10
ELMB71	4969.4 mV	4977.3 mV	7.9 mV	0.16
ELMB72	4949.2 mV	4952.9 mV	3.7 mV	0.07

Table 5.11: *Measurement of the analog supply voltage before and after the irradiation for all ELMBs.*

Device	Before (MIC5203)	After	Change	Change %
ELMB61	3274.0 mV	3281.4 mV	7.4 mV	0.23
ELMB62	3292.4 mV	3294.4 mV	2.0 mV	0.06
ELMB63	3303.5 mV	3307.7 mV	4.2 mV	0.13
ELMB64	3275.8 mV	3279.9 mV	4.1 mV	0.13
ELMB65	3290.3 mV	3294.2 mV	3.9 mV	0.12
ELMB66	3304.5 mV	3308.3 mV	3.8 mV	0.12
ELMB67	3294.7 mV	3298.3 mV	3.6 mV	0.11
ELMB69	3305.5 mV	3309.7 mV	4.2 mV	0.13
ELMB70	3318.3 mV	3321.9 mV	3.6 mV	0.11
ELMB71	3292.7 mV	3294.7 mV	2.0 mV	0.06
ELMB72	3265.2 mV	3268.7 mV	3.5 mV	0.11

Table 5.12: *Measurement of the digital supply voltage before and after the irradaition for all ELMBs.*

Device	Before (MIC5203)	After	Change	Change %
ELMB61	4958.4 mV	4971.4 mV	13.0 mV	0.26
ELMB62	4934.2 mV	4941.5 mV	7.3 mV	0.15
ELMB63	5008.2 mV	5022.7 mV	14.5 mV	0.29
ELMB64	4984.5 mV	4992.8 mV	8.3 mV	0.17
ELMB65	4966.3 mV	4978.8 mV	12.5 mV	0.25
ELMB66	4973.5 mV	4983.7 mV	10.2 mV	0.20
ELMB67	4973.0 mV	4982.8 mV	9.8 mV	0.20
ELMB69	4998.5 mV	5007.3 mV	8.8 mV	0.18
ELMB70	4976.0 mV	4991.3 mV	15.3 mV	0.31
ELMB71	4945.2 mV	4955.0 mV	9.8 mV	0.20
ELMB72	4961.2 mV	4973.8 mV	12.6 mV	0.25

Table 5.13: *Measurement of the CAN supply voltage before and after the irradiation for all ELMBs.*

Device	Before	After	Change	Change %
ELMB61	2496.7 mV	2497.8 mV	1.1 mV	0.04
ELMB62	2495.0 mV	2493.9 mV	-1.1 mV	-0.04
ELMB63	2493.8 mV	2492.6 mV	-1.2 mV	-0.05
ELMB64	2499.0 mV	2500.1 mV	1.1 mV	0.04
ELMB65	2495.5 mV	2497.2 mV	1.7 mV	0.07
ELMB66	2492.7 mV	2494.3 mV	1.6 mV	0.06
ELMB67	2491.9 mV	2492.6 mV	0.7 mV	0.03
ELMB69	2492.4 mV	2493.6 mV	1.2 mV	0.05
ELMB70	2493.2 mV	2491.8 mV	1.4 mV	-0.06
ELMB71	2495.4 mV	2496.5 mV	1.1 mV	0.04
ELMB72	2494.3 mV	2495.6 mV	1.3 mV	0.05

Table 5.14: *Measurement of the reference voltage (AD680JR circuit) before and after the irradiation for all ELMBs.*

5.1.5 Accelerated ageing test

The accelerated aging test was performed with two ELMBs. The irradiated ELMB3 and an unirradiated ELMB that was labeled ELMB4. When the ELMB3 irradiation ended it was decided that we should test the programming function of the master controller. It turned out that the programming function was lost during the irradiation. Therefore the ELMB was not running as normal in this test. Since the master controller was erased, the slave controller had taken control of the ELMB.

The test was started by placing the ELMBs in the climate chamber at room temperature. It was decided to increase the temperature in steps to see how the ELMBs reacted to the temperature variations, this to avoid destroying the ELMBs by increasing the temperature to fast. The temperature was increased in four steps. In the first step the temperature was increased to 50 °C. As seen on the figure 5.24, the digital current drawn by ELMB3 increased from about 32mA to 38mA, and showed a small decrease as time went by. The unirradaited ELMB4 did not show much change. When the temperature was increased to about 75 °C, the digital current increased again, but even higher. The ELMB4 current did not change much. The ELMBs was left at this temperature for almost 5 days. During these days the digital current (ELMB3) had decreased down to about the same level the test was started at. Again the temperature was increased and the digital current increased about 2mA. After about one day at 85 °C, the temperature was increased to 100 °C. When the temperature was increased to 100 °C the ELMB3 digital current started to pulsate and none of the ELMBs responded to any CANopen command. As seen on the current plot for ELMB4 the current did fall around 7 mA in this last temperature step. The current drop can be explained by the fact that the ELMBs stopped to work properly (the microcontrollers are not running, e.g. it was no clock signal from CAN controller). It should be mentioned that some of the components have a maximum operating temperature of 75 °C. During the cool down the ELMBs became functional again this is shown in the figure were the digital currents increased again. During the cool-down period the ELMB4 digital current went back to its normal value. Also the ELMB3 digital current went back to a normal value, almost the same as before irradiation.

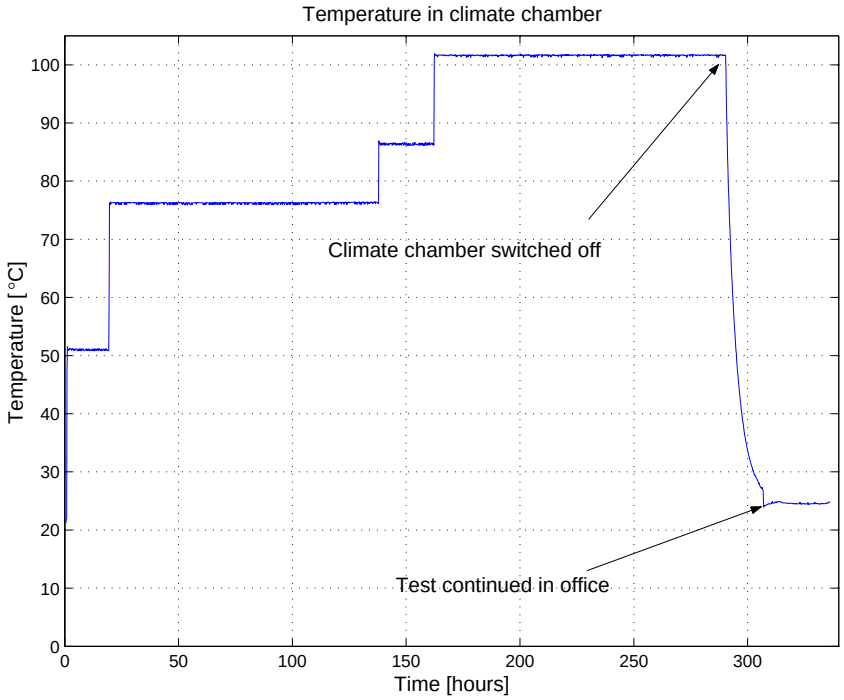

Figure 5.23: *Plot of the temperature in the climate chamber during the accelerated ageing test.*

During the accelerated aging test, the CAN current and the analog current was also measured. Figure 5.25 shows a plot of the analog current for ELMB3 and ELMB4. When the temperature were increased to 50 °C the analog current for ELMB3 dropped about 1mA. The current continued to decrease during the rest of the test, but when the temperature was increased to 100 °C the analog current started to pulsate like the digital current for ELMB3. The analog current for ELMB4 did like the ELMB3 analog current decrease when the ELMBs stopped to work properly. Both currents stabilized at normal values during the cool down period. The CAN currents for ELMB3 and ELMB4 are plotted in figure 5.26. The currents did not change much except for a lower current when the ELMBs was not working properly. Also these currents went back to normal values during the cool down when the ELMBs became operational. Table 5.15 shows results from measurements of the three currents drawn by ELMB3 before irradiation, after irradiation and after the accelerated aging test. After the accelerated aging test, the ELMB3 currents went back to more or less the same currents as measured before the irradiation.

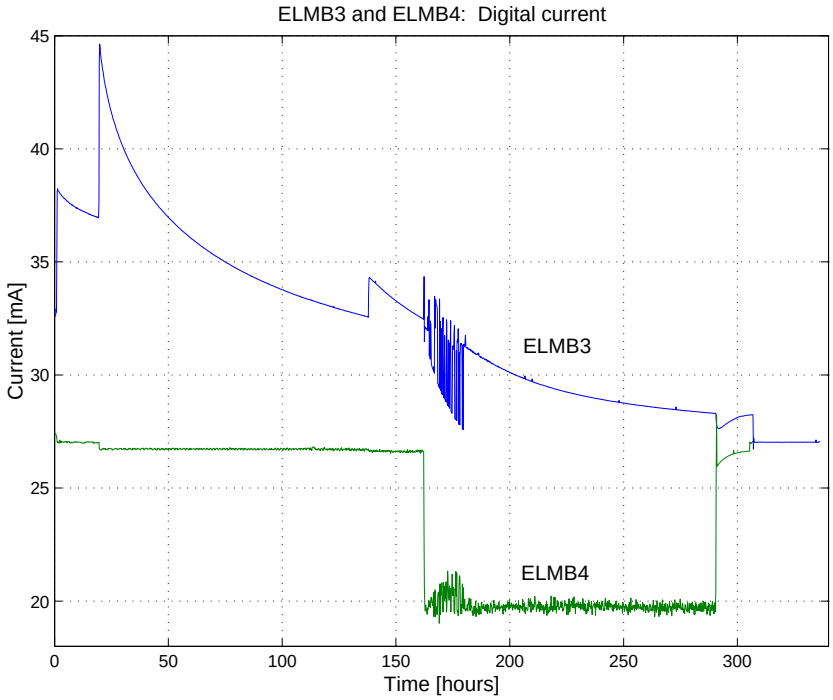

Figure 5.24: *Plot of the ELMB3 and ELMB4 digital currents during accelerated aging test.*

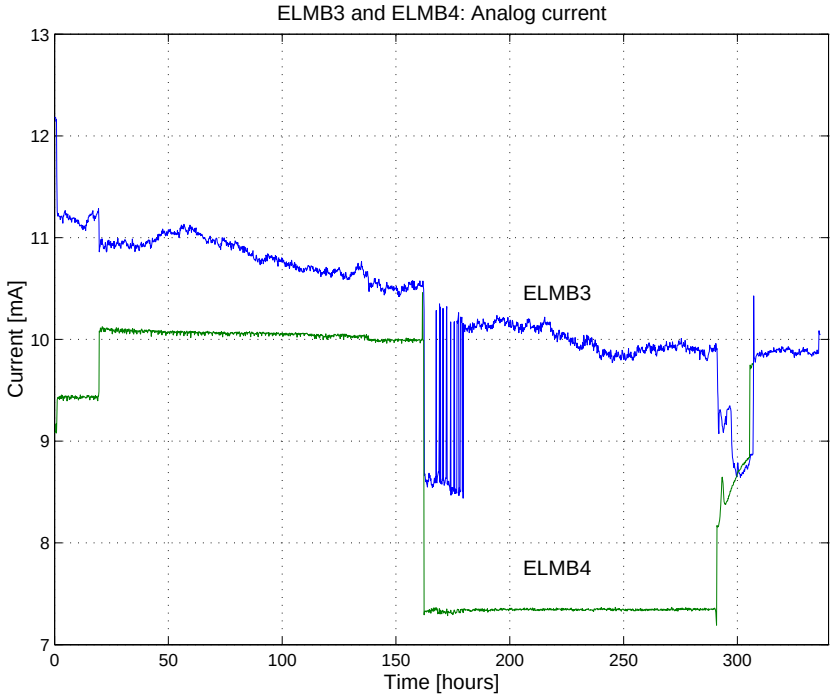

Figure 5.25: *Plot of the ELMB3 and ELMB4 analog currents during accelerated aging test.*

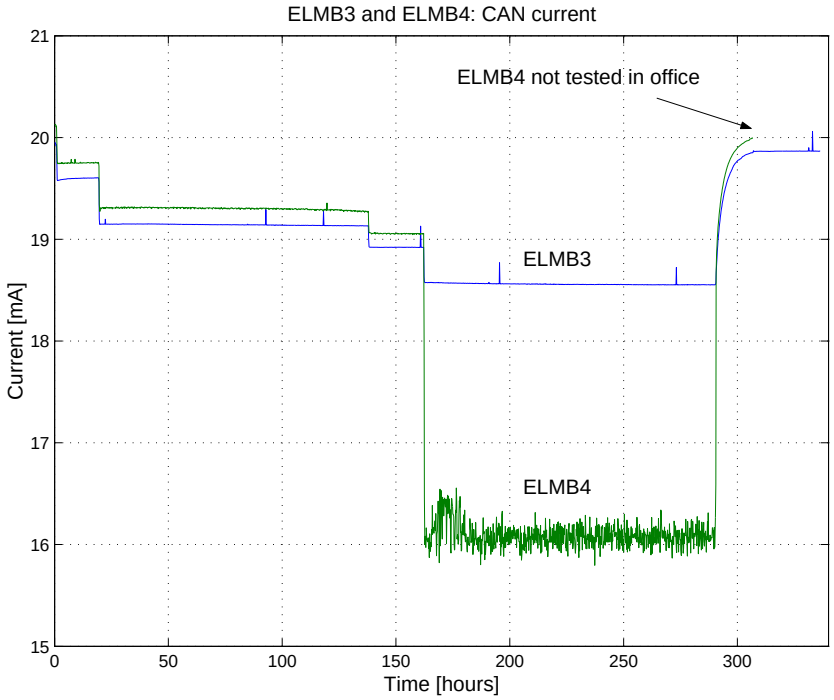

Figure 5.26: *Plot of the ELMB3 and ELMB4 CAN currents during accelerated aging test.*

Supply current	Before	End [43 Gy(Si)]	After ageing test
Digital	27.2 mA	32.4 mA	26.8 mA
Analog	9.6 mA	11.8 mA	9.5 mA
CAN	20.5 mA	20.5 mA	20.4 mA

Table 5.15: *Digital, analog and CAN currents measured on ELMB3 before irradiation, after irradiation and after the accelerated aging test.*

Also the three supply voltages and the reference voltage (also the operational amplifier buffered reference voltage) on ELMB3 was measured before and after the accelerated aging test. The results is shown in table 5.16. All voltages except the voltage reference decreased. When compared with the values measured before the irradiation (table 5.5) the values has recovered more or less back to the original value measured before the irradiation.

DC voltages measured	Before test	After test	Change
Voltage regulator MIC5203 CAN (IC 38)	5004 mV	5000.8 mV	-3.2 mv
Voltage regulator MIC5203 Digital (IC 37)	4961.5 mV	4959.1 mV	-2.4 mV
Voltage regulator MIC5203 Analog (IC 36)	5003.1 mV	4994.7 mV	-8.4 mV
Reference voltage circuit AD680 (IC 23)	2489.0 mV	2490.0 mV	1.0 mV
Op-Amp LMC6084 ch0-15 (on motherboard)	2492.8 mV	2491.3 mV	-1.5 mV
Op-Amp LMC6084 ch16-31 (on motherboard)	2492.5 mV	2491.7 mV	-0.8 mV
Op-Amp LMC6084 ch32-47 (on motherboard)	2491.6 mV	2490.6 mV	-1.0 mV
Op-Amp LMC6084 ch48-63 (on motherboard)	2493.2 mV	2492.4 mV	-0.9 mV

Table 5.16: *Voltage measurements of the voltage regulators and the voltage reference circuit after the irradiation.*

After the test, the ELMBs was inspected and tested. The ELMB4 did not show any sign of the accelerated aging process. It was working normally after the test, which corresponds to about 40000 hours of operation at 25 °C. Before the accelerated aging test was started the programming function of the master controller was checked. The test showed that the programming function had failed during the irradiation. After the accelerated aging test the programming function was tested again. The programming function was now working as normal and it was possible to load the firmware into the flash memory. The ELMB3 was reprogrammed and tested with the same test setup as used during the irradiation. It was found to be fully working.

5.1.6 Summary of the TID measurements

In total, four different TID tests has been performed. The purpose of the first test was to gain some experience with the test procedure, and with the ELMB in a radioactive environment. Both ELMBs used in this test showed a rapid increase in the digital current after the ELMBs had received an integrated dose of about 35Gy(Si). Investigation of the ELMBs showed that the three most complex digital circuits (the two microcontrollers and the CAN controller) was affected by the γ-ray radiation. Also the programming function in the microcontrollers was lost. Since the dose-rate at the first test was quite high (77Gy(Si)/h) it was decided to redo the test at a lower dose-rate. This decision was based on previous results from Temic [29], which showed that the dose-rate could have a great impact on the current increase (leakage). The second test was done at the GIF at CERN. At this facility the test was done with a much lower dose-rate, the dose-rate was 0.48Gy(Si)/h. The measurements from this test showed that the digital current started to increase at more or less the same total integrated dose as with the two first ELMBs. Also in this test the programming function in the microcontrollers was lost.

The third TID test was done to investigate at which total integrated dose the programming function in the microcontrollers was lost. This test was also done at the GIF. The ELMB was irradiated with a dose-rate of 0.45Gy(Si)/h (theoretical), but the source was not on all the time. The ELMB was irradiated in periods with the source on for about 10 hours and off for the next 14 hours. After each irradiation period the programming function was tested. The programming function was lost after the ELMB had received an integrated dose between 33.8Gy(Si) and 37.9Gy(Si). The digital currents from the first three TID tests is shown in figure 5.27.

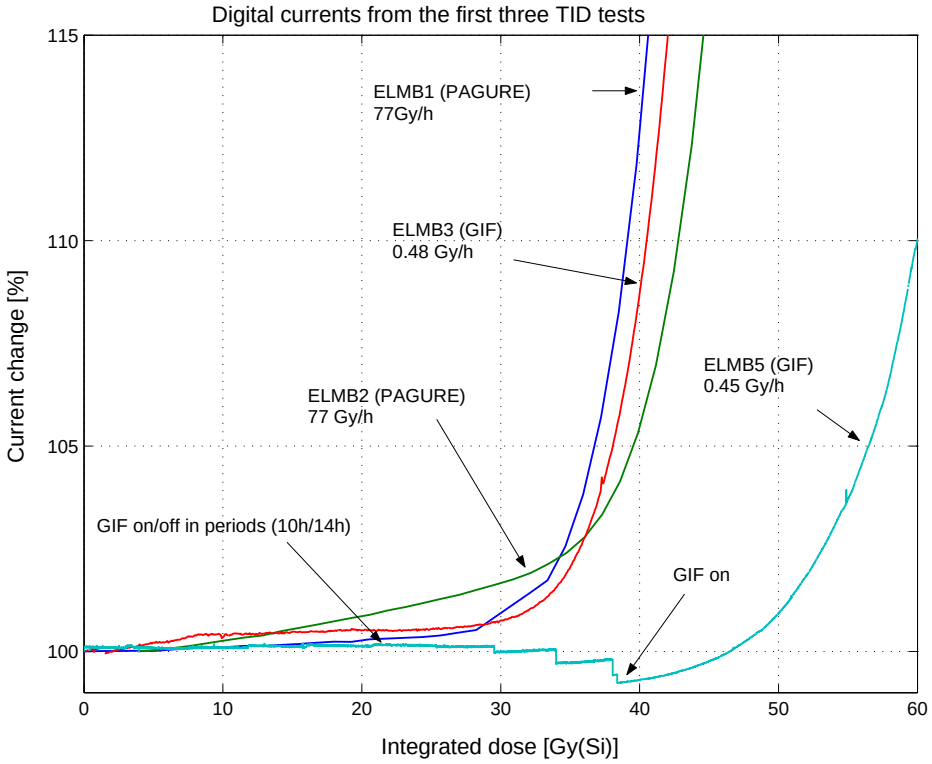

Figure 5.27: *Plot of the digital current from the three first TID tests (ELMB1, ELMB2, ELMB3 and ELMB5).*

The CAN current was not measured during the ELMB1 and ELMB2 test. This was because there was something wrong with the measurement equipment. However, the currents were measured before and after the irradiation. Table 5.17 compares the CAN currents from the three TID tests. The ELMB2 current was more or less unchanged, while the ELMB1 current had increased a bit. The magnetic coupler ADuM1100 caused this current increase. The CAN currents from the ELMB3 and ELMB5 test did not change much. As seen there is current drop in the ELMB1 CAN part after 48 hours. This is probably caused by an annealing effect in the ADuM1100 magnetic coupler.

Device	Received dose	Current before	Current after	After 48 hours
ELMB1	85 Gy(Si)	14 mA	28 mA	32 mA
ELMB2	94 Gy(Si)	19 mA	19 mA	19 mA
ELMB3	43 Gy(Si)	20.5 mA	20.5 mA	n/a
ELMB5	38 Gy(Si)	18.1 mA	18.2 mA	n/a

Table 5.17: *Comparison of the CAN currents measured during the first three TID tests.*

The analog current was not directly measured during the ELMB1 and ELMB2 test. These currents were measured together with the digital current during the test, but were measured individually before and after the irradiation. Table 5.18 shows a comparison of the analog currents from the three TID tests. Detailed measurements showed that there is a small increase in the analog current. This is clearly shown for the ELMB3 where the current increase is 2.5mA

after 43Gy(Si), and the ELMB5 test where the current increase is 75μA after 38Gy(Si).

Device	Received dose	Current before	Current after	After 48 hours
ELMB1	85 Gy(Si)	7 mA	7 mA	n/a
ELMB2	94 Gy(Si)	9 mA	10 mA	9 mA
ELMB3	43 Gy(Si)	9.5 mA	12 mA	n/a
ELMB5	38 Gy(Si)	7.42 mA	7.5 mA	n/a

Table 5.18: *Comparison of the analog currents measured during the first three TID tests.*

Table 5.19 shows a comparison of the digital currents measured during the TID tests. As seen there is a large current increase in the digital currents. The ELMB5 current shows a small decrease. This current did actually decrease in the first part of the test where the source was on in periods, but the current started to show a rapid increase after the programming function of the microcontrolles was lost. Another interesting observation is the decrease in the ELMB2 current after 48 hours. This effect was also observed for ELMB5 when it was left to anneal (not shown in table).

Device	Received dose	Current before	Current after	After 48 hours
ELMB1	85 Gy(Si)	7 mA	121 mA	n/a
ELMB2	94 Gy(Si)	35 mA	130 mA	118 mA
ELMB3	43 Gy(Si)	27.2 mA	32.3 mA	n/a
ELMB5	38 Gy(Si)	14.1 mA	13.9 mA	n/a

Table 5.19: *Comparison of the digital currents measured during the first three TID tests.*

During the SEE test all three currents was measured for each ELMB. The current change from the beginning of the test and after the test was in general very small, but during the test some small current jumps was observed. The standard deviation for each current has been calculated and the values are plotted in figure 5.28. As seen the changes are quite small.

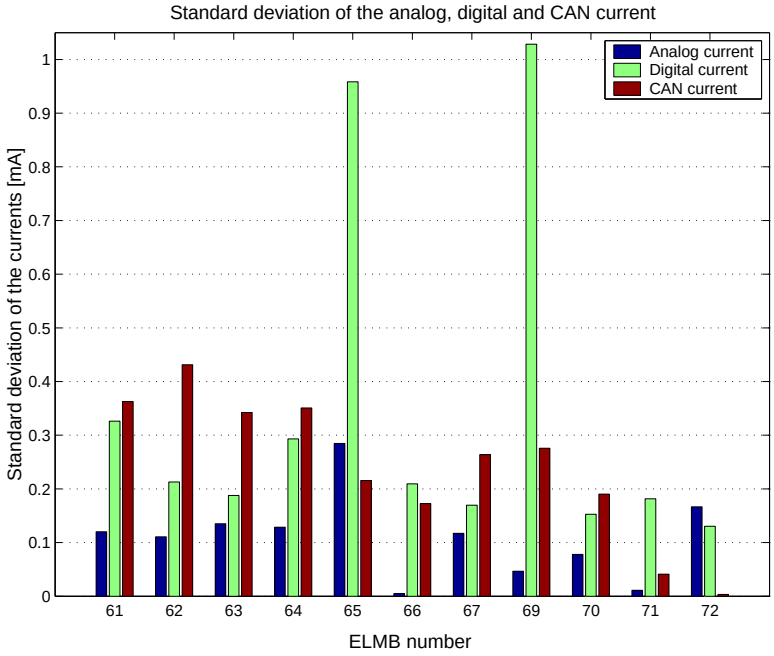

Figure 5.28: *Plot of the standard deviation of the analog, digital and CAN currents from the SEE test.*

During the ELMB1 test the CAN bus was blocked. The ELMB1 had magnetic couplers between the digital part and the CAN part, while all other ELMBs used opto-couplers. It is believed that the ADuM1100 magnetic coupler is responsible for this blockage. This could probably happen in at least two ways. The coupler is defective and is holding the CAN transmission lines at a dominant level. This would prevent other node to access the bus. A second possibility is that the digital current was limited by the voltage regulator (the microcontrollers, the CAN controller and the magnetic coupler caused an increased current), this caused the magnetic coupler to stop working, and the CAN bus lines was held at the dominant level. This would create the same scenario as described for the first possibility. Anyway, this was a test to see if this new device was a good replacement for the opto-couplers. With the increased current and this failure, the device was ruled out as a replacement for the opto-coupler.

The three supply voltages and the reference voltage were measured before and after the SEE test. The change is plotted in figure 5.29 and 5.30. The reference voltage is quite stable. The worst case change is about 0.07%. The worst case voltage change for the MIC5203 voltage regulator was about 0.35%. All supply voltages showed an increase, while the reference voltage did change in both positive and negative direction.

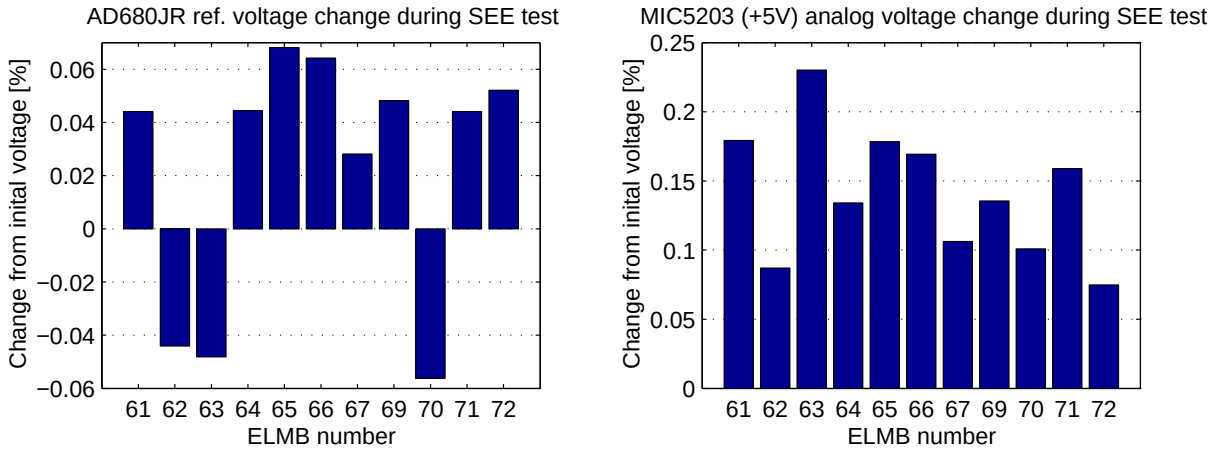

Figure 5.29: *Plot of the voltage change on the reference voltage and the analog supply voltage during the SEE test.*

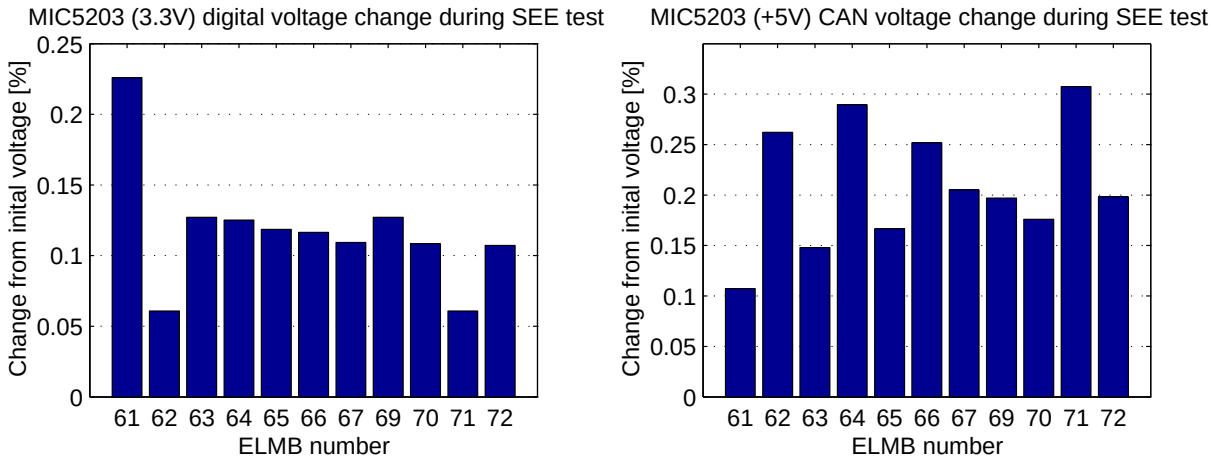

Figure 5.30: *Plot of the voltage change on the digital supply voltage and the CAN supply voltage during the SEE test.*

The voltages for the regulators and the voltage reference circuit were also measured during the TID tests. The voltage change on the three regulators and the voltage reference was also measured on ELMB3. The worst-case change of the MIC5203 regulator was about 0.7%. The reference voltage (AD680 = Bipolar circuit) is very stable. The change was only 0.004%. The measurements from the TID tests showed that the supply voltages (MIC5203) and the reference voltages (AD680) were within the specification given in the product datasheets [37], [42].

The ADC read-out for ELMB1 showed a drift. This drift is explained by the fact that the analog supply voltage was used as the reference voltage on the motherboard (the voltage that fed the analog input channels). The ELMB2 and ELMB3 showed a significant lower drift in the analog read-out. The standard deviation of the analog input values for ELMB2 is shown in figure 5.31 while the standard deviation for the analog inputs for ELMB3 is shown in figure 5.32. It should also be noted that the drift in the ADC can be even smaller if a re-calibration sequence is done on the ADC on a regularly basis. This can be seen from the ELMB5 ADC read-out. During the

ELMB5 test the ADC was re-calibrated after each reprogramming sequence. Figure 5.33 shows the standard deviation of the analog input values for ELMB5. When the ADC was tested, it was configured with an input rage of 1V a conversion frequency of 1.88Hz and it was operating in the unipolar mode. This gives an ADC LSB of 15.3μV. A comparison between the figures shows that there is a large reduction in the standard deviation if the ADC is re-calibrated on a regular basis.

It should be pointed out that the operational amplifier that is used as a current buffer for the reference voltage (LMC 6064, National Semiconductor) is not radiation tolerant. This part has been tested earlier [31], but the results was not known when the TID tests was done.

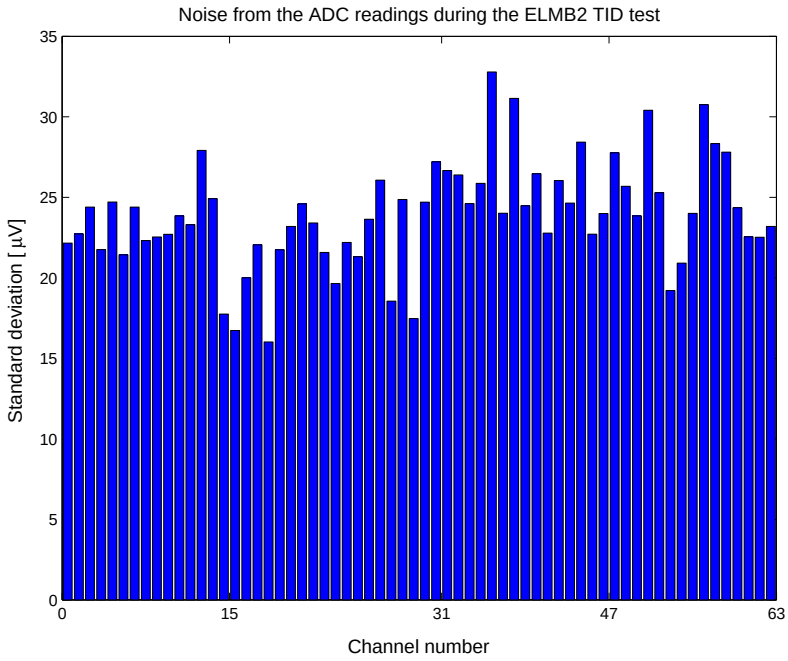

Figure 5.31: *Plot of the standard deviation for the analog input channels for ELMB2 during the TID test.*

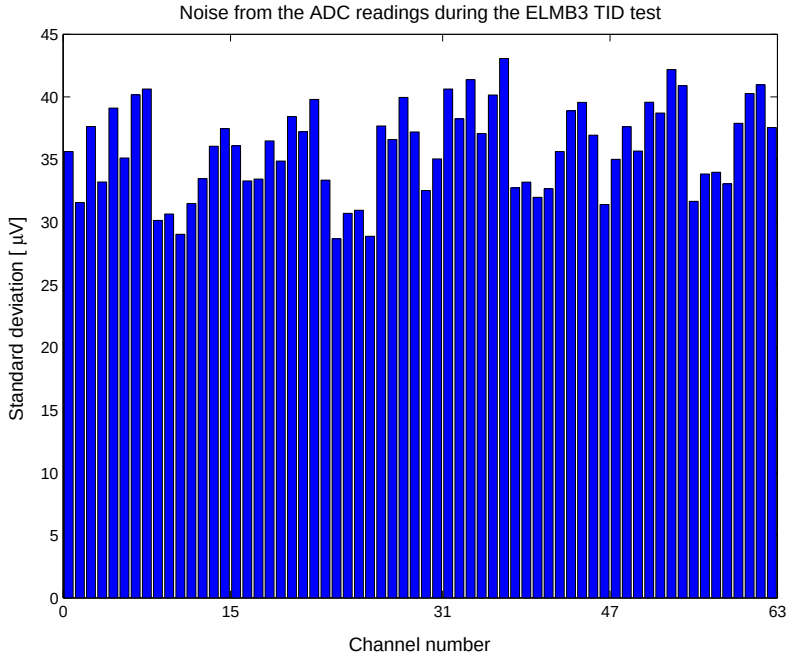

Figure 5.32: *Plot of the standard deviation for the analog input channels for ELMB3 during the TID test.*

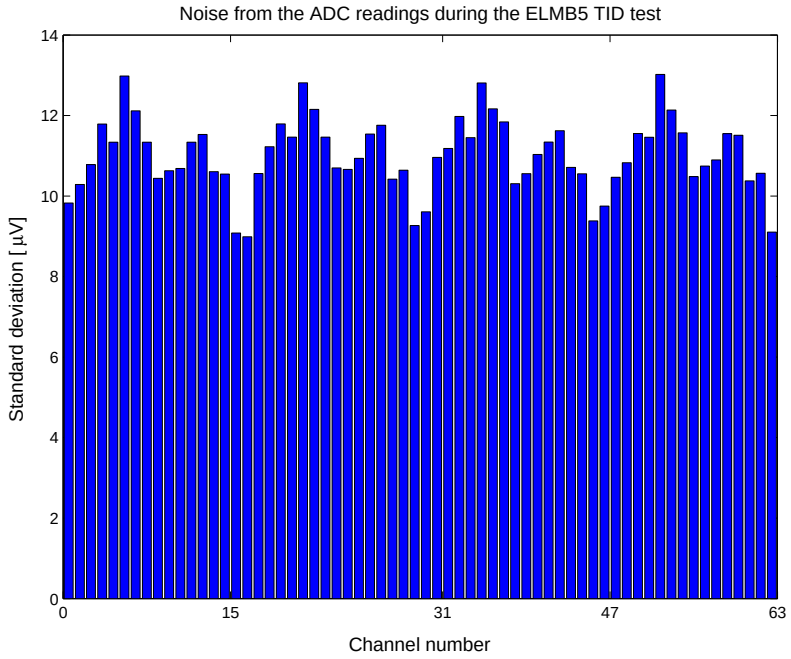

Figure 5.33: *Plot of the standard deviation for the analog input channels for ELMB5 during the TID test.*

During the TID tests it was found that the programming function of the microcontrollers was lost. The microcontrollers should not be exposed to a higher dose than around 30Gy(Si) (γ-ray irradiation) otherwise the programming function might be lost.

The programming function of the microcontrollers was also tested after the SEE test. In this test non-of the microcontrollers was affected by the proton irradiation even though the average total integrated dose was 46Gy(Si). It seems that there is a difference between the γ-ray radiation and the proton radiation concerning the charge build-up in the components.

According to the "ATLAS Policy on Radiation Tolerant Electronics" [14], the low dose rate effects can be simulated by performing an accelerated aging test at 100 °C for 168 hours. An accelerated aging test on one irradiated and on unirradiated ELMB has been performed. To minimize the stress on the electronics and to observe the temperature effect the temperature was increased in four steps to the final temperature of 100 °C. The test lasted for about 360 hours. This corresponds to about 40000 operating hours at 25 °C. The temperature increase did not have much impact on the unirradiated ELMB. Except that the ELMB stopped working when the temperature was put to 100 °C. It should be noted that many of the components used in the ELMB has a maximal operating temperature of 75 °C. However, the temperature did have a major impact on the irradiated ELMB. The essence of the test was that the digital and the analog currents for the irradiated ELMB went back to normal values as measured before the irradiation. In addition to the current decrease the programming function of the affected microcontrollers was recovered. The irradiated ELMB was also reprogrammed (master controller) and was found to be fully working. In this accelerated aging test no problems were found, and the components did not show any low dose-rate effect.

As described in chapter 3, γ-ray radiation can have a degrading effect on CMOS components. Table 5.20 shows a summary of the components used on the ELMB and the problem which was measured. As seen the CMOS components showed the largest change.

Device	Technology	Comment
ATmega103	CMOS	Increased current/loss of prog. function
AT90S2313	CMOS	Increased current/loss of prog. function
SAE81C91	CMOS	Increased current
MIC2754	CMOS	No functional effect[a]
MIC5203	CMOS	Voltage drift
74HC1G66	CMOS	No functional effect[b]
ADP3607	CMOS	Not measured[d]
NC7SZ00	CMOS	No functional effect[b]
MAX4582	CMOS	No functional effect[c]
CS5523AS	CMOS	No functional effect[c]
MAX871	CMOS	No functional effect[e]
74HC1G14	CMOS	No functional effect[b]
74HC74ADT	CMOS	No functional effect[b]
ADuM1100	CMOS	Increased current
ADP680	Bipolar	Very stable
BAT54W	Bipolar	No functional effect[c]
PCA82C250	Bipolar	No functional effect[c]
BAV70W	Bipolar	No functional effect[c]
HCPL0601	Opto	No functional effect[c]
HCPL0731	Opto	No functional effect[c]

[a] This components could not be measured directly since the ELMB was tested as a complete system. This component should be tested separately if detailed information is required.

[b] These components is logic circuits. No errors in the ELMB could be traced to any of these components. However, if it is necessary to check if the logic levels is within the specification (e.g. input and output levels) it is necessary to do a test on the components separately.

[c] These components did not show any problems during the TID test. Since the ELMB was tested as a complete system it was just possible to measure the functionality of these components.

[d] This component is an auxiliary voltage generator (regulator) and was not involved in the ELMB test.

[e] The negative 5V voltage was never measured, but the ADC and the multiplexers which uses the voltage did not show any problems.

Table 5.20: *Summary of the various effects that the TID test had on the components which is used in the ELMB design.*

The bipolar components used in the ELMB design did not show any problems during the TID test. Especially the voltage reference circuit (AD680) is very stable.

The components used in the ELMB design has not been tested individually, but has undergone a functional test. Due to this not all parameters could be measured on each component.

TID results compared to the TID requirements

The limiting factor in the ELMB is the rapid increase in the digital current and the loss of the programming function in the microcontrollers. The rapid current increase started when the ELMB had received an integrated dose of about 35Gy(Si). The programming function of the microcontrollers was also lost at around 30-35Gy(Si), the data from the SEE test showed that the ELMB could withstand a higher dose, but we should use the worst-case results when we compare the results to the requirements. This means that the ELMB has a TID acceptance of about 30Gy(Si). To be able to qualify the ELMB for the TID, it is necessary to use the safety factors given in table 5.21. These safety factors gives a RTC_{TID} of 22Gy(Si). There is still a small margin until the 30Gy(Si) limit is reached. Table 5.22 gives a summary of the different TID tests concerning the dose-rates, the observed problem, the integrated dose where the problem occurred and the total integrated dose which was received by the device under test.

Test	**SRL_{sim}**	**SRL_{ldr}**	**SRL_{lot}**
TID	$\times$ 3.5	$\times$ 1.0	$\times$ 1.0

Table 5.21: These safety factors can be used when the extended qualification test is performed, and homogeneous component batches are used in the ELMB.

The use of these safety factors implies that the extended TID test must be performed during the TID qualification. In other words, the test must me done on a homogeneous component batch and the accelerated aging test must be performed.

Test	**Dose-rate/Φ_p**	**Effect**	**Problem dose**	**Total dose**
$TID1_1$	77 Gy(Si)/h	Inc. current/loss of prog. func.	35-40 Gy(Si)	85 Gy(Si)
$TID1_2$	77 Gy(Si)/h	Inc. current/loss of prog. func.	35-40 Gy(Si)	94 Gy(Si)
TID2	0.48 Gy(Si)/h	Inc. current/loss of prog. func.	35-40 Gy(Si)	43 Gy(Si)
TID3	0.45 Gy(Si)/h	Inc. current/loss of prog. func.	$\sim$35 Gy(Si)	80 Gy(Si)
SEE	5×10^7 p/cm^{2}s	No effect	-	46 Gy(Si)

Table 5.22: *Summary of the dose-rates, the integrated dose and the problems the was observed.*

5.2 Single event effect test results

In this section the results from the SEE test is presented, except the results related to the TID effect. The TID part of the SEE test have already been discussed. The results are treated as individual faults, the effect of the SEE, and the possible solution to the SEE problem in the affected component. During the test the digital input lines (PORTF) was left unconnected (floating). After the analysis of the data this turned out to be a good indication of the on/off time of the proton beam. Normally the input lines would be read as logic "0", but this was not the case when the proton beam was turned on. The input value changed to a logic "1". This is shown in figure 5.34. The figure shows the input port of ELMB63. The time scale on this figure is the recorded time in the CAN analyzer. In the following, the time scale is called "time". This is the test time for each ELMB. During this time the proton beam was on, but in some cases the beam was shut off due to recovery from various problems, e.g. fault requiring a power cycle.

Table 5.23 shows the total fluence, Ψ_{tot}, and the effective fluence, Ψ_{eff}, received by each ELMB during the test. The effective fluence is the flunce received by the device when the test software was running (e.g. protons received during a power cycle or a node hang is not included). This fluence is used in the following cross-section calculations.

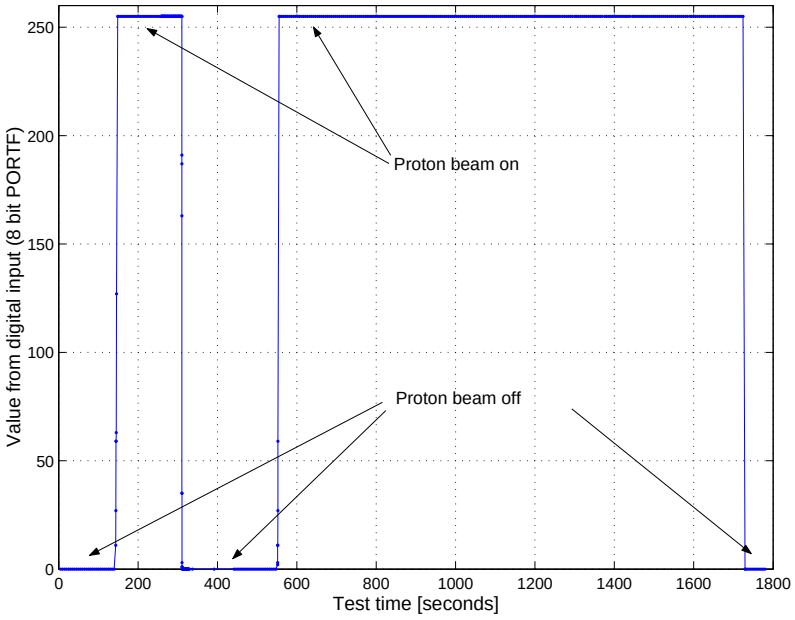

Figure 5.34: *Plot of the byte value read from the input port during the SEE test for ELMB63.*

Device	Total fluence, Ψ_{tot}	Effective fluence, Ψ_{eff}
ELMB61	3.07×10^{10} p/cm^2	2.43×10^{10} p/cm^2
ELMB62	3.00×10^{10} p/cm^2	3.00×10^{10} p/cm^2
ELMB63	3.42×10^{10} p/cm^2	2.42×10^{10} p/cm^2
ELMB64	3.09×10^{10} p/cm^2	2.86×10^{10} p/cm^2
ELMB65	3.11×10^{10} p/cm^2	3.10×10^{10} p/cm^2
ELMB66	4.00×10^{10} p/cm^2	4.00×10^{10} p/cm^2
ELMB67	3.75×10^{10} p/cm^2	3.75×10^{10} p/cm^2
ELMB69	3.12×10^{10} p/cm^2	3.12×10^{10} p/cm^2
ELMB70	3.54×10^{10} p/cm^2	3.02×10^{10} p/cm^2
ELMB71	2.91×10^{10} p/cm^2	2.03×10^{10} p/cm^2
ELMB72	3.18×10^{10} p/cm^2	3.18×10^{10} p/cm^2
Sum	$\mathbf{3.86 \times 10^{11}}$ p/cm^2	$\mathbf{3.39 \times 10^{11}}$ p/cm^2

Table 5.23: *List of the total and the effective fluence for each ELMB. The total fluence it the overall fluence received by the device, and the effective fluence is the fluence received while the test software was running.*

5.2.1 Functional test of the microcontrollers and the CAN controller

During the SEE test only the master processor was checked for SEE. In addition, the programming function of both controllers was checked after the test. This was done to see if the TID effect had any influence on the programming function. It was also of great interest to find out which memory type that was sensitive to upsets. The SRAM memory and registers was expected to be most sensitive to SEE. During the test 2k bytes of SRAM was checked on each ELMB every fifth second. In total there were reported 2312 single bit-flips and 3 double bit-flips in the SRAM (a single bit-flip is where only one bit has changed in the tested byte). Figure 5.35 shows two graphs of the bit flips in the SRAM. The bit-flips are shown for bit-flips from logic "1" to "0" and from logic "0" to "1" for each bit in the byte that was checked. The graphs shows that there was about the same number of bit-flips from "1" to "0" (1169 bit-flips) as from "0" to "1" (1149 bit-flips). The bits were also more or less evenly affected in each byte.

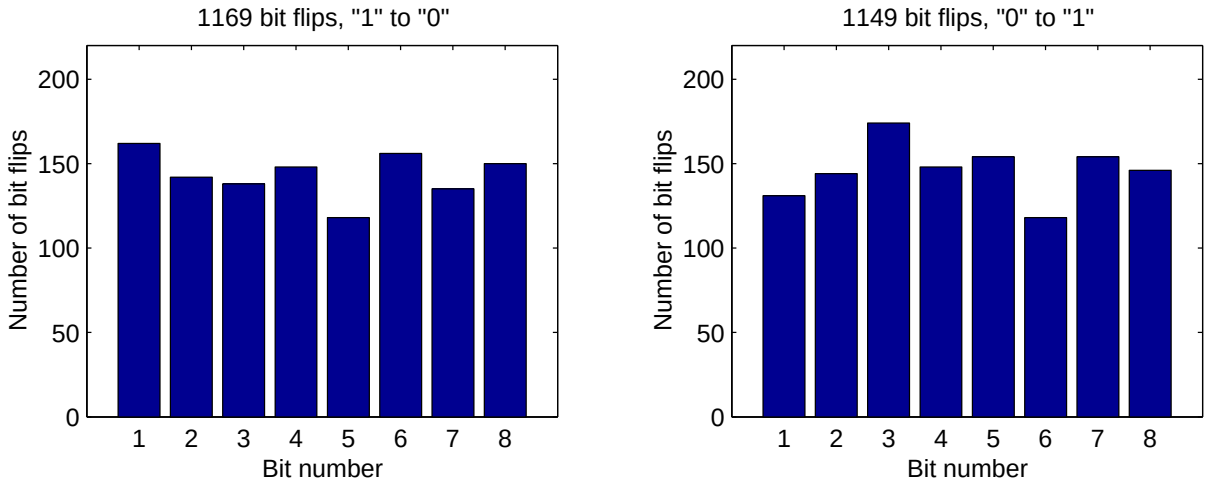

Figure 5.35: *Changes in the SRAM for all ELMBs during the test. The figures shows the number of bit-flips for each bit in the data byte that changed from a logic one, to a logic zero, and vice versa.*

During the irradiation, the eleven ELMBs received an effective fluence of 3.39×10^{11} protons/cm^2. This gives a total cross-section of 4.17×10^{-13} cm^2/bit for the SRAM. This is illustrated in the second plot in figure 5.36. As seen the number of SEE follows the proton/cm^2 with a linear increase. This is also the case when the proton flux was increased from 2.5×10^7 protons/cm^{2}s to 5×10^7 protons/cm^{2}s. The flux increase was done after the first 5 ELMBs was irradiated, which corresponds to a fluence of about 1.5×10^{11} proton/cm^2. The first plot shows the distribution of the detected SEE in the tested 2k bytes of SRAM. It is clear that the errors seem to be distributed evenly over the tested address space (0x400 to 0xBFF). Figure 5.37 shows the number of SEE versus the address. The figure shows that almost every SRAM location has received at least one bit-flip.

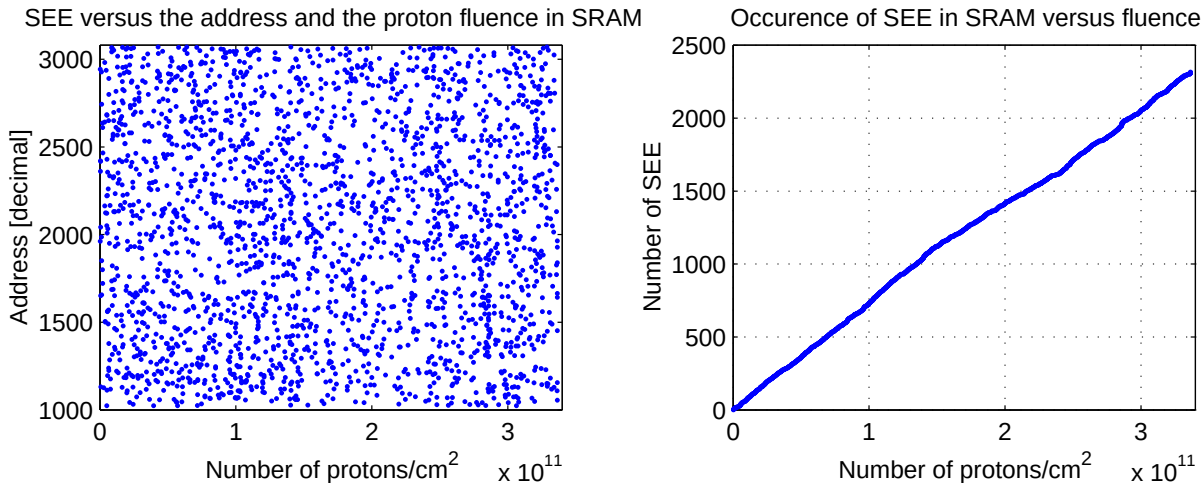

Figure 5.36: *Plot of the distribution of the errors in the SRAM, and the number of errors during the irradiation for all ELMBs.*

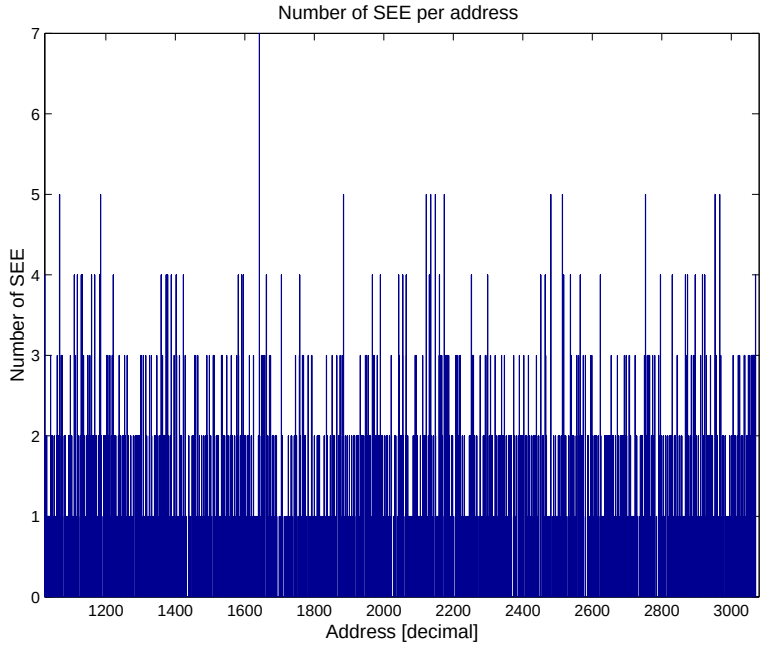

Figure 5.37: *The total number of bit changes versus the SRAM address for all ELMBs.*

The SEE test also involved a test of the EEPROM. During each test cycle 3.5k bytes of the EEPROM was tested. Not a single bit flip was reported in this test. Also the flash memory was tested. 64k bytes of the available 128k bytes were tested during each test cycle. In this test it was reported two errors. The errors was reported by one error summary message which is supposed to be sent after the error reports as described in section 4.3.2. The data collected did not show any error reports before the summary message. This is probably caused by a SEE bit-flip in some of the SRAM/registers used during the flash memory test cycle. After the test the entire flash memory of all ELMBs was tested, but no errors was found. This means that the

summary message received from the flash memory of ELMB65 was a false error.

Errors that affected the operation of the ELMB

In addition to the mentioned errors in the SRAM there were a few errors that affected the operation of the ELMB. The errors and a description of how the errors were cancelled are given in the following list.

1. During the ELMB61 test, a rapid current increase in the digital power supply was observed. This is believed to be a SEL (single event latch-up). Since the ELMB is equipped with current limiting voltage regulators the current was limited and the ELMB was not damaged, but the operation was interrupted and a power off/on cycle was needed to regain control of the ELMB.

2. The period between each test cycle was defined to be 5 seconds. This period was implemented by using a timer in the master controller (ATmega103). During the irradiation, this period changed for four of the ELMBs. The affected ELMBs was ELMB61 (period changed to 21 s), ELMB65 (period changed to 21 s) ELMB70 (period changed to 37 s) and ELMB72 (period changed to 85 s). For ELMB61, ELMB70 and ELMB72 this problem was solved by doing a software reset of the ELMB (sending a CANopen "reset node" command). The ELMB65 was reset, by doing a power cycle sequence. This was done by a mistake. The increased cycle period is shown in the ADC readings in section 5.2.2.

3. The ELMB71 stopped sending messages from the test cycles. A software-reset command was sent, but the ELMB did not respond. The ELMB was reset by performing a power off/on cycle. The currents was still read while the ELMB was not responding so the CAN bus was still operational. The missing data can be seen in the plot for the ADC read-out where there is missing values.

4. The ELMB software did also poll the digital input lines PORTF during the test. This function is part of the original ELMB software and did not have anything to do with the SEE test, but it turned out that a SEE changed the polling interval. The polling interval was changed to 1mS. This caused the ELMB63 to send digital input data on the CAN bus all the time. This caused blockage of the CAN bus, and it was not possible to receive any data from the current reading (LMB). This is shown in the plot for the ELMB63 current readings. Also the data from the read-out is missing. This fault was corrected by doing a power off/on cycle.

5. During the test the ELMB65 and ELMB67 transmitted a boot-up message. This is a message that is transmitted after the software has been re-started (reset). A reset command was not sent so there is a possibility that a SEE triggered a reset of the microcontroller.

6. The ELMB 72 did not respond to a CAN command. The fault did recover automatic. It is not known what kind of fault this was.

Errors related to the CAN part

During the test 40 bytes of data were checked in the CAN controller registers. In total 23 bit flips was observed during the test. There was 12 bit flips from logic "1" to "0" and 11 bit flips from "0" to "1". This correspond to a cross-section of 2.12×10^{-13} cm^2/bit. In addition to the

errors that was found in the CAN controller registers there were three errors that interrupted the operation of the controller. These errors were reported via emergency messages. This kind of message is specified in the CANopen standard and is standard in the ELMB software. The SEE test showed that the emergency functionality worked as normal. One of the errors forced a re-initialization of the CAN controller. The two other errors were created from interrupts in the error counters. This is a counter that counts the number of errors in the CAN controller (e.g. communication errors). Since setting a bit in a register triggers this interrupt it is likely that there was a SEE in this register or circuitry related to the interrupt mechanism. Since all bus communication was logged with two CAN bus analyzers it was even possible to find out if there was any problems with the CAN messages. During the test five CAN bus error frames was reported. It is unknown what the cause of the error frames was. This could be anything from a SEE in the CAN controller to a SEE in the CAN interface chip or the opto-couplers between these chips. The CAN controllers have a built-in error checking circuit. If an error is found the message is rejected and a re-transmission request is issued. During the irradiation of the ELMB64 there was something wrong with the ADC read-out CAN massage. In total 92 CAN frames with the ADC read-out identifier was sent without any data. The length of the message was zero bytes, the "data length code" in the message was "0". This can be seen in section 5.2.2 where the ADC data is missing in the ELMB64 ADC read-out plot. The problem with the "data length code" was also encountered when the ELMB61 was tested ("data lenght code" was "0"). In this test the ADC read-out was not affected, but the SDO replay from the ELMB was affected. To test the ELMB receive mechanism, a SDO message was sent from the computer to the ELMB on a regular basis. The ELMB should answer this SDO by sending a SDO replay. The SDO message which was received did not have the correct "data length code".

5.2.2 Functional test of the ADC

During the SEE test four of the analog input channels on each ELMB were read-out. The setup used for the input channels are described in section 4.3. Figure 5.38, 5.39, 5.40 and 5.41 shows plots of the ADC raw values. The ADC was configured to work in the unipolar input mode, the input voltage range was set to 1V and the conversion rate was set to 61.6Hz. With this input range the ADC LSB is about 15μV. The ADC on-chip digital filter is not very effective for power line noise when the conversion rate is 61.6Hz. This means that there can be a noise component from power lines etc. in the measurements. The conversion rate was set to this value to introduce some noise in the reading. The reason was to have a change in the ADC readings (to indicate if something was "stuck" in the analog input part). As seen on the plots, the ADC raw value is not complete stable there is a small noise component in the read-out. During the SEE test, five bit errors were observed. The ELMB64 had four errors in the ADC read-out three in channel 0 and one in channel 1. ELMB70 had a wrong value in channel 3. Table 5.24 shows the value which was read, and the value which was expected. The analog input channels were read-out once every test cycle. The test cycle period was set to five seconds. During the irradiation, the test cycle period changed to a different time. This is clearly shown in the plots of the analog input channels. This is indicated by a longer period between the data in the plots. The test cycle changed during irradiation of ELMB61 (changed to 21 s), ELMB65 (changed to 21 s) ELMB70 (changed to 37 s) and ELMB72 (changed to 85 s).

Device	Channel	Time	Read value	Expected value
ELMB64	ch0	75 s	0x107C	0x147C
ELMB64	ch1	225 s	0x0344	0x1344
ELMB64	ch0	609 s	0x132C	0x142C
ELMB64	ch0	664 s	0x1439	0x1479
ELMB70	ch3	0 s	0x1330	0x1370

Table 5.24: *Errors in the ADC read-out during the SEE test for all ELMBs.*

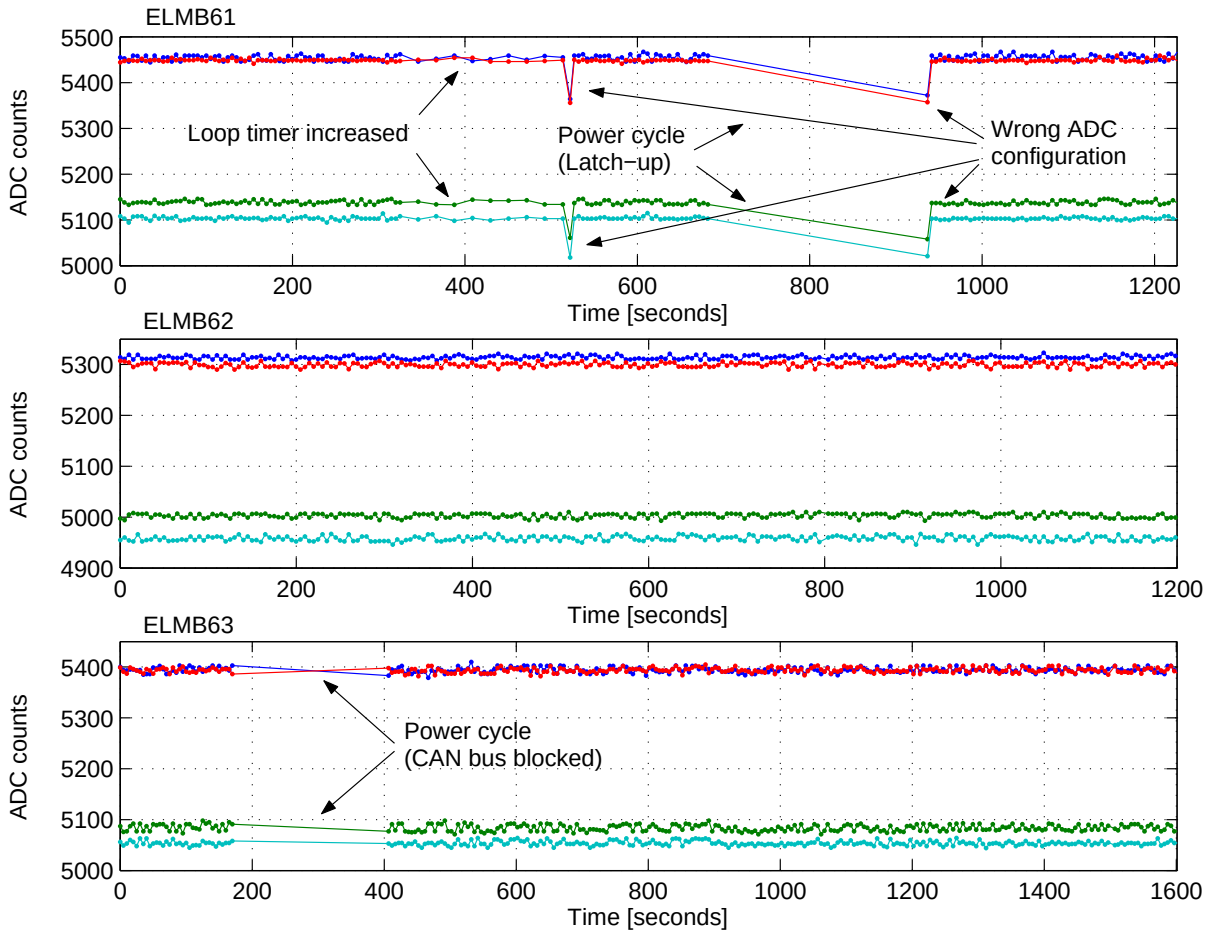

Figure 5.38: *Plot of ADC raw values from ELMB 61-63 during the SEE test.*

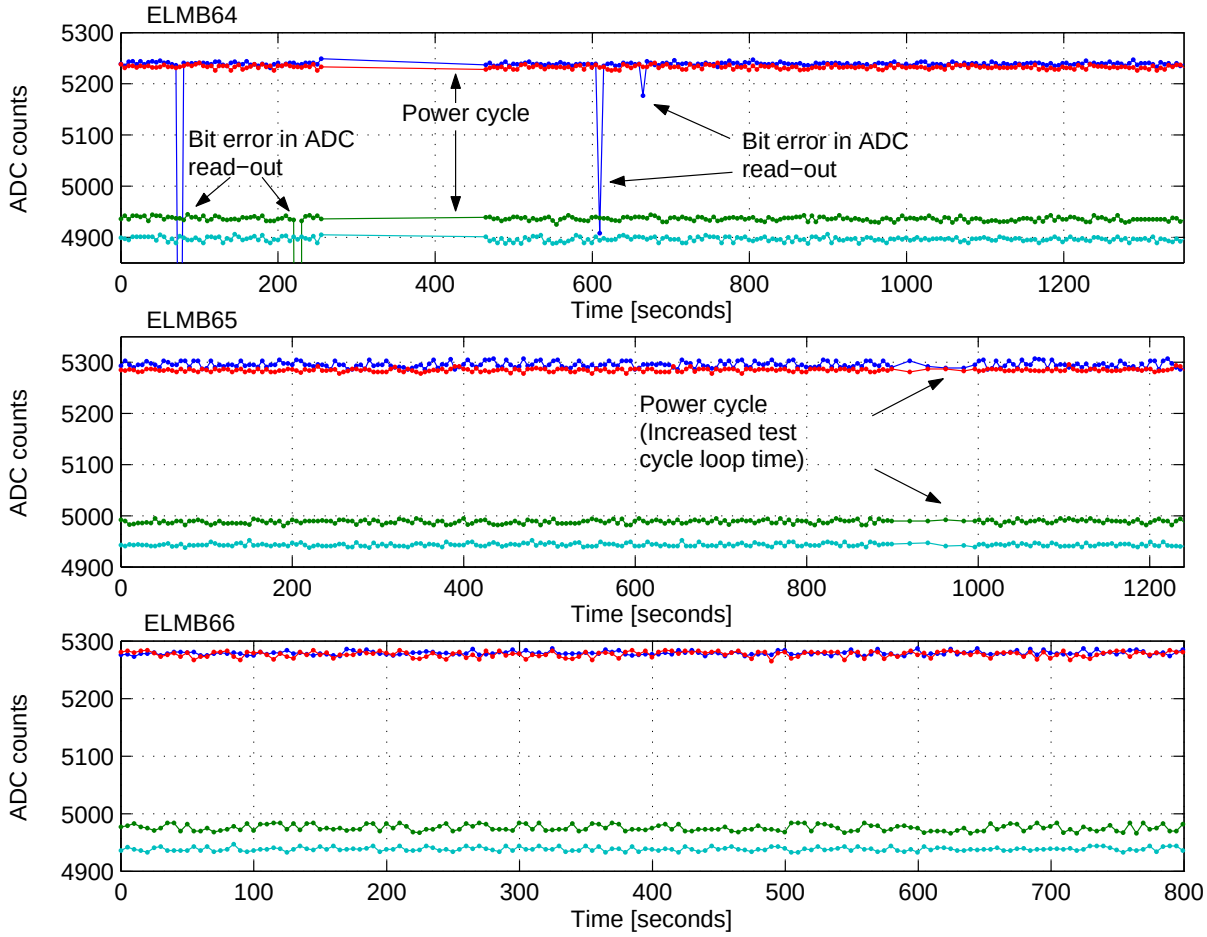

Figure 5.39: *Plot of ADC raw values from ELMB 64-66 during the SEE test.*

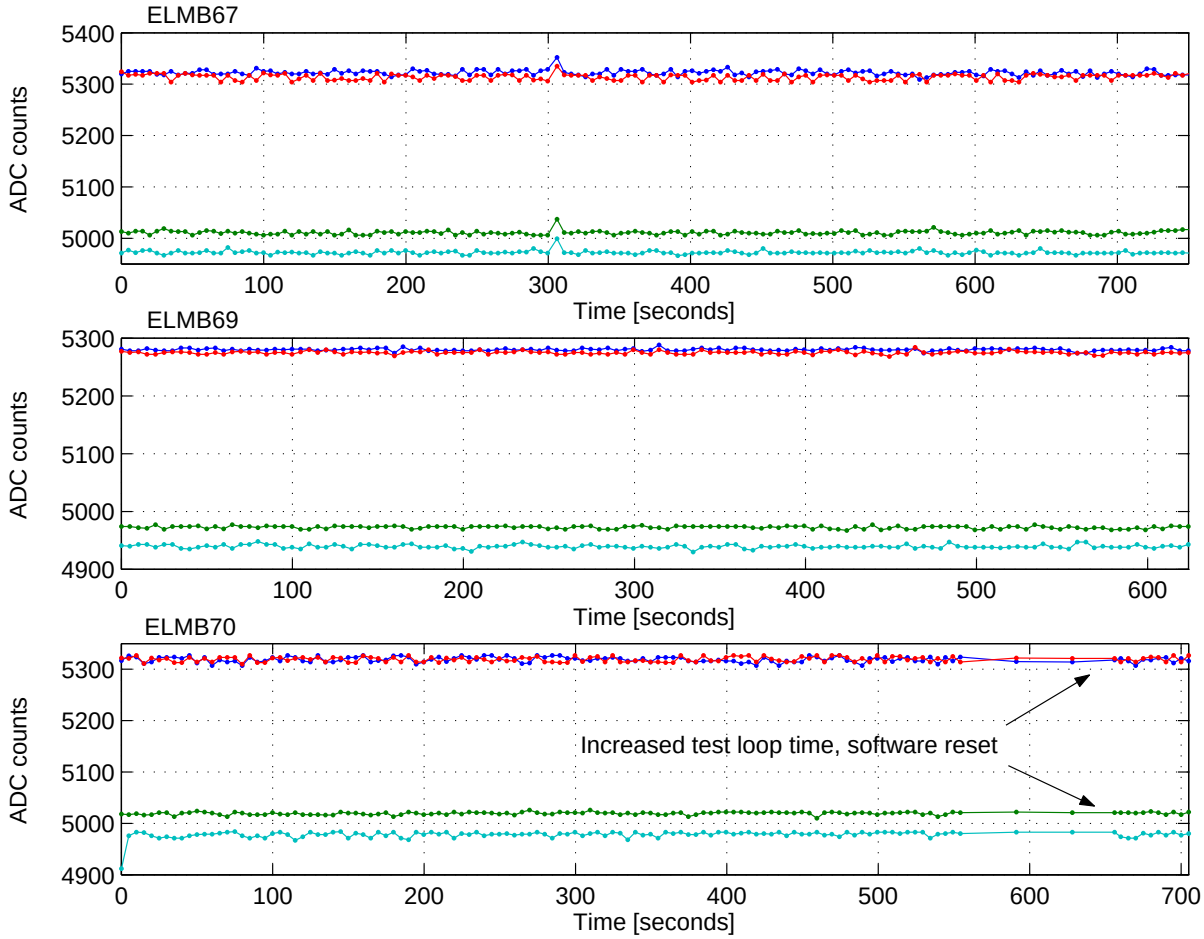

Figure 5.40: *Plot of ADC raw values from ELMB 67,69,70 during the SEE test.*

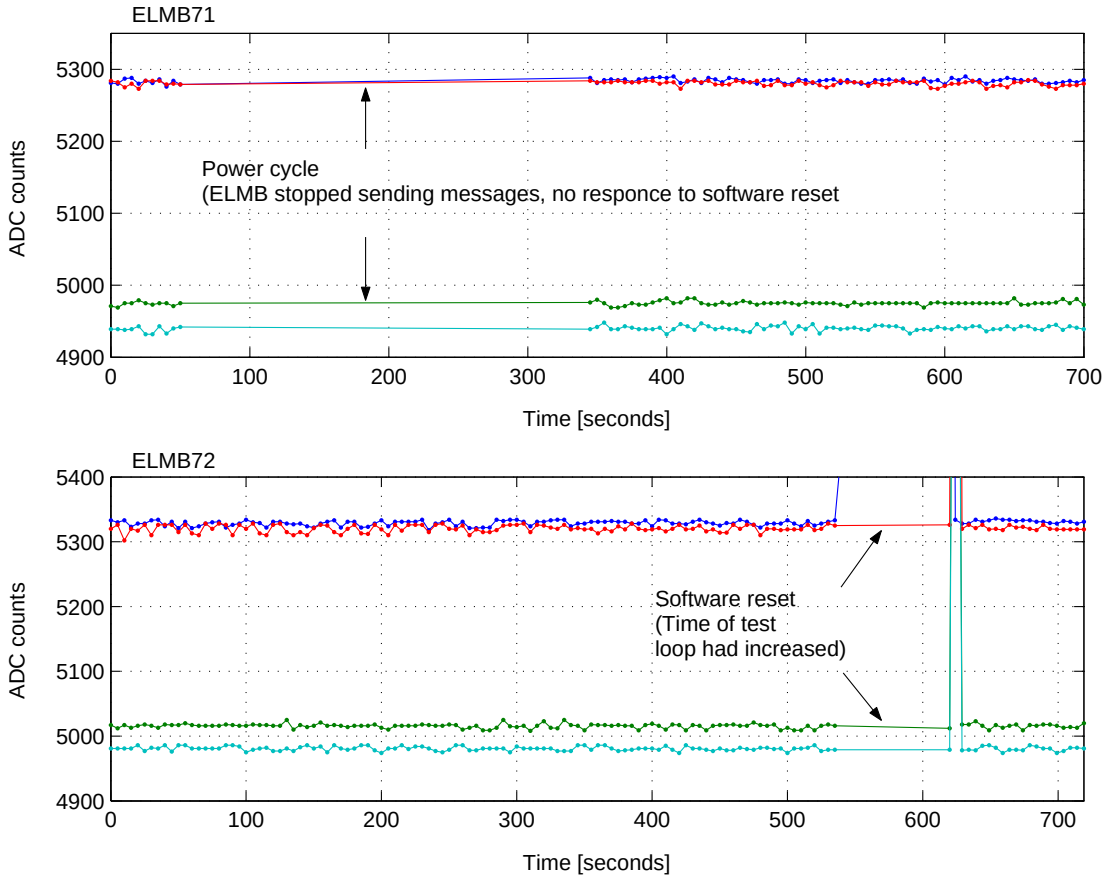

Figure 5.41: *Plot of ADC raw values from ELMB 71-72 during the SEE test.*

The ADC on-chip registers were also tested during the irradiation. In total 33 bytes of internal registers in the ADC was tested during each test cycle. After a fluence, Ψ_p, of 3.39×10^{11} protons/cm^2 the total number of single bit flips was counted to 23, and one double bit flip. All bit flips was from logic "1" to "0". This gives a cross-section of 2.8×10^{-13} cm^2/bit. In addition to the errors found in the ADC registers the ADC chip (communication with the chip) encountered a few other problems. In total 5 emergency messages with ADC related problems was received. During data read-out from ELMB62 and ELMB63 there was an ADC conversion time-out (emergency messages). This resulted in missing data values for all four channels during one test cycle. The time between succeeding data was 10 seconds. In ELMB65 there was a problem with the ADC initialization (emergency message) and problems with the ADC conversion timeout for channel 0 (emergency message). This did also result in missing data. Time between succeeding data was 13 seconds. ELMB70 did also have an ADC conversion timeout in channel 1 (emergency message). In ELMB72 there was also an error in the ADC read-out. Channel 0 was missing in one test cycle, but the three other channels were read. This error was not reported with an emergency message. It is unknown way channel 0 is missing. It is likely that some of the conversion time-out errors are caused by SEE in a timer used to keep track of the conversion time.

5.2.3 Summary of the SEE measurements

SEE tests have been performed on eleven ELMBs. The test was done with a 60MeV proton beam. The first five ELMBs was irradiated (effective) for about 1100 seconds each, with a proton flux of 2.5×10^7 protons/cm^{2}s, while the six remaining ELMBs was irradiated with a proton flux of 5×10^7 protons/cm^{2}s. In total the eleven ELMBs received a total fluence of 3.39×10^{11} protons/cm^2. This resulted in several errors in the microcontroller (ATmega103L) SRAM, in the registers in the CAN controller, and the ADC. The proton beam did not influence the flash memory or the EEPROM. The errors are summarized in table 5.25. It should be mentioned that the flash size listed is for 128k bytes since all bytes in the memory was tested after the test.

Memory	**Bit tested**	**SEE detected**	**Cross-section [cm^2/bit]**
SRAM	16384	2318	4.17×10^{-13}
EEPROM	28672	<1	$< 1.03 \times 10^{-16}$
Flash	1048576	<1	$< 2.81 \times 10^{-18}$
CAN	320	23	2.12×10^{-13}
ADC	264	25	2.79×10^{-13}

Table 5.25: *Summary of all SEEs which was detected in the memory and registers*

Table 5.26 shows all additional errors detected during the test. There were three categories of errors. The first is an error that could be corrected automatic by the ELMB software, e.g. ADC read-out where a SEE had altered the ADC settings. The second category is an error where the ELMB needed a software reset. Sending the CANopen command "reset node" does a software-reset. This requires that the ELMB is capable of receiving the message and to interpret it. The reset command restarts the ELMB application from the first instruction. The last category of errors can only be treated by a power cycle off/on sequence. Table 5.27 summarizes the detected SEEs for each ELMB, type of error, and how the error was corrected. Also the effective fluence received by each ELMB is given.

Description	**No.**	**Recovery**	**Comment**
Emergency msg. ADC related	5	Automatic	Treated as 5 SEE
Emergency msg. CAN related	3	Automatic	Treated as 3 SEE
Bit errors in the ADC read-out	5	Automatic	Treated as 5 SEE
CAN bus error frames	5	Automatic	Treated as 5 SEE
Unexpected boot up messages	2	Automatic	Treated as 2 SEE
ADC readout error (missing data)	1	Automatic	Treated as 1 SEE
Software hang/abnomal behaviour	1	Automatic	Treated as 1 SEE
ADC data missing in CAN msg.	92	Software reset	Treated as 1 SEE
SDO data missing in CAN msg.	90	Software reset	Treated as 1 SEE
Increased loop period	3	Software reset	Treated as 3 SEE
Increased loop period	1	Power cycle	Treated as 1 SEE
Single Event Latch-up	1	Power cycle	Treated as 1 SEE
Software hang/abnormal behaviour	2	Power cycle	Treated as 2 SEE

Table 5.26: *Summary of additional SEE encountered during the test.*

ELMB	Errors	Fluence, Ψ_{eff}	Failure description	Corrected by
ELMB61	4	2.43×10^{10} p/cm^2	Digital power SEL	Power cycling
			Increased test loop period	Software reset
			Missing DLC in CAN message	Software reset
			CAN remote frame interrupt	Auto recovery
ELMB62	2	3.00×10^{10} p/cm^2	CAN error frame	Auto recovery
			ADC conversion time-out	Auto recovery
ELMB63	2	3.42×10^{10} p/cm^2	To many CAN messages (bus load)	Power cycling
			ADC conversion time-out	Auto recovery
ELMB64	6	2.86×10^{10} p/cm^2	CAN error frame	Auto recovery
			Missing DLC in CAN message	Software reset
			ADC read-out error (ADC value)	Auto recovery
			ADC read-out error (ADC value)	Auto recovery
			ADC read-out error (ADC value)	Auto recovery
			ADC read-out error (ADC value)	Auto recovery
ELMB65	4	3.10×10^{10} p/cm^2	Increased test loop period	Power cycling
			Unexpected boot message	Auto recovery
			ADC initialization problem	Auto recovery
			ADC conversion timout	Auto recovery
ELMB66	0	4.00×10^{10} p/cm^2		
ELMB67	2	3.75×10^{10} p/cm^2	Unexpected boot message	Auto recovery
			CAN error frame	Auto recovery
ELMN69	0	3.12×10^{10} p/cm^2		
ELMB70	3	3.02×10^{10} p/cm^2	Increased test loop period	Software reset
			ADC read-out error (ADC value)	Auto recovery
			ADC conversion time-out	Auto recovery
ELMB71	2	2.03×10^{10} p/cm^2	Infinite program loop (hang)	Power cycling
			CAN emergency message	Auto recovery
ELMB72	6	3.18×10^{10} p/cm^2	Increased test loop period	Software reset
			No replay from node	Auto recovery
			CAN life guarding time-out	Auto recovery
			CAN error frame	Auto recovery
			CAN error frame	Auto recovery
			ADC error (missing data)	Auto recovery

Table 5.27: *Summary off all SEE detected during the test.*

The SEE requirements for the ATLAS muon MDT end-cap 1 location is described in section 4.1.4. Table 5.28 shows a comparison between the ATLAS requirements and the results gained in this test. Since the SEE test was done with a proton fluence, Ψ_p, of 3.39×10^{11} protons/cm^2, the number of errors must be scaled to the simulated hadron fluence, Ψ_h, for the muon MDT end-cap 1 location. The analysis of the results shows that the measured values for the soft SEU is well below the maximum allowed error rate. However, it should be noted that the requirement for the hard SEU could not be fulfilled since no error was observed. The statistics is limited, higher proton fluence are required to determine whether the ELMB fulfills the SEE requirements or not.

SEE category	Number of SEE per ELMB		
	$\Psi_p = 3.39 \times 10^{11}$ p/cm^2	$\Psi_h = 4.83 \times 10^{11}$ h/cm^2	
	Test results	**Requirement**	**Result after scaling**
Soft SEE, Auto recover	22	2604	31
Soft SEE, Software	5	1157	7
Soft SEE, Power cycle	4	18	6
Hard SEE	0	0.006	0

Table 5.28: *Comparison between the SEE results and the SEE requirements for the ATLAS end-cap 1 location.*

The ELMB ADC was read-out out every fifth second during the SEE test. The ADC was configured with an input range of 1V, unpolar mode and with a conversion rate of 61.6Hz. This gives a LSB of 15.3μV. With this input configuration, the ADC is specified to have a noise free resolution of 12 bits [39]. The RMS noise is specified to 92μV. The mean standard deviation noise from all ELMBs (channel 0-3), is calculated to be 60μV. This corresponds to about 4×LSB. The standard deviation for the analog input channels 0-3 (all ELMBs) is plotted in figure 5.42. It should be noted that the wrong ADC readings are not included in the calculation.

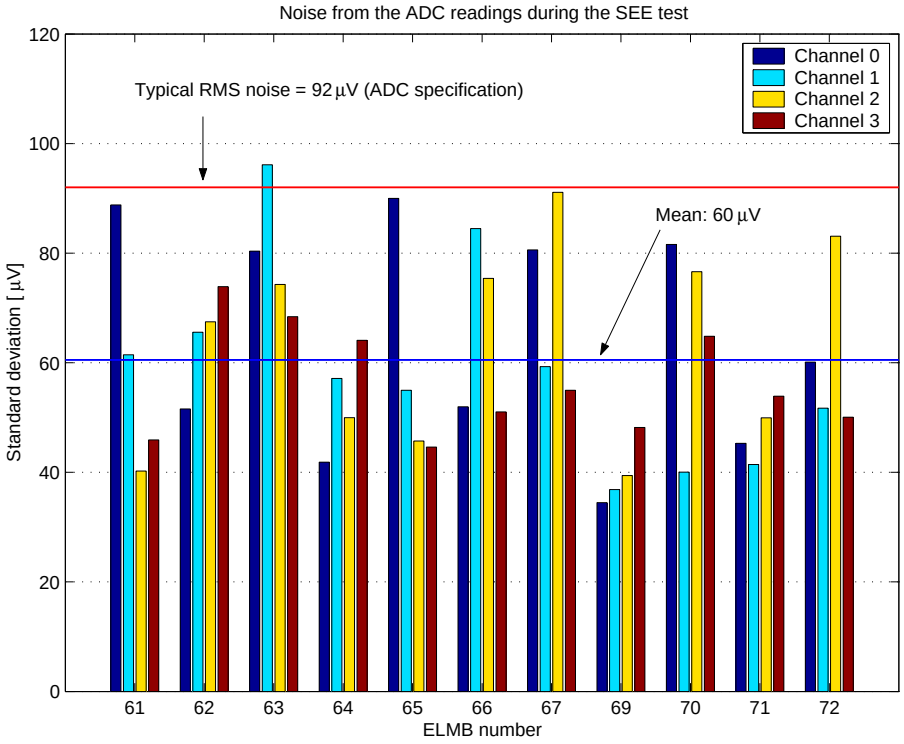

Figure 5.42: *Plot of the standard deviation for the analog input channels 0-3 during the SEE test.*

Chapter 6

Conclusion

This thesis has given a detailed presentation of the TID and the SEE tests performed on the ELMB. The results are summarized in section 5.1.6 and 5.2.3. The purpose of the first TID tests was to gain some experience with the test procedures, and the behavior of the ELMB in a radioactive environment. During the first TID test we experienced some problems with both the measuring equipment and the ELMB itself. Measurements showed that the ELMB did not tolerate as high total integrated dose (γ) as we had hoped for. The digital current showed a rapid increase after the ELMBs had received a dose of about 30-35Gy(Si) this is over ten times lower than required for the worst-case location in the ATLAS detector (MDT end-cap 1 area) with the worst-case safety factors.

A TID test done by Temic [29] showed that there could be a correlation between the dose-rate, and the leakage current in a memory cell. Based on this test it was decided to do a second TID test. This test was done with a significant lower dose-rate than the dose-rate used in the first TID test. The measurements from this test showed more or less the same current increase as in the first TID test. Also the programming function of the microcontrollers was lost during this test, this was also the case in the first TID test.

The loss of the programming function needed further investigation to find the total integrated dose when the programming function ceased to work. This was the purpose of the third TID test. In this test it was found the programming function was lost after the ELMB had received a dose of about 35Gy(Si).

The three TID tests showed the same problem, the loss of the programming function for the microcontrollers, and a rapid increase in the digital current. If the ELMB was to be qualified for the MDT end-cap 1 location something needed to be done with the safety factors. According to the *ATLAS policy on radiation tolerant electronics* document [14], it is possible to reduce some of the safety factors if special care is taken. It is possible to reduce the low dose-rate safety factor if it can be proven that the device does not suffer from such effects. The low dose-rate effect can be simulated by doing an accelerated aging test. An accelerated aging test has been performed on one irradiated ELMB and on one unirradiated ELMB. The conclusion of the test was that the ELMB does not suffer from these effects. This means that the safety factor can be reduced down to one. However, this is not enough, it would be required to also reduce the safety factor related to component batches. Investigation among the various semiconductor manufacturers showed that it is possible to obtain components from homogenous batches. This reduces the lot safety factor to one. The only remaining safety factor is the radiation simulation safety factor. With the mentioned reduction in the safety factors it is possible to obtain a radiation tolerance

criteria which satisfies the worst-case location in the detector where the ELMB has been foreseen to be used.

The second type of radiation test was the SEE test. In this test the ELMB was exposed to a proton beam and the number of errors was counted. The proton beam can cause different SEU, but also the method to recover from such SEU is important. A comparison between the requirements and the results from the test showed that the ELMB fulfills the requirements for the soft SEU, but since no hard SEU error was detected it is not possible to say if this requirement is satisfied. The total fluence from the test was not large enough to judge whether the requirement if fulfilled or not.

In addition to a possible SEU, a proton will also contribute to an integration of charge in the semiconductor. In other words, the ELMBs had undergone a fourth TID test. The SEE test was done with eleven ELMBs and it was not observed any current increase in the currents as in the TID tests, even though the average integrated dose was 46Gy(Si).

The TID results from the SEE test and the results from the three previous TID tests showed convincing results. Even though the rules for pre-selection (TID test method) was not strictly followed, it has been approved by the ATC group (the group responsible qualification of electronics to be used in the ATLAS experiment) as a pre-selection of the components for the ELMB (TID). Also the SEE test results provides convincing results for the soft SEUs, but not for the hard SEUs. In addition to the TID and SEE test a NIEL test has also been performed. The result from this test is also convincing for pre-selection of components (NIEL) [22].

To summarize, the three necessary radiation tests that are required for the pre-selection of components has been performed on the ELMB. The measurements from the tests showed convincing results (except for the hard SEU - the ELMB must be re-tested for the hard SEU before the components can be qualified), and the components has therefore been selected (pre-selection) to be used in the ELMB. This is the first step in the ELMB qualification process. This pre-selection test has in addition to the component selection, contributed to a good understanding of the radiation test procedures, and how they should be performed in the qualification test.

When the components used in the ELMB is qualified they will be registered in a database. The intention of this database is that other users can select components from this database and use them without further test as long as they are used under the same conditions as the tested components.

6.1 Further work

The radiation tests performed on the ELMB so fare has been so-called pre-selection tests. A pre-selection test is done to find out if a component can be used at all. If the results from such pre-selection are promising, further test should be done to qualify the component for use in the ATLAS experiment. The procedure for the qualification is described in [14].

The pre-selection of the components for the ELMB has now been done. The next step is to qualify them for use in the ATLAS experiment (muon MDT end-cap 1 area). Before the qualification can be done, it is necessary to obtain components from known homogeneous component batches. This is required if the ELMB is to be qualified for TID. Without known homogeneous batches, the safety factors would be too large, and this would cause a problem with the TID acceptance. Since no hard SEU was detected, and the received proton fluence was lower then the simulated level (with safety factors) it is necessary to do a test where it is possible to judge if the hard SEU requirement is fulfilled. Before the ELMB can be qualified for the use in the ATLAS experimental area, the following must be done:

- Purchase components from homogeneous batches. All components required for the ELMB production for the ATLAS experiment should be purchased.
- The components must undergo and pass a NIEL test, a SEE test and a TID test with accelerated aging testing.
- The ELMB must be tested and qualified for hard SEU.

Bibliography

[1] G.C. Messenger, M.S. Ash, *The effects of radiation on electronic systems*, 1992, ISBN 0-442-23952-1.

[2] T.P.Ma, Paul V. Dressendorfer, *Ionizing radiation effects in MOS devices and circuits* 1989, ISBN 0-471-84893-X.

[3] M. Menichelli et al., *Total Dose Test of Commercial Off-The-Shelf Components To Be Used in Power supply for Space Experiments*, IEEE Transactions on Nuclear Science, vol. 47, No. 6, December 2000.

[4] C.I. Lee, B.G. Rax, A.H. Johnston, *Hardness Assurance and Testing Techniques for High Resolution (12- to 16-bit) Analog-to-Digital Converters*, IEEE Transactions on Nuclear Science, vol. 42, No. 6, December 1995.

[5] B. Hallgren, H. Boterenbrood, H.J. Burckhart, H. Kvedalen, *The Embedded Local Monitor Board (ELMB) in the LHC Front-end I/O system.*

[6] H.J. Burckhart, B. Hallgren, H. Kvedalen, *Radiation test at GIF and accelerated aging of the ELMB*, CERN ATLAS Internal Working Note DCS-IWN9, 9^{th} March 2001

[7] J. Cook, B. Hallgren, H. Kvedalen, *Irradiation Measurements of the ATLAS ELMB*, CERN ATLAS Internal Working Note DCS-IWN10 2^{nd} May 2001

[8] B. Hallgren, H. Kvedalen, *Radiation test of the 3.3V version ELMB at GIF*, CERN ATLAS Internal working note DCS-IWN11 31^{st} August 2001

[9] H. Boterenbrood, H.J. Burckhart, B. Hallgren, H. Kvedalen, N. Roussel, *Single Event Effect Test of the Embedded Local Monitor Board* CERN ATLAS Internal working note DCS-IWN12, 10^{th} September 2001

[10] H.J.Burckhart, *Detector control system*, CERN, Geneva, Switzerland.

[11] *ATLAS technical proposal for a general purpose PP experiment at the Large Hadron Collider at CERN*, December 1994, ISBN 92-9083-067-0

[12] *ATLAS High-level triggers, DAQ and DCS, Technical design proposal,* CERN/LHCC 2000,17 31 March 2000, ISBN 92-9083-160-0

[13] *ATLAS Level-1 trigger Technical design report,* ATLAS TDR-12, 20 August 1998

[14] *ATLAS Policy on Radiation Tolerant Electronics.*, ATC-TE-QA-0001, Rev. no 2. 21 July 2000.

[15] B.Hallgren, H.J.Burckhart, *Frontend I/O via CANbus of the ATLAS detector control system*, CERN, Geneva, Switzerland.

[16] W.R. Leo, *Techniques for nuclear and particle physics experiments, A How to Approach* Second Revised edition, Springer Verlag, ISBN 3-540-57280-5

[17] A. Colder et al, *Study of Radiation Effects on Bipolar Transistors*

[18] B.G. Henson, P.T. McDonald and W.J. Stapor, *SDRAM Space Radiation Effects Measurements and Analysis*, Innovative Concepts Incorporated, McLean, VA 22102, www.innocon.com

[19] P.T. McDonald, W.J. Stapor and B.G. Henson, *PC603E 32-bit RISC μP Radiation Effects Study*, Innovative Concepts Incorporated, McLean, VA 22102, www.innocon.com

[20] B.G. Henson, P.T. McDonald and W.J. Stapor, *16Mb SDRAM Proton Radaition Effects Measurements and Analysis*, Innovative Concepts Incorporated, McLean, VA 22102, www.innocon.com

[21] S. Agosteo et al., *A facility for the test of large muon chambers at high rates* CERN-EP-2000-031, February 16, 2000

[22] J.Cook and B.Hallgren, *Non Ionising Energy Loss Test of the Embedded Local Monitor Board*, ATLAS Internal working note DCS-IWN14, 22^{nd} January 2002

[23] Kenneth S. Krane *Introductory Nuclear Physics*, 1988, ISBN 0-471-80553-X

[24] A global radiation test plan for CMS electronics in HCAL, Muons and Experimetal Hall, Updated draft 17/12/1999

[25] Robert Bosch GmbH, *CAN specification*, version 2.0, 1991

[26] NSI, *CAN auto 2000 training*, papers from CAN cource at CERN.

[27] CAN in Automation, *CiA webpage*, www.can-cia.de

[28] G. Baribaud et al., *Recommendations for the use of fieldbuses at CERN*, CERN ECP 96-11 June 1996, http://itcowww.cern.ch/fieldbus/report1.html

[29] Temic, *TEMIC Semiconductor Radiation Policy*, July 03 2000.

[30] H. Boterenbrood, *ELMBio test objects*, v3.3, may 2001.

[31] C. Bayer, S. Kersten, P. Kind, P. Sicho, *Results from the first Interlock Box irradiation* http://www-hep.fzu.cz/pixpage/IRR/REPORTS/IntBox.pdf

[32] Wolfhard Lawrenz, *CAN System Engineering, From Theory to Practical Applications*, ISBN 0-387-94939-9, Springer-Verlag 1997

[33] Maxim datasheet, *MAX870/MAX871 Switched-Capacitor Voltage Inverters*, Rev. 0, 6/97

[34] Siemens datasheet, *SAE81C90/91 standalone Full-CAN controller* 01.97 Preliminary.

[35] Maxim datasheet, *MAX4518/MAX4519 Precision 4-Channel/Dual 2-Channel, Low voltage CMOS Analog Multiplexers*, Rev 1, 5/98

[36] Analog devices, *ADP3607, 50mA Switched Capacitor Voltage Boost with Regulated Output*, rev 0, 1999

[37] Analog devices, *AD680, Low Power 2.5 V reference*, rev D. 2001

[38] Analog devices, *ADuM1100AR/ADuM1199BR Preliminary datasheet* Rev. Prg. November 6 2000.

[39] Cirrus Logic, *CS5521/22/23/24/28 datasheet*, DS317F2 May 2000.

[40] Atmel Corporation, *ATmega103 datasheet*, Rev. 0945E-01/00

[41] Atmel Corporation, *AT90S2313 datasheet*, Rev. 0839E-04/99

[42] Micrel, *MIC5203 80mA Low-Dropout Voltage Regulator*, December 1998

[43] Micrel, *MIC2753/2754 Power Supply Supervisors*, June 1999

[44] ATLAS-DCS *LMB technical documentation*, http://atlasinfo.cern.ch/ATLAS/GROUPS/DAQTRIG/DCS/lmb.html

[45] ATLAS-DCS *ELMB technical documentation*, http://atlasinfo.cern.ch/ATLAS/GROUPS/DAQTRIG/DCS/ELMBinfo.html

[46] Philips semiconductors, *PCA82C250 CAN controller interface*, january 2000

[47] Atmel Corporation, *Atmel Reliability Monitor Report* November 9 2000.

[48] CIS bio international commercial flyer, *Irradiation des composants électroniques et systèmes*

[49] Henriksen, Ingebretsen, Storruste, Strand, Svendby, Wethe, *Stråling og helse*, 1995, ISBN 82-992073-2-0

[50] European Space Agency, *Single Effects Test Method and Guidelines* ESA/SCC Basic Specification No. 25100, Issue 1, Oct. 1995

[51] F. Faccio, *Radiation effects in the electronics for CMS*, radiation course slides

[52] ATLAS web page, http://atlasinfo.cern.ch/ATLAS/internal/Welcome.html

[53] Daniel Montgomery MacQueen, *Total Ionizing Dose Effects on Xilinx Field-Programmable Gate Arrays*, University of Alberta, 2000

Appendix A

This appendix includes the schematics for the 3.3V version of the ELMB.

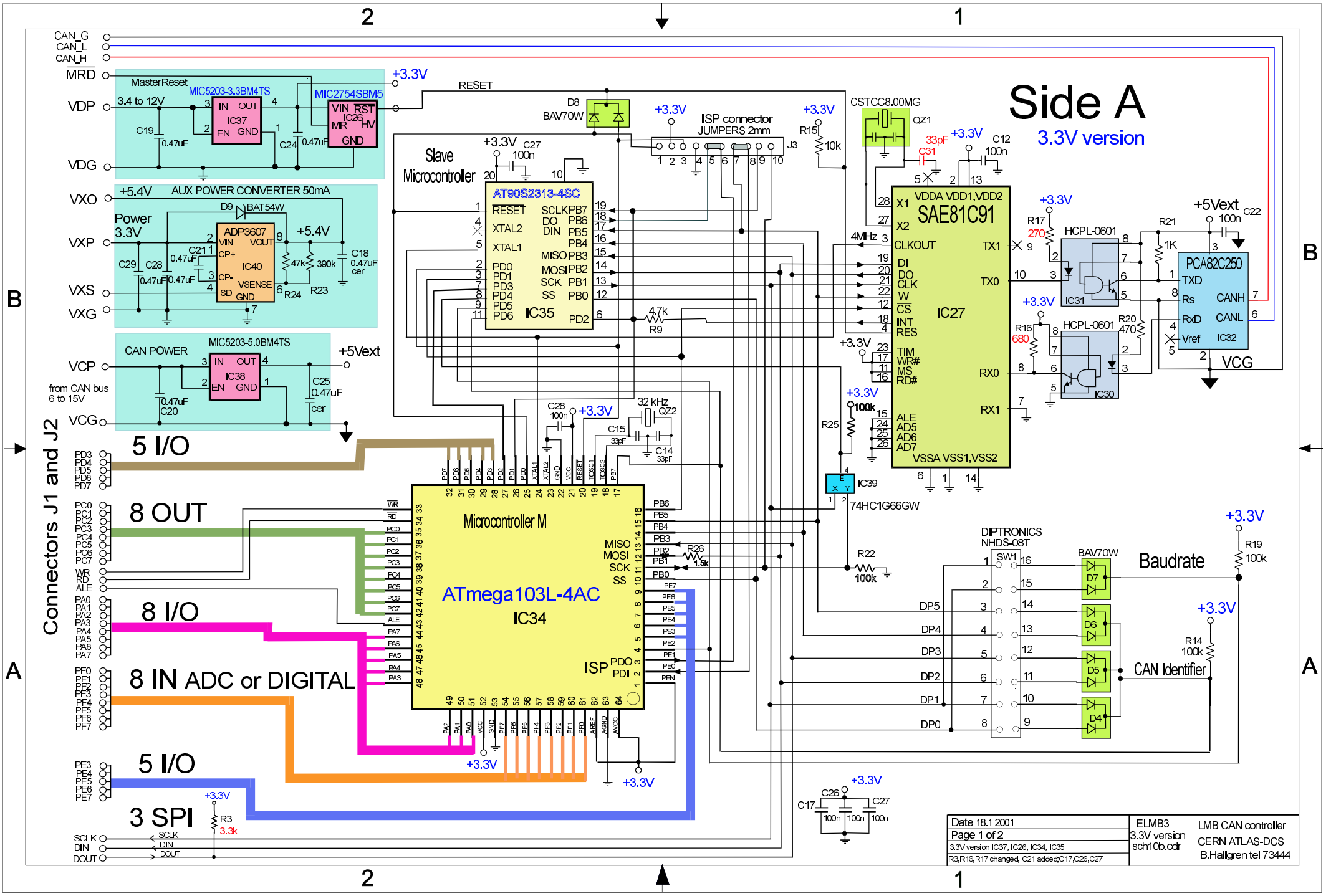
Side A
3.3V version
CAN_G
CAN_L
CAN_H
MRD
VDP
VDG
VXO
VXP
VXS
VXG
VCP
VCG
from CAN bus 6 to 15V
MasterReset
MIC5203-3.3BM4TS
MIC2754SBM5
3.4 to 12V
+3.3V
AUX POWER CONVERTER 50mA
+5.4V
Power 3.3V
ADP3607
BAT54W
CAN POWER
MIC5203-5.0BM4TS
+5Vext
RESET
D8 BAV70W
ISP connector JUMPERS 2mm
Slave Microcontroller
AT90S2313-4SC
IC35
CSTCC8.00MG
QZ1
33pF
SAE81C91
IC27
VDDA VDD1,VDD2
VSSA VSS1,VSS2
4MHz
HCPL-0601
IC31
IC30
PCA82C250
IC32
VCG
32 kHz
QZ2
IC39
74HC1G66GW
Microcontroller M
ATmega103L-4AC
IC34
ISP
DIPTRONICS NHDS-08T
SW1
BAV70W
Baudrate
CAN Identifier
DP5
DP4
DP3
DP2
DP1
DP0
Connectors J1 and J2
5 I/O
8 OUT
8 I/O
8 IN ADC or DIGITAL
5 I/O
3 SPI
SCLK
DIN
DOUT
Date 18.1 2001
Page 1 of 2
3.3V version IC37, IC26, IC34, IC35
R3,R16,R17 changed, C21 added;C17,C26,C27
ELMB3
3.3V version
sch10b.cdr
LMB CAN controller
CERN ATLAS-DCS
B.Hallgren tel 73444

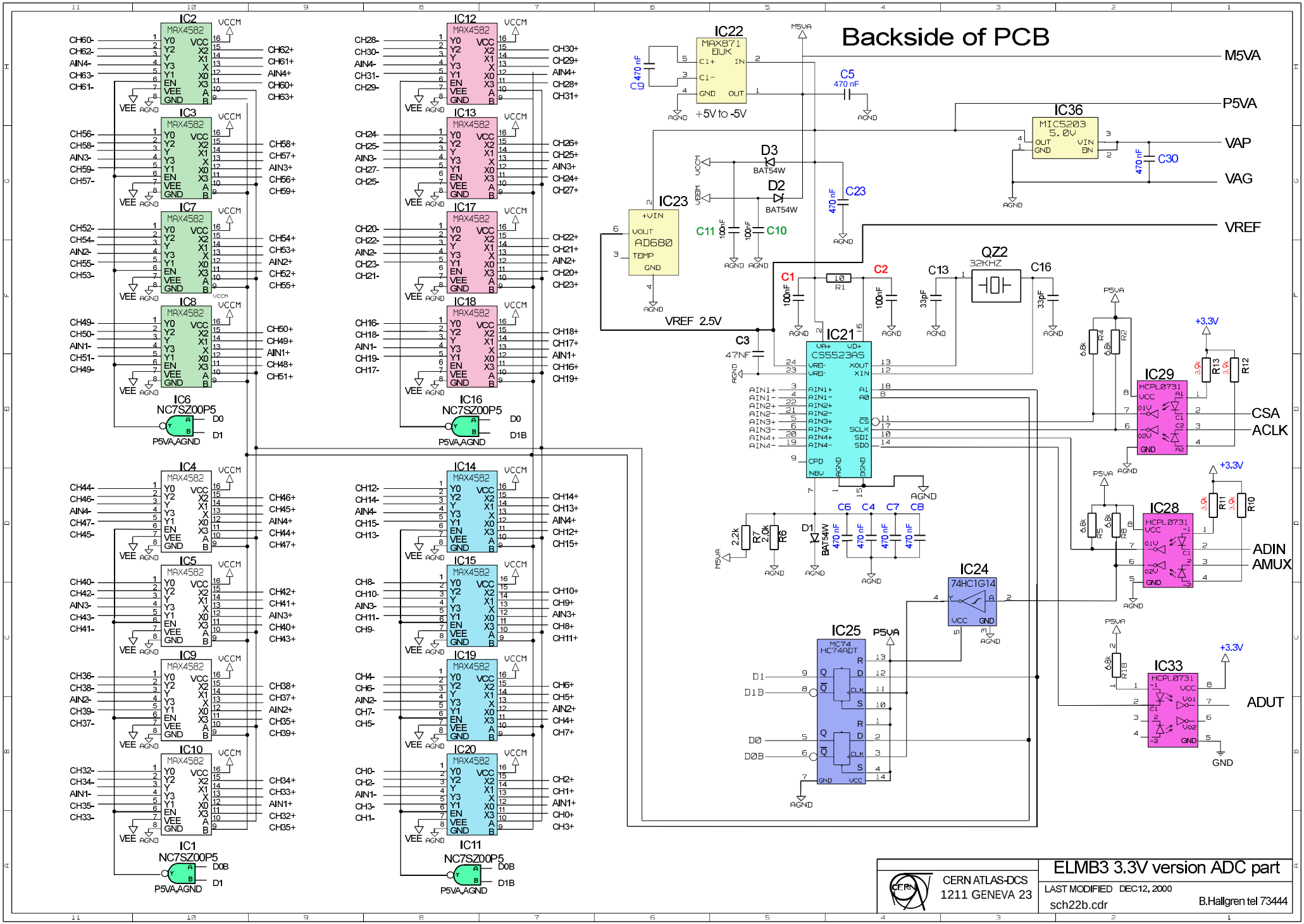
Backside of PCB
IC2
IC3
IC7
IC8
IC12
IC13
IC17
IC18
IC4
IC5
IC9
IC10
IC14
IC15
IC19
IC20
IC1
IC6
IC16
IC11
MAX4582
NC7SZ00P5
IC22
MAX871
EUK
+5V to -5V
IC23
AD680
IC21
CS5523AS
IC24
74HC1G14
IC25
MC74
HC74ADT
IC36
MIC5203
5.0V
IC29
IC28
IC33
HCPL0731
QZ2
32KHZ
D3
BAT54W
D2
BAT54W
D1
BAT54W
M5VA
P5VA
VAP
VAG
VREF
CSA
ACLK
ADIN
AMUX
ADUT
+3.3V
GND
VREF 2.5V
P5VA,AGND
CERN ATLAS-DCS
1211 GENEVA 23
ELMB3 3.3V version ADC part
LAST MODIFIED DEC12, 2000
sch22b.cdr
B.Hallgren tel 73444

Appendix B

This appendix shows the "The Embedded Local Monitor Board (ELMB) in the LHC Front-end I/O Control System" paper which was presented at the "7th Workshop on Electronics for LHC Experiments", Stockholm, Sweden, 10 to 14 September, 2001 [5].

Also the CERN ATLAS internal working note DCS-IWN11 "Radiation test of the 3.3V version ELMB at GIF" is included.

1. The Embedded Local Monitor Board (ELMB) in the LHC Front-end I/O Control System, B.Hallgren, H.Boterenbrood, H.J.Burckhart, H.Kvedalen

2. Radiation test of the 3.3V version ELMB at GIF, B.Hallgren, H.Kvedalen

The Embedded Local Monitor Board (ELMB) in the LHC Front-end I/O Control System

B. Hallgren[1], H.Boterenbrood[2], H.J. Burckhart[1], H.Kvedalen[1]

[1]CERN, 1211 Geneva 23, Switzerland, [2]NIKHEF, NL-1009 DB Amsterdam, The Netherlands
bjorn.hallgren@cern.ch, boterenbrood@nikhef.nl, helfried.burckhart@cern.ch, hallvard.kvedalen@cern.ch

Abstract

The Embedded Local Monitor Board is a plug-on board to be used in LHC detectors for a range of different front-end control and monitoring tasks. It is based on the CAN serial bus system and is radiation tolerant and can be used in magnetic fields. The main features of the ELMB are described and results of several radiation tests are presented.

I. INTRODUCTION

A versatile general-purpose low-cost system for the front-end control, the Local Monitor Box (LMB) was designed in 1998 and tested by ATLAS sub-detector groups in test-beam and other applications [1]. Based on this experience and to match all the needs of the ATLAS sub-detector groups a modified version, the Embedded Local Monitor Board (ELMB) was designed. The main difference as compared to the LMB is the plug-on feature and the small size (50x67 mm). It can either be directly put onto the sub-detector front-end electronics, or onto a general-purpose motherboard which adapts the I/O signals. In order to make the ELMB available for evaluation a small-scale production of 300 boards has been made.

A. Environmental Requirements

The ELMB is intended to be installed in the underground cavern of LHC detectors. As an example of such radiation environments the simulated radiation levels [2] for 10 years of operation of the ATLAS Muon MDT detectors are given below:

- Total Ionising Dose (TID): 6.4 Gy,
- Non-Ionising Energy Loss (NIEL): $3*10^{11}$ neutrons/cm^2 (equivalent to 1 MeV Si)
- Single Event Effect (SEE): $4.8*10^{10}$ hadrons/cm^2 (>20 MeV)

The magnetic field in which the Muon detectors operate is 1.5 Tesla, which makes it difficult to use DC to DC converters and other ferromagnetic components including transformers that are often used in commercial, off-the-shelf systems. These components have been avoided in the design of the ELMB. Another requirement is remote operation up to a distance of 200 m.

II. DESCRIPTION OF THE ELMB

The ELMB has an on-board CAN-interface and is in-system programmable, either via an on-board connector or via CAN. There are 18 general purpose I/O lines, 8 digital inputs and 8 digital outputs. Optionally a 16-bit ADC and multiplexing for 64 analogue inputs is provided on-board as shown in Figure 1.

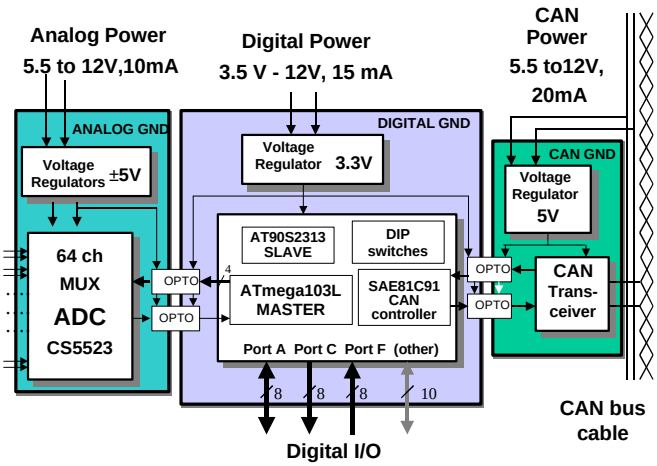

Figure 1: Simplified block diagram of the ELMB module

A. Power distribution

As seen from Figure 1 the ELMB is divided into three sections: analog, digital and CAN. They are separated with optocouplers to prevent current loops. The three parts are each equipped with a Low Dropout (LDO) 80 mA voltage regulator from Micrel (MIC5203). These regulators provide current and thermal limitations, which is a useful feature for protection against Single Event Latch-up (SEL). The analog circuits need ±5V, which is generated by a separate CMOS switched-capacitor circuit. The total analog current consumption is 10 mA. The power supply of the digital section is 3.3V, 15mA. The CAN part of the ELMB may be powered via the CAN cable and needs 20mA at 5.5V.

B. The Analog Circuits -ADC

A 16 bit differential delta-sigma ADC with 7 bit gain control (Crystal CS5523) is used and placed on the back-side of the printed circuit board. The CS5523 is a highly integrated CMOS circuit, which contains an instrumentation

chopper stabilised amplifier, a digital filter, and calibration circuits. 16 CMOS analog differential multiplexers expand the number of inputs to 64. The AD680JR from ANALOG DEVICES supplies a stable voltage reference. The ADC input can handle a range between +4.5 and –4.5V. Figure 2 shows the backside of the printed circuit board with the ADC, the voltage reference and 16 multiplexer circuits.

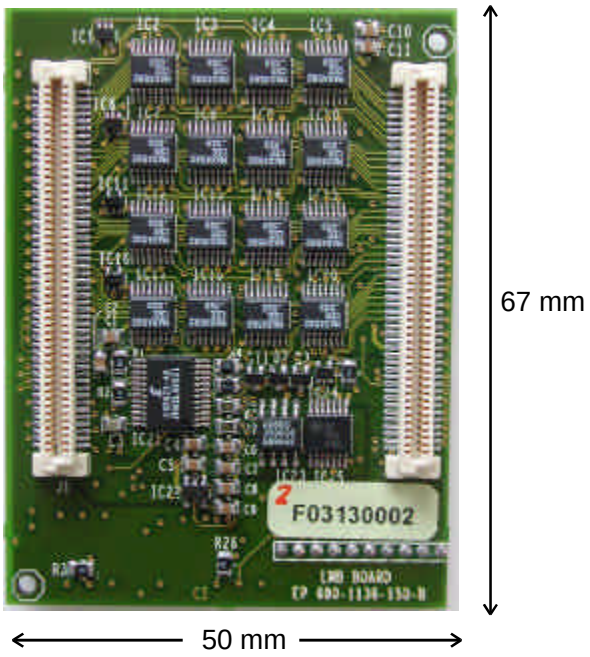

Figure 2: The backside of the ELMB printed circuit board

C. The Digital Circuits

The local intelligence of the ELMB is provided by 2 microcontrollers of the AVR family of 8-bit processors, manufactured by ATMEL. This family of microcontrollers is based on a RISC processor developed by Nordic VLSI and is particularly efficient in power consumption and instruction speed. The ELMB's main processor is the ATmega103L running at 4 MHz. This CMOS integrated circuit contains on-chip 128 Kbytes of flash memory, 4 Kbytes of SRAM, 4 Kbytes of EEPROM and a range of peripherals including timers/counters and general-purpose I/O pins. The main monitoring and control applications are running on this processor.

The second on-board microcontroller is a much smaller member of the same AVR family, the AT90S2313 with 2 Kbytes flash-memory, 128 bytes of SRAM and 128 bytes of EEPROM. The main purpose of this processor is to provide In-System-Programming (ISP) via CAN for the ATmega103L processor. In addition it monitors the operation of the ATmega103L and takes control of the ELMB if necessary. This feature is one of the protections against SEE. In turn the ATmega103L monitors the operation of the AT90S2313 and provides ISP for it. Figure 3 shows the front-side of the ELMB printed circuit board with the two microcontrollers and the CAN circuit.

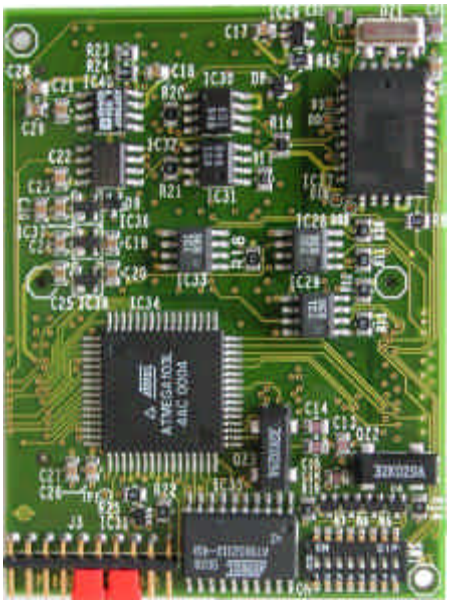

Figure 3: The front side of the ELMB

D. CAN circuits

CAN is one of the three CERN recommended fieldbuses [3]. It is especially suited for sensor readout and control functions in the implementation of a distributed control system because of reliability, availability of inexpensive controller chips from different suppliers, ease of use and wide acceptance by industry. The error checking mechanism of CAN is of particular interest in the LHC environment where bit errors due to SEE will occur. The CAN controller registers a node's error and evaluates it statistically in order to take appropriate measures. These may extend to disconnecting the CAN node producing too many errors. Unlike other bus systems, the CAN protocol does not use acknowledgement messages but instead signals any error that occurs.

For error detection the CAN protocol implements three mechanisms at the message level:

- Cyclic Redundancy Check (CRC)
- Message frame check
- Acknowledgement errors

The CAN protocol also implements two mechanisms for error detection at the bit level:

- Monitoring
- Bit stuffing

If one or more errors are discovered by at least one station using the above mechanisms, the current transmission is aborted by sending an error message. This prevents other stations accepting the faulty message and thus ensures the consistency of data throughout the network. When the transmission of an erroneous message has been aborted, the

sender automatically re-attempts transmission (automatic repeat request).

The on-board CAN-controller is the Infineon SAE81C91, a so-called 'Full-CAN controller' with buffers for 16 messages. It is connected to the CAN bus via high-speed optocouplers to an interface circuit (Philips PCA82C250) which translates the logic levels to CAN levels. This bipolar integrated circuit has an operating temperature range of -40 to 125 °C and contains several protection features. The microcontrollers communicate with the CAN-controller via a serial interface.

E. Software

CANopen [4] has been chosen as the higher layer protocol. CANopen standardises the way data is structured and is communicated. Of particular relevance for LHC applications is the network management. A master watches all the nodes to see if they are operating within their specifications. The most recent version of CANopen recommends using heartbeat messages for the supervision of the nodes. A general purpose CANopen embedded software program (ELMBio) for the ELMB Master processor has been developed [5]. 64 analog input channels, up to 16 digital inputs (PORTF and PORTA) and up to 16 digital outputs (PORTC and PORTA) are supported. The ELMBio conforms to the CANopen DS-401 Device Profile for I/O-modules and provides sufficient flexibility to make it suitable for a wide range of applications.

The ELMBio source code is available as a framework for further developments and additions by users, who want to add or extend functionality, e.g. support for specific devices [6].

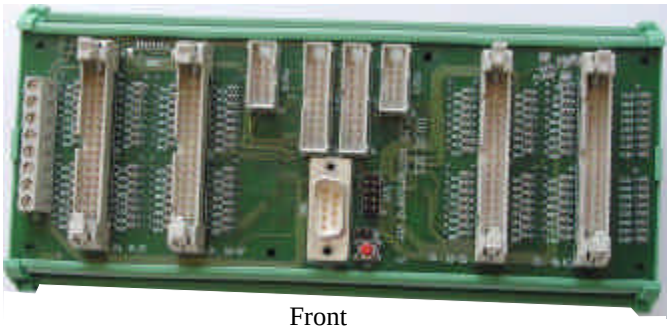

Front

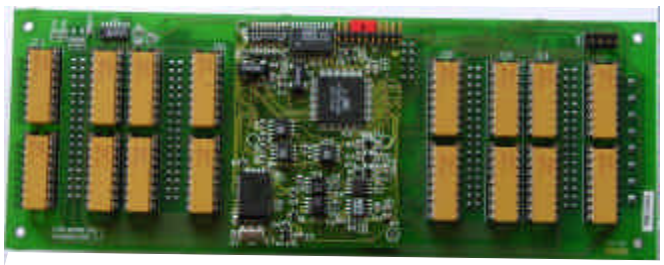

Back

Figure 4: The ELMB motherboard

III. ELMB MOTHERBOARD

A motherboard is available in order to evaluate the ELMB and for non-embedded applications, see Figure 4. It contains two 100-pin SMD connectors for the ELMB and sockets for adapters for the 64 channel ADC. The purpose of the adapters is to convert the input signals to levels suitable for the ADC. Adapters are available for voltage measurements and for resistive sensors in 2- and 4-wire connections. The motherboard may be mounted in DIN rail housing of the size 80x190 mm^2. On the front side are connectors for the ADC inputs, digital ports, a SPI interface, the CAN interface and power connectors.

IV. RADIATION TESTS

Several radiation tests for TID, SEE effects and NIEL have been performed.

A. TID tests

Three pre-selection TID tests have been made on 4 different ELMBs. Three of the ELMBs were of the first prototype series powered with 5V, while the 4th was from the 3.3V series.

1) The Pagure test

Two ELMBs were exposed to a Co^{60} γ-source [1 MeV] at the PAGURE facility [8]. They worked without problems until 30 Gy. At this point the power supply current started to increase by up to a factor of 10. Except for this increase, the ELMBs were basically working up to about 80 Gy when the measurements were stopped. The cause for the increase in the current was found to be the three CMOS components ATmega103L, AT90S2313 and the SAE81C91. The dose rate at this test was 77 Gy/h, which is 10^5 times higher than the ELMB is expected to receive at LHC. It was therefore decided to repeat tests at lower rates at CERN.

2) The first GIF test

The CERN Gamma Irradiation Facility (GIF) has a Cs^{137} γ-source [0.6 MeV]. The dose rate can be chosen in a wide range from 0.5 Gy/h down to 0.02 Gy/h. A test was done with one ELMB (given the identifier ELMB3) with a dose rate of 0.48 Gy/h [9]. The result was similar to the PAGURE test with the current increase starting at about 35 Gy. The test was stopped at 43 Gy when the current had increased by 20%. Both microcontrollers were still functional. However the in-system programming function of the master failed. The slave processor was found to be working without any faults.

3) Accelerated ageing test

After the radiation test the ELMB3 was tested for 12 days in a climate chamber [9]. At the same time a non-irradiated ELMB (ELMB4) was also tested for comparison. The total number of equivalent device hours reached was about 40000 h at 25 °C. Figure 5 shows how the current varied during the test. The current of the irradiated ELMB increased after each

temperature increase but then decreased exponentially. The current of the non-irradiated ELMB did not show this behaviour. Both ELMBs were still operating at 85 °C, but stopped working at a temperature of 100 °C, which is outside the specifications of the components. After the test the current of both ELMBs returned to the original value. The master processor had fully recovered and could be reprogrammed.

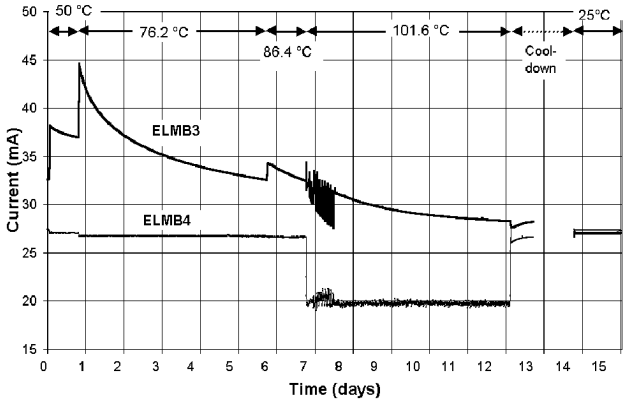

Figure 5: Current variations during the temperature test

4) GIF test 2

In order to test when the reprogramming function of the ELMB microcontrollers cease to work, an additional test of a 3.3V ELMB (ELMB5) was performed [10]. The irradiation was done in periods of approximately 10 hours and thereafter 14 hours break. After each step the reprogramming function was checked. This function failed after 35 Gy. At this moment a small current decrease could be observed. From then on the ELMB received a continuous dose and the current increased. Figure 6 shows how the digital currents changed for all the TID tests.

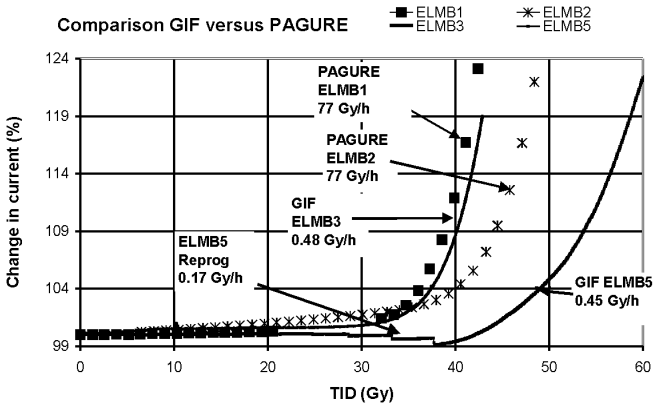

Figure 6: Comparison of the digital current for all TID tests

5) Conclusions from the TID test of the ELMBs

It was observed that the re-programming function of the flash memory and EEPROM in the master microcontroller ceases to work at a total received dose of around 35 Gy. Also the digital current increases substantially for a total dose of about 40 Gy. However this did not influence the operation of the ELMB up to about 80 Gy

B. SEE tests

The ELMB was irradiated with 60 MeV protons at the CYClotron of LOuvain-la-NEuve (CYCLONE) of the Université Catholique de Louvain, in Belgium [11]. The main purpose was to study SEE effects on the ELMB but also some TID measurements were made. A total fluence of $3.28*10^{11}$ protons/cm^2 was divided among 11 ELMBs. Each ELMB received an ionising dose of 39 Gy. Two types of tests were performed: a systematic test of memories and register and a functional test. They are described in detail in [11].

1) Result of the systematic memory and register tests

Special software was run in the ELMB, which in addition to the normal program also performed systematic bit tests of the different memories and registers in the ELMB. Figure 7 shows the addresses of the ATmega103L SRAM where the bit errors were located versus fluence. (The total fluence reached was $3.28*10^{11}$ protons/cm$^{2)}$.

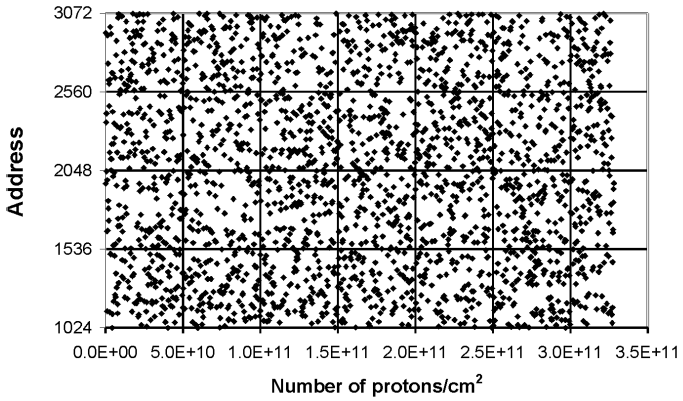

Figure 7: Addresses of the SRAM where SEE occurred versus fluence

A summary of the memory and register errors is shown in Table 1. No error was found in the flash memory or in the EEPROM. Many errors were found in the SRAM as expected. The SRAM is twice as sensitive as the registers in the CAN controller SAE81C91 and ADC CS5523.

Table 1: Results of the systematic SEU test

	No of bits Tested	**No of errors**	**Cross-section cm^2/bit**
SRAM	16384	2320	$4.3*10^{-13}$
EEPROM	28672	<1	$<1.1*10^{-16}$
FLASH	1048576	<1	$<2.9*10^{-18}$
CAN registers	320	23	$2.2*10^{-13}$
ADC registers	264	22	$2.5*10^{-13}$

2) The result of the functional SEE test

There will be in the order of 3000 ELMBs installed in ATLAS. For topological and operational reasons at most 64 ELMBs will form a CAN branch. As shown in this paper, errors due to radiation will occur. Table 2 lists the different types of errors with their symptoms, the method to recover from them and their maximally allowed rate.

Table 2: Maximum allowed SEE rates in DCS system

SEE category / Symptoms	Error recovery	Maximum allowed rate
Soft SEE / Data readout errors	Automatic recovery	1 every 10 minutes per CAN branch
Soft SEE / CAN node hangs	Software reset	1 every 24 hours per CAN node
Soft SEE / CAN branch hangs	Power cycling	1 every 24 hours per CAN branch
Hard SEE / Permanent error	Replace ELMB	1 every 2 months for 3000 ELMBs
Destructive SEE/ Damage	Power limitation	Not allowed

In total there were 29 abnormal situations detected in 131157 CAN messages recorded for $3.28*10^{11}$ protons/cm^2, These events are divided in categories according to how the normal behaviour was restored, see Table 3.

Table 3: Results of the SEE test compared with requirements

SEE category/ Recovery	Result of the SEE test	Requirements
Soft SEE / Automatic recovery	20	2604
Soft SEE / Software reset	5	1157
Soft SEE / Power cycling	4	18
Hard SEE	0	0.006

Of the SEEs, which required power cycling, one was due to an increase in the digital current and therefore believed to be a SEL. All other SEEs are soft SEE. No hard or destructive SEEs were found. All ELMBs were working perfectly after the test.

4) TID effects

The dose amounted to 39 Gy for 10 of the ELMBs and to 44.5 Gy for one of the ELMBs. The TID is estimated using a conversion factor $1.0*10^{10}$ protons/cm^2 corresponding to an ionising dose of 13 Gy for 60 MeV protons. The average fluence per ELMB was $3.0*10^{10}$ protons/cm^2. The power supply currents were measured on-line. The change measured was negligible (< 0.3%). All voltages of the LDO regulators and the ADC voltage reference were also found to be unchanged. Finally all ELMBs were checked to see if the reprogramming function of the microcontrollers was still working. They all proved to work perfectly.

C. NIEL

Tests on 10 ELMBs at the PROSPERO reactor with 1 MeV neutrons were done to test the bipolar components of the ELMB. 5 of the ELMBs were irradiated to $6*10^{11}$ n/cm^2 (equiv. 1 MeV Si) while the other 5 to $3*10^{12}$ n/cm^2 (equiv. 1 MeV Si). All 10 were found to be perfectly working after the test. Measurements on the bipolar LDO voltage regulators and the voltage references AD680JR showed that they were all within specifications.

V. Conclusions

The ELMB has proven to be a versatile general-purpose I/O device, very well matched to the needs of the LHC experiments. All ATLAS subdetectors have decided to use it on a large scale - the biggest system comprising 1200 ELMBs. CAN is an excellent choice for the read-out due to its robustness and error handling facilities. It has also been shown that by using COTS a certain level of radiation tolerance can be achieved. For example the requirements for the ATLAS Muon detector MDT are fulfilled concerning SEE and NIEL. The required TID figures including a safety factor of 7 varies from 9.3 Gy to 44.7 Gy for the different MDT chambers. For more than 97% of them the requirements are fully satisfied. More investigations and possibly some special measures may be required to use the ELMB for the rest of the chambers.

VI. Acknowledgements

We would like to thank M.Dentan for helping us with the definition and execution of the radiation tests. We are grateful to the EP-ESS group for collaborating in the production of the ELMB and to the EP division for the support as a Common Project.

VII. References

[1] B. Hallgren et al, “A Low-Cost I/O Concentrator using the CAN fieldbus”, ICALEPS99conference, Trieste, Italy, 4 – 8 October, 1999

[2] http://atlas.web.cern.ch/Atlas/GROUPS/FRONTEND/WWW/RAD/RadWebPage/RadConstraint/Radiation_Tables_031000.pdf

[3] G.Baribaud et al, "RECOMMENDATIONS FOR THE USE OF FIELDBUSES AT CERN", CERN ECP 96-11, June 1996. http://itcowww.cern.ch/fieldbus/report1.html.

[4] CAN in Automation (CiA), D-91058 Erlangen (Germany). http://www.can-cia.de/

[5] H.Boterenbrood, “Software for the ELMB (Embedded Local Monitor Board) CANopen module”, NIKHEF, Amsterdam, 25 July 2001.

[6] http://www.nikhef.nl/pub/departments/ct/po/html/ELMB/ELMBresources.html

[7] CAN in Automation (CiA), “CANopen Device Profile for Generic I/O Modules”, CiA DS-401, Version 2.0, 20 December 1999.

[8] H.Burckhart, B. Hallgren and H. Kvedalen, ' Irradiation Measurements of the ATLAS ELMB', CERN ATLAS Internal Working Note, DCS- IWN9, 8 March, 2001

[9] J. Cook, B. Hallgren and H. Kvedalen, ' Radiation test at GIF and accelerated ageing of the ELMB ', CERN ATLAS Internal Working Note, DCS- IWN10, 2 May, 2001

[10] B. Hallgren and H. Kvedalen, ' Radiation test of the 3.3V version ELMB at GIF ', CERN ATLAS Internal Working Note, DCS- IWN11, 31 August, 2001

[11] H. Boterenbrood, H.J. Burckhart, B. Hallgren H. Kvedalen and N. Roussel, 'Single Event Effect Test of the Embedded Local Monitor Board',CERN ATLAS Internal Working Note, DCS- IWN12, 20 September, 2001

Radiation test of the 3.3V version ELMB at GIF

B. Hallgren and H. Kvedalen

Abstract: A total ionizing dose (TID) test of a 3.3V version of the ELMB has been performed at the CERN GIF facility with a dose rate of 0.46 Gy/h. No significant difference in the results from the two previous ELMB TID test was found. The irradiation was done in periods of approximately 10h on and 14 h off. After each period with radiation the programming function of the flash memory was tested. The programming function failed after receiving a dose of approximately 35 Gy. A very small linear current increase could be observed in the analog current. The digital current started to increase after the source was left on continuously. The CAN current showed small changes. No changes or drift was found in the ADC readout.

1.0 Introduction

The purpose of this TID test was to test the new 3.3V version of the ELMB, and to find out when the programming function in the micro controllers is lost. This test was also done to see whether a periodical irradiation sequence had any influence on the known current increase in the digital part [2,3]. The test was done with intervals with irradiation and no irradiation. The irradiation periods were about 10h per day. After each period the source was turned off and the master processor (Atmega103) was reprogrammed.

2.0 ELMB5 test

The ELMB5 is a standard board from the small series production of 300 pieces. The ELMB was mounted on a second-generation motherboard. All analog inputs were connected to a resistor network that derived a reference voltage to 16 different DC voltages. The reference voltage was derived from the ADC reference voltage through an operational amplifier. The available digital I/O lines was connected in a pattern so the ELMB could do a digital I/O test.

The setup consisted of a standard 3.3V ELMB connected to 30m of cable carrying power and the CAN bus. This cable was connected to a PC running a SCADA DAQ application for ELMB readout and currents measurement. It was also connected to a CAN bus analyzer serving as a CAN bus monitor while reprogramming tests was carried out. To measure the three currents (analog, digital and CAN), a setup with the older LMB was used. This setup was also placed inside the GIF radiation zone, but hidden behind a concrete wall for protection.

As mentioned, the ELMB was exposed to radiation for about 10 hours during the day, it was left without radiation the following 14 hours. After the source was turned off, the programming function of the program memory in the ATmega103 processor was tested. The test was done by using a special loader program[1]. With this program it was possible to change the program in the ELMB via the CAN bus. The reason for using this method was due to the fact that is was very inconvenient to remove the ELMB from the GIF for testing, and it was not practical to do the testing inside the GIF zone.

2.1 Radiation tests at GIF

The ELMB were placed in the small side-beam at the GIF. It was placed at a distance of 25cm from the source. The setup is shown in figure 1. At this distance the theoretical dose-rate is

[1] Custom made loader program made for uploading a program to the ELMB via the CAN bus. Program can be downloaded from: http://www.nikhef.nl/pub/departments/ct/po/html/ELMB/ELMBresources.html

0.45Gy/h. Dose measurements was done with four L-Aniline dosimeters. Two of them were removed from the source when the programming function failed, the last two was removed when the test was finished. During the test, the three currents were measured, the ambient temperature, a digital IO test was performed and the 64 ADC channels were read. The reading of these values was done every minute.

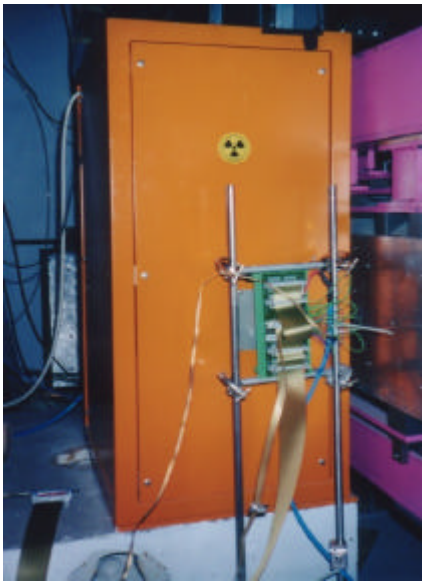

Figure 1. *Picture of the test setup using the side beam of the GIF.*

2.1.1 The Analog part

The readings from the 64 ADC channels during the whole test period (source on and off) are shown in figure 2 and 3. During the data acquisition, the ADC was configured with 1V range and with a 15Hz conversion rate. The gaps in the data in the figure are due to wrong configuration of the ADC. In the first gap, the ADC was not reprogrammed to the correct setting after a test of the program memory in the main processor, ATmega 103 (the ADC setting was reset when this was done). The next gap (only involving a few channels) was changed during the test. The reason way this changed is unknown. After a reset (reprogramming test) the ADC readings was correct and was correct till the end of the test.

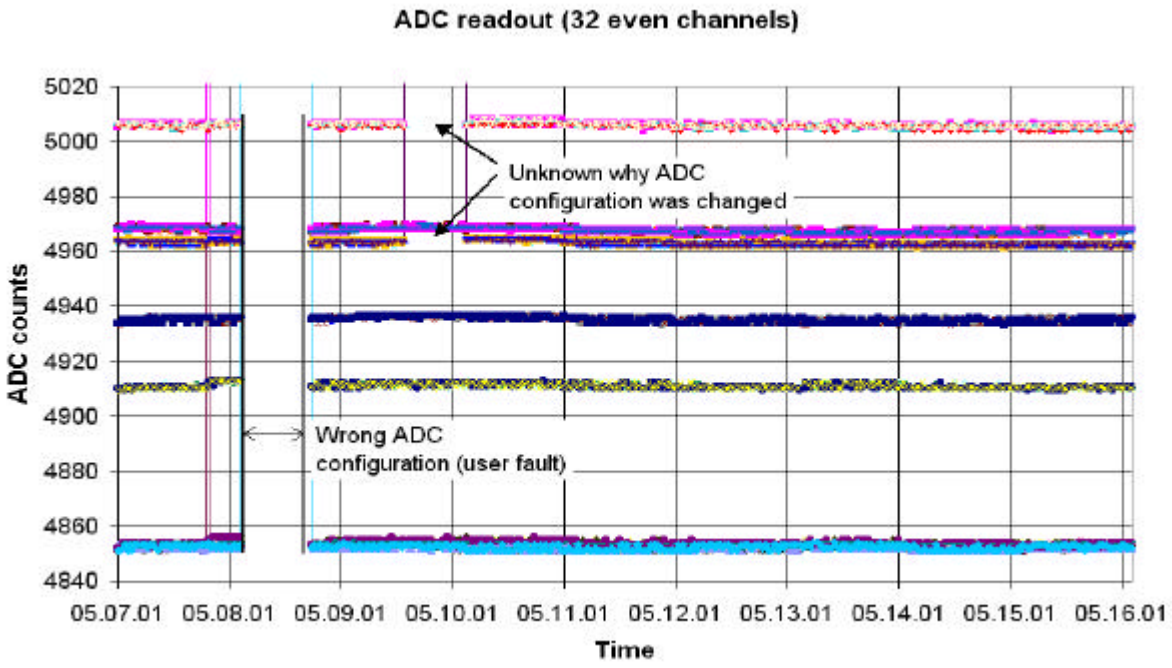

Figure 2. *ADC readout form even channels during the test.*

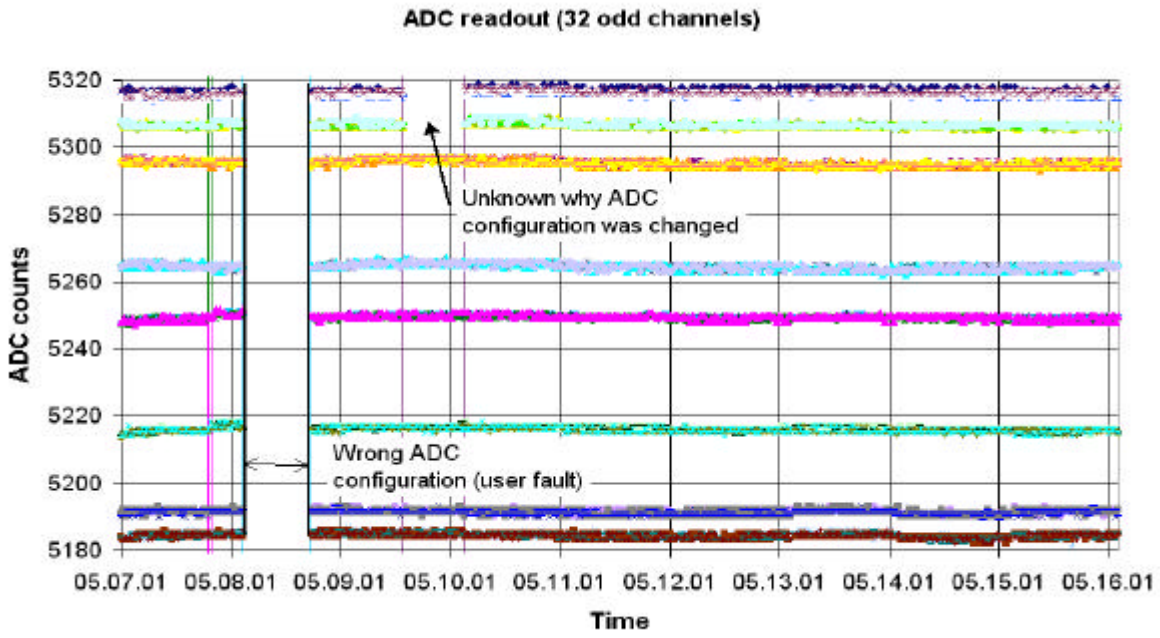

Figure 3. *ADC readout form odd channels during the test*.

2.1.2 The Analog current

Figure 4 show the behavior of the analog current during the test. As seen there is a small variation in the current (photo-current) during the test when the source was switched on and off periodically. There is also a small linear increase in the current (around 1%). After 9 days the source was left on until the test was ended (due to failure of reprogramming of ATmega103 processor). When the source was left on, the current had decreased a bit, but continued to increase, but after a while the current started to decrease rapidly. This current decrease is believed to be correlated with the increase in the digital current shown in figure 7. An increase in the digital current will make the digital voltage regulator quite hot. This regulator is placed side by side with the analog and the CAN voltage regulators and therefore also heats these regulators. As seen in the figure, when the source is switched of, the currents stabilizes around a small ripple. This ripple is believed to be the day – night temperature variation. The temperature during the test is shown in figure 5. The current measurement is done with very high resolution and the total change in the current is just 150 A. Such small current change does not have any significance for operation, but it is important that we understand as much as possible about the effects of radiation on the ELMB.

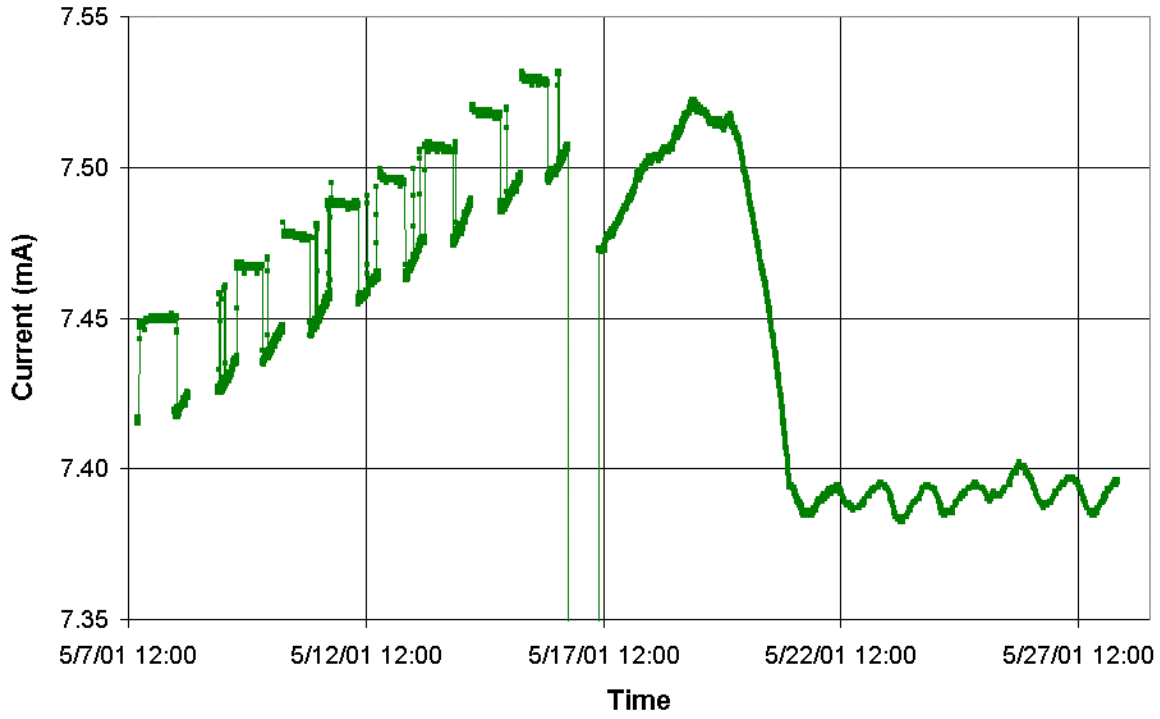

Figure 4. *Analog current during the test*.

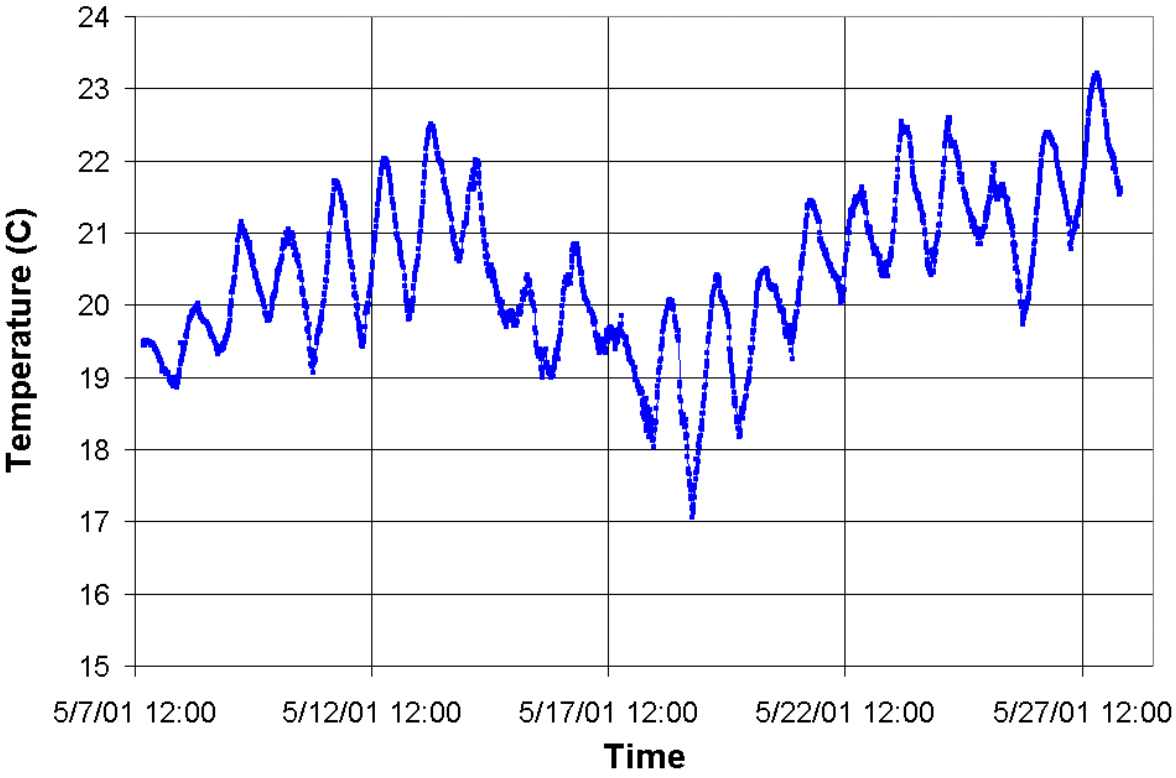

Figure 5. *Temperature variation during the test.*

2.1.3 The Digital part

After each period of radiation the master processor was reprogrammed with a different program to find out if the programming circuitry was still working. After receiving a dose between 35-40 Gy the programming function did not work anymore. Figure 6 show the digital current up till the point here the programming function failed. As seen a small change in the digital current could be observed after each programming sequence. Table 1 show when the programming took place and at which accumulated does. After the programming function failed the ^{137}Cs source was left continuously on for ~4 days. As seen in figure 7 the digital current then started to increase rapidly. After reaching 80 Gy the source was turned off and the ELMB was left to anneal in ambient temperature.

Period	Time	Digital current (mA)	Cumulated dose (Gy)
START	5/7/01 16:31	14.100	0.0
1	5/8/01 11:38	14.100	0.5
2	5/9/01 19:24	14.109	7.9
3	5/10/01 18:31	14.111	12.2
4	5/11/01 18:46	14.112	16.3
5	5/12/01 18:21	14.105	20.8
6	5/13/01 19:01	14.103	25.2
7	5/14/01 17:54	14.083	29.4
8	5/15/01 18:53	14.045	33.8
9	5/16/01 18:58	13.999	37.9
STOP	5/21/01 10:15	39.622	80.3

Table 1. *Time and received dose when programming function was tested.*

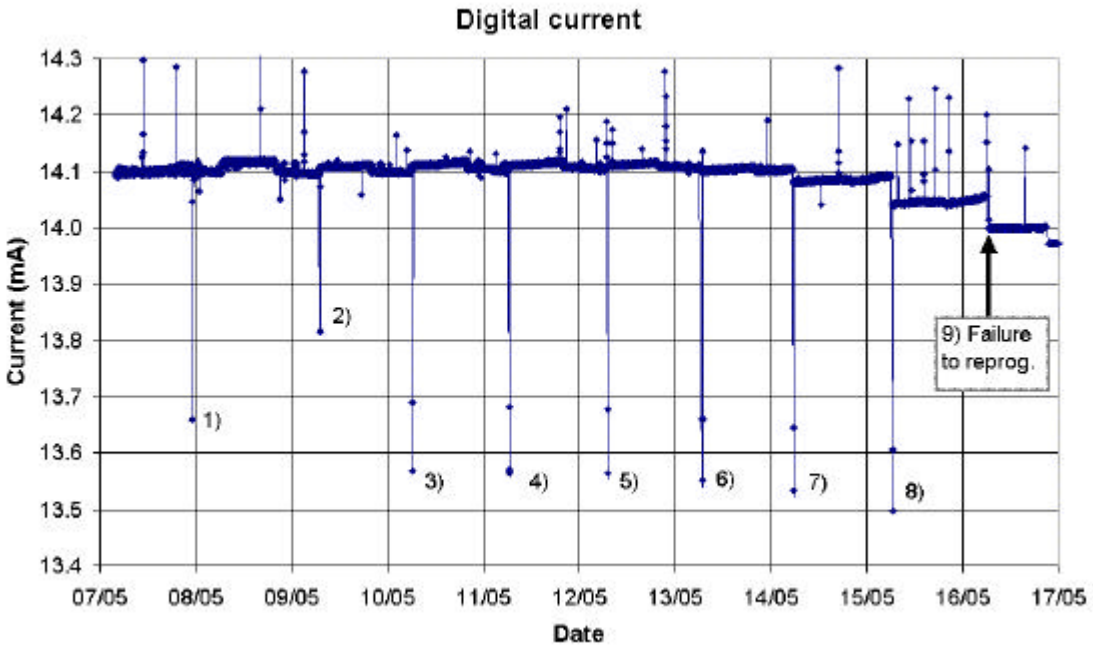

Figure 6. *Digital current up the point where the programming function stopped working.*

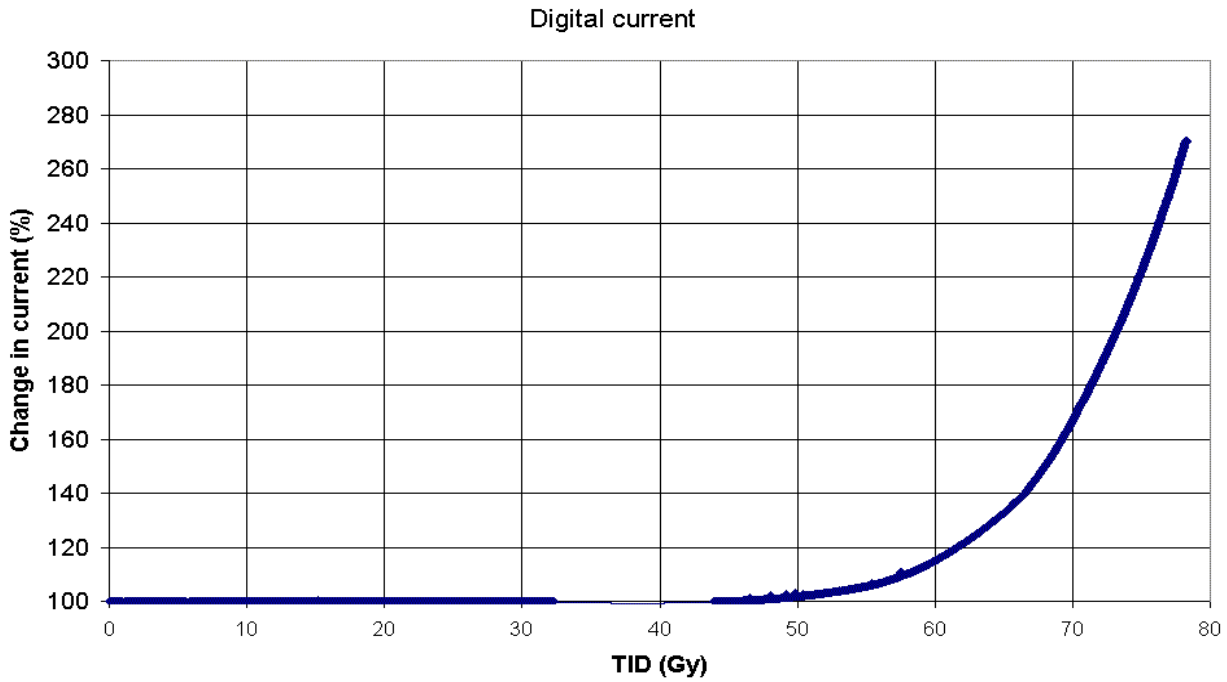

Figure 7. Digital current as function of total integrated dose.

Figure 8 show the digital current as function of the time. After the source was turned off the ELMB5 was left with power. This was done to see if there was any annealing effect. As seen in the figure there is an annealing effect on the digital current. Also in this figure there is some ripple, the reason for this is the day-night temperature variation.

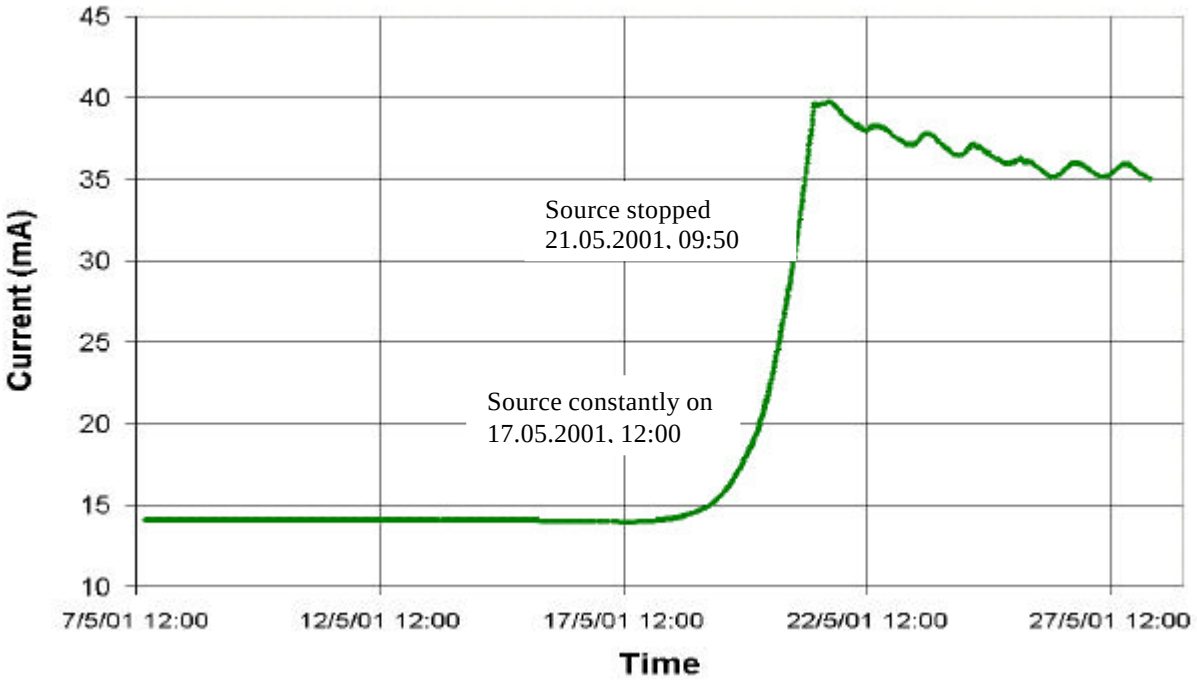

Figure 8. *Digital current as function of time.*

2.1.4 CAN current

The CAN circuits did work normally when the test was ended at 80 Gy. Figure 9 show the CAN current. The change in the current after receiving 80Gy is less than 1%. The peaks in the figure are caused by the fact that the current measurement is done when the CAN part is operational. When there is activity on the CAN bus, the CAN current will vary a bit.

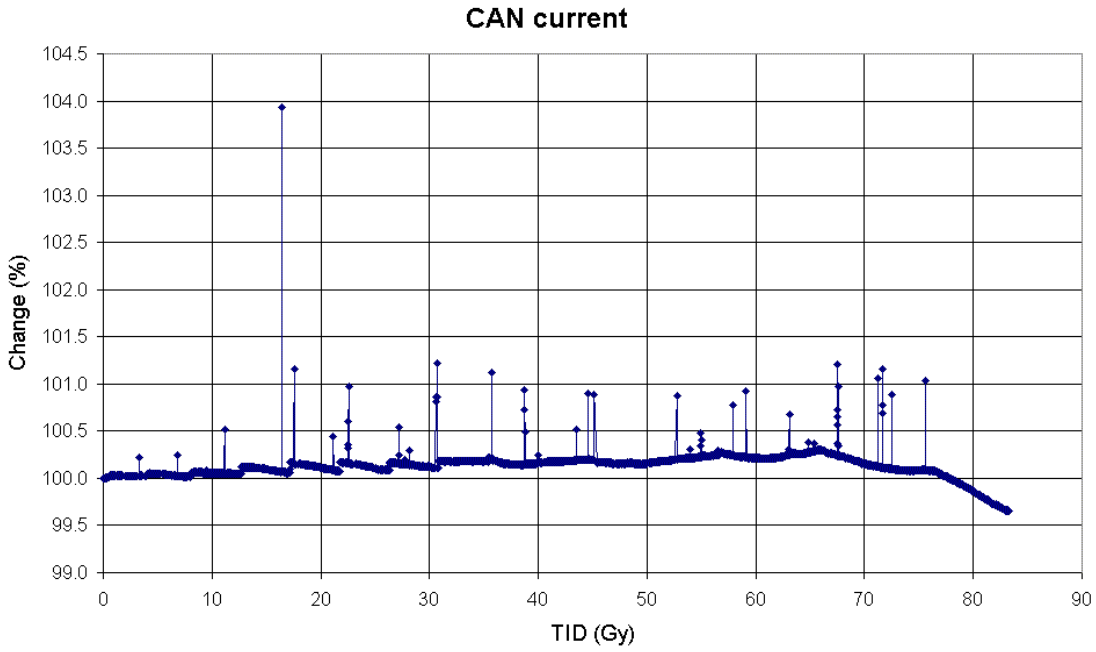

Figure 9. *CAN current as function of the total integrated dose. Peaks are due to activity on the CAN bus.*

Figure 10 shows the CAN current as function of time. In this figure the CAN current shows the same behavioral as the analog current, figure 4. Mind the scale on the figure, the total current variation is only 200 A.

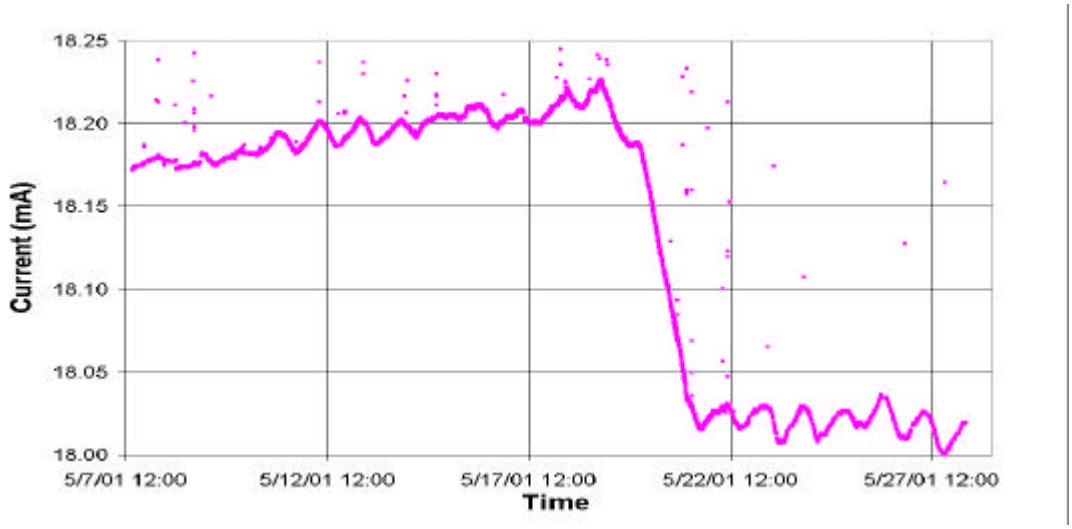

Figure 10. *CAN current as function of time.*

2.1.5 Functional test of the microcontrollers

While the ELMB was installed in the GIF, the program memory of the master processor (ATmega 103) was programmed remotely by the slave processor (AT90S2313) to verify the programming function. After test, the ELMB was removed from the GIF and both processors were checked with the programming environment from Kanda Systems[2]. This environment gives access to the EEPROM and the Flash memory via in system programming connector on the ELMB. These to different memories are of interest to test since we have found problems with the programming function of these memories in earlier tests [2,3].

ATmega 103

During the test: The ATmega 103 were reprogrammed 8 times and was found to be fully working. When attempting to reprogram the 9^{th} time the programming function failed. It was not possible to upload a new program to the processor anymore.

After the test (after 80Gy): After the ELMB was removed from the GIF, the ATmega 103 processor was carefully checked directly via the in system programming connector. It was found that all program memory locations were erased to 0xFF except for one location. After a re-programming sequence the entire memory was "erased" to 0xFF (unknown if this location was erased to 0xFF or it was programmed to the value). However, no program could be stored in the flash. The programming function was destroyed. During this test it was found that it was still possible to program the EEPROM in the ATmega103 processor, but the erase circuit did not work (still possible to program 0xFF).

AT90S2313

During test: The AT90S2313 was not reprogrammed during the irradiation sequence. Only serving as programming interface between computer and the ATmega103.

After the test (after 80Gy): It was possible to reprogram the EEPROM in the slave processor AT90S2313, and the erase circuitry worked. It was also possible to erase the flash memory, but it was not possible to re-program it. Note: the processor was fully working before reprogramming. Therefore, if no reprogramming functionality is needed, the processor can be used up to this integrated dose without any problems except increased current consumption.

[2] Kanda Systems: www.kanda-systems.com

2.1.6 Measurements after the test campaign

The following DC voltages were measured after the test, the voltages are within the specifications.

Description	Voltage
ADC reference voltage AD681-JR	2.498V
Digital voltage MIC 5203	3.327V
Analog voltage MIC 5203	5.064V
CAN voltage MIC 5203	5.013V
Op-Amp LMC6084 ch.0-15	2.499V
Op-Amp LMC6084 ch.16-31	2.500V
Op-Amp LMC6084 ch.32-47	2.503V
Op-Amp LMC6084 ch.48-63	2.503V

Table 2. *DC voltages measured after the test.*

3.0 Comparison with previous test

3.1 Comparison of the digital currents

Figure 11 show a comparison of the three TID testes. As seen the ELMB5 current behaves differently than the ELMB1, ELMB2 and ELMB3 up to a TID dose of 38 Gy. Until this dose the ELMB5 was operated in different manner than the other three ELMBs: 1) the dose was applied in 9 steps and 2) the reprogramming function of the microcontroller was exercised. From a TID dose of 38 Gy ELMB5 received a continuous dose as the other ELMBs and behaves similarly

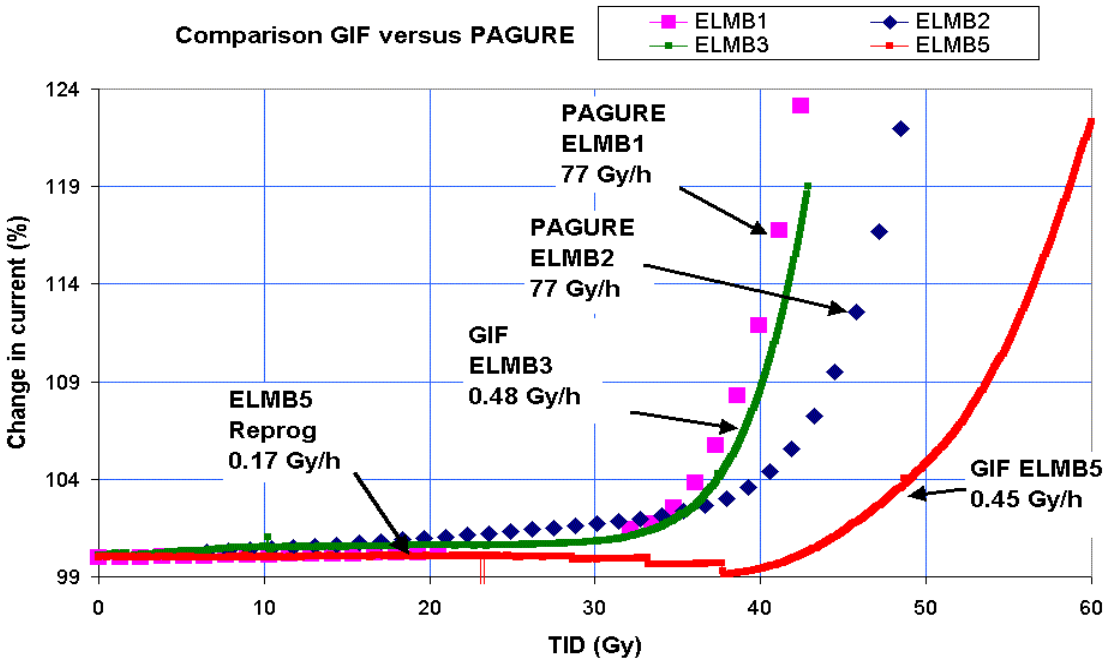

Figure 11. *Comparison of the digital current from all for tests [2,3].*

3.2 Comparison of the analog currents

Figure 12 shows the behavior of the analog currents from ELMB3 and ELMB5. The ELMB3 current did vary quite a bit, but there is an increasing trend. The ELMB5 current does not show this variations, but there is a small constant increase in the current.

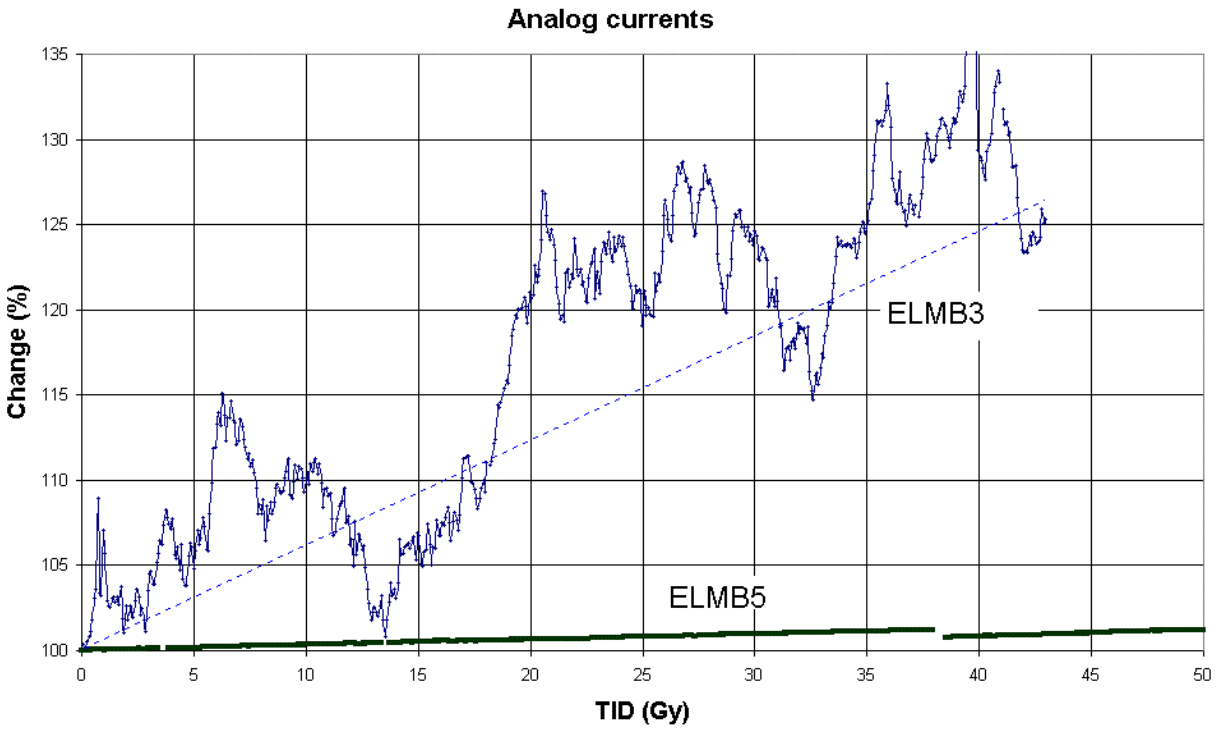

Figure 12. *Comparison of the analog current from the first GIF test [3] with the current obtained in the latest test.*

3.3 Comparison of the analog readout

Figure 13 show the ADC readout during the ELMB3 test. In this figure we can see a small increase in the values read from the ADC. In figure 2 and 3 (ELMB5) we do not see this effect. The reason for this can be that the ADC was re-calibrated after each reprogramming. This was not the case in the ELMB3 test.

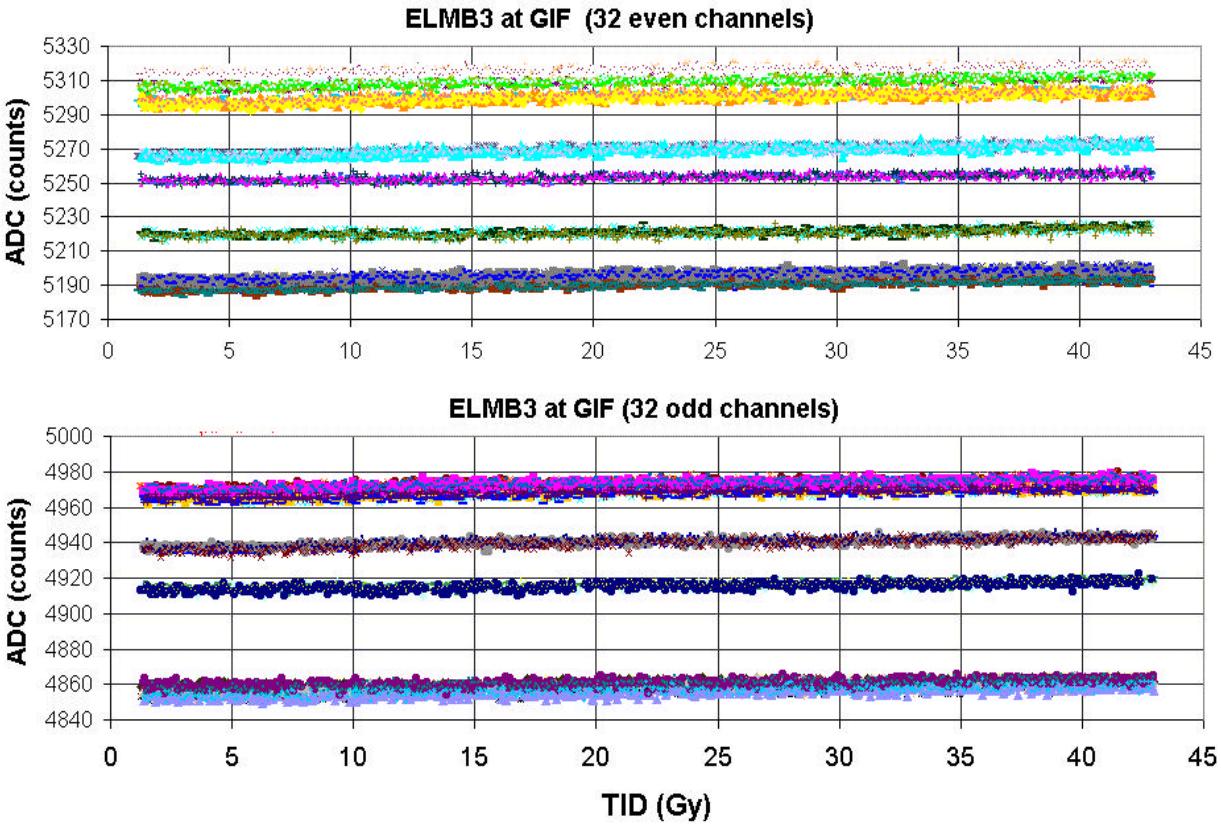

Figure 13. *ADC readings from the ELMB3 test.*

4.0 Conclusion

- Programming function of the ATmega103 cease to work at a total received dose of around 35Gy. The slave processor still worked at a dose of 80 Gy, but reprogramming of flash memory not possible. However, programming of the EEPROM worked in both processors, but problems with the erase function were observed in the ATmega 103.
- The digital current of the ELMB5 increased 10% for a total dose of 55 Gy.
- The small changes in the currents of the analog and CAN parts did not influence the operation of the ELMB5.
- Results show that a 3.3V version behaves quite similar to the 5V version.

5.0 References

[1] S. Agosteo et al, 'A facility for the test of large area muon chambers at high rates' CERN-EP-2000-031, February 16, 2000.

[2] H.Burckhart, B. Hallgren and H. Kvedalen, ' Irradiation Measurements of the ATLAS ELMB', CERN ATLAS Internal Working Note, DCS- IWN9, 8 March, 2001

[3] J. Cook, B. Hallgren and H. Kvedalen, ' Radiation test at GIF and accelerated aging of the ELMB ', CERN ATLAS Internal Working Note, DCS- IWN10, 2 May, 2001